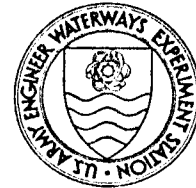LEVEL II

MICROGRAVIMETRIC TECHNIQUES FOR GEOTECHNICAL APPLICATIONS

by

Dwain K. Butler

Geotechnical Laboratory
U. S. Army Engineer Waterways Experiment Station
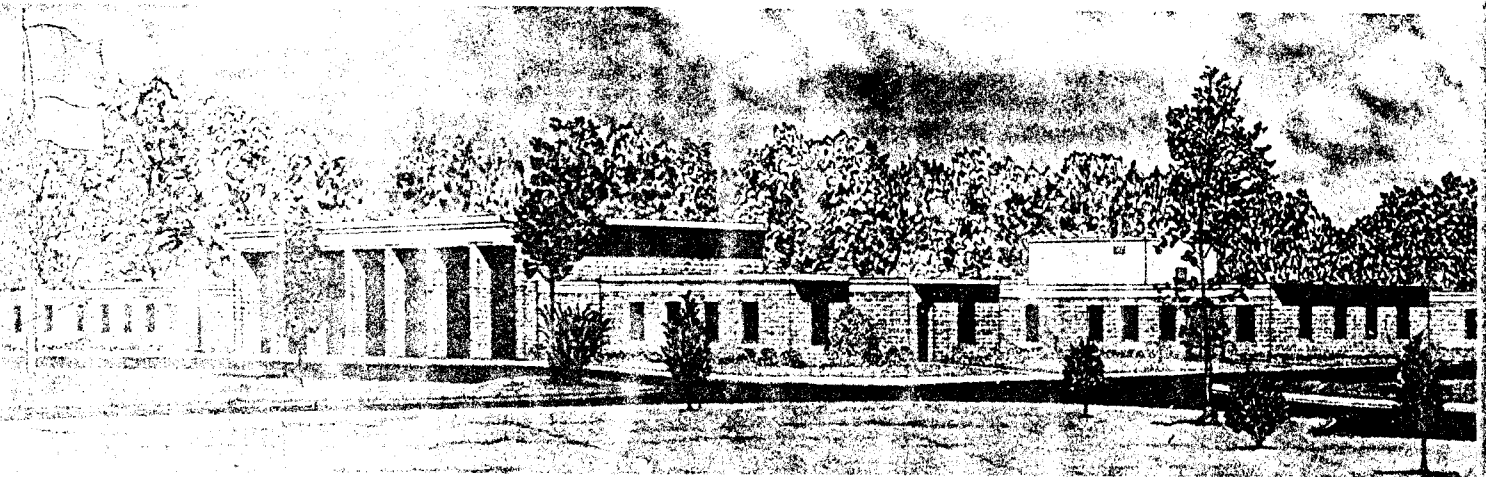P. O. Box 631, Vicksburg, Miss. 39180

September 1980

Final Report

Approved For Public Release; Distribution Unlimited

DTIC
SELECTED
OCT 1 5 1980

A

80 10 14 235

REPORT DOCUMENTATION PAGE	READ INSTRUCTIONS BEFORE COMPLETING FORM

1. REPORT NUMBER WES/MP/GL-80-13 MISCELLANEOUS PAPER GL-80-13	2. GOVT ACCESSION NO. AD A090874	3. RECIPIENT'S CATALOG NUMBER

4. TITLE (and Subtitle)
MICROGRAVIMETRIC TECHNIQUES FOR GEOTECHNICAL APPLICATIONS

5. TYPE OF REPORT & PERIOD COVERED
Final report NOV 78 - MAY 80

6. PERFORMING ORG. REPORT NUMBER

7. AUTHOR(s)
Dwain K. Butler

8. CONTRACT OR GRANT NUMBER(s)

9. PERFORMING ORGANIZATION NAME AND ADDRESS
U. S. Army Engineer Waterways Experiment Station
Geotechnical Laboratory
P. O. Box 631, Vicksburg, Miss. 39180

10. PROGRAM ELEMENT, PROJECT, TASK AREA & WORK UNIT NUMBERS
Project No. 4A161101A91D

11. CONTROLLING OFFICE NAME AND ADDRESS
Assistant Secretary of the Army (R&D)
Department of the Army
Washington, D. C. 20310

12. REPORT DATE
September 1980

13. NUMBER OF PAGES
129

14. MONITORING AGENCY NAME & ADDRESS(if different from Controlling Office)

15. SECURITY CLASS. (of this report)
Unclassified

15a. DECLASSIFICATION/DOWNGRADING SCHEDULE

16. DISTRIBUTION STATEMENT (of this Report)

Approved for public release; distribution unlimited.

17. DISTRIBUTION STATEMENT (of the abstract entered in Block 20, if different from Report)

18. SUPPLEMENTARY NOTES

19. KEY WORDS (Continue on reverse side if necessary and identify by block number)

20. ABSTRACT (Continue on reverse side if necessary and identify by block number)

Application of high-resolution gravimetry to geotechnical problems is properly termed microgravimetry and is a relatively recent addition to the list of geophysical methods available for geophysical site investigations and other geotechnical applications. This report investigates the applicability of microgravimetry to the wide range of geotechnical problems of interest to the Corps of Engineers.

Microgravimetry should be viewed as a complement to other geophysical methods for site investigations. For sites with strata which are (Continued)

DD , FORM 1 JAN 73 1473 EDITION OF 1 NOV 65 IS OBSOLETE

411412

20. Abstract (Continued)

nearly horizontal (i.e., a "layer cake" type structure), microgravimetry will be of little use. However, microgravimetry is ideally suited for sites with bedrock irregularities, faults, fracture zones, cavities, buried channels, etc. Use of microgravimetry accompanied by other complementary geophysical methods (such as seismic refraction and/or electrical resistivity) and only selective drilling can achieve adequate site definition at considerably less cost than the comprehensive drilling program alone necessary to achieve the same site definition.

Pertinent aspects of gravitational potential theory are reviewed and the concept of gravity anomalies is explored. Model studies are presented which investigate the detectability of subsurface structures by gravity surveys. Using a detection threshold of 10 µGal, based on the sensitivity and accuracy of state-of-the-art microgravimeters, the detectability of spherical, horizontal cylindrical, and truncated horizontal slab models is assessed. As a rule of thumb, compact structures which can be approximated as spherical in shape, can be detected at a depth to center of about two times the effective diameter at the 10-µGal threshold level.

A substantial portion of the report is devoted to the practical field survey procedures for microgravity work. The emphasis is on acquiring high-quality data. Topographic survey requirements and gravity data acquisition procedures are discussed in detail. The corrections which must be made to gravity data are discussed and a practical example of the drift correction procedure is presented.

Three case histories of the application of microgravimetry to the detection and delineation of subsurface cavities are presented. Also, the results of a full-scale microgravity field investigation at a natural cavity site in Florida are presented and analyzed. With only one exception, all known cavities at the site were delineated by the gravity results. Other negative gravity anomalies were investigated by drilling and found to be due either to cavities or to clay pockets in the top of the limestone. Even very subtle geologic features were correctly expressed in the gravity data.

There is considerable fundamental and practical importance in the measurements of horizontal and vertical gravity gradients. In particular, gravity-gradient profiles (a) have diagnostic properties which make subsurface structure identification more straightforward, and (b) tend to selectively filter out anomalies caused by deeper-seated structures and hence enhance anomalies caused by shallower structures of interest in geotechnical investigations. Results of a field gravity-gradient study are presented demonstrating successful determination of both vertical and horizontal gravity-gradient profiles over a shallow man-made structure.

Finally, two more exotic applications of microgravimetry are discussed. Microgravimetry can be used to study deflections of the crust due to reservoir loading, underground fluid injection or withdrawal, and earthquakes. Elevation changes due to reservoir loading are specifically addressed. Examples of the use of the gravimeter to record earth tides and as a long-period vertical seismometer are presented. The value of theoretical and recorded earth tide records in the analysis of microgravity field data is also emphasized.

Microgravimetry has many varied applications to geotechnical problems. It should be carefully considered for application to geophysical site investigations as well as other areas discussed in this report.

PREFACE

The study reported herein was performed during the period November 1978 to May 1980 under Department of the Army Project No. 4A161101A91D, In-House Laboratory Independent Research (ILIR) Program, sponsored by the Assistant Secretary of the Army (R&D).

The report was prepared by Mr. Dwain K. Butler of the Earthquake Engineering and Geophysics Division (EEGD), Geotechnical Laboratory (GL), U. S. Army Engineer Waterways Experiment Station (WES), Vicksburg, Mississippi, under the general supervision of Drs. Paul F. Hadala and William F. Marcuson, III, former Chief and Acting Chief, respectively, EEGD, and Messrs. James P. Sale and Clifford L. McAnear, former Chief and Acting Chief, respectively, GL. Field work was performed at Vicksburg, Mississippi; Reddick, Florida; and Bryan, Texas. Mr. Rodney Walters assisted in the topographic survey at the Reddick, Florida, site. Special appreciation is expressed to Professor Robert Neumann and his colleagues at the Compagnie Generale de Geophysique, Massy, France, for assistance in processing data from the Medford Cave site near Reddick, Florida. Professor Neumann has been instrumental in encouraging geotechnical applications of microgravimetry. Assistance with field programs at the Medford Cave site was provided by Messrs. J. D. Gammage, William Steltz, and Bill Wisner, and Dr. Robert Ho of the Florida Department of Transportation, Gainesville, Florida.

The microgravity survey at the Medford Cave site near Reddick, Florida, was closely coordinated with work planned by Mr. Joseph R. Curro, Jr., under CWIS Work Unit 31150 entitled "Remote Delineation of Cavities and Discontinuities in Rock." Various analytical and data processing considerations involved in this work were closely coordinated with work planned by Mr. Butler under the Project 4A161102AT22, Work Unit 002/Q6 entitled "Analytical and Data Processing Techniques for Interpretation of Geophysical Properties."

Commanders and Directors of the WES during the performance of this work and the preparation of this report were COL John L. Cannon, CE, and COL Nelson P. Conover, CE. Technical Director was Mr. Fred R. Brown.

1

CONTENTS

MICROGRAVIMETRIC TECHNIQUES FOR GEOTECHNICAL APPLICATIONS

PART I: INTRODUCTION

Background

1. Microgravimetry is a geophysical method that offers special advantages over other subsurface exploration methods in a variety of applications. At the Symposium on Detection of Subsurface Cavities held at the U. S. Army Engineer Waterways Experiment Station (WES), July 1977, Professor Robert Neumann (1977) commented

> "I have been involved in microgravimetry from its inception. It is now a healthy teenager, but I must deplore the small amount of material relating to gravity in this symposium: only one paper devoted to the subject, and moreover from France. Are there really no micro-gravity case histories available in the U. S.? If a symposium like this were organized in Europe, the number of gravity papers would account for 50 percent of the geophysical subjects. Such a difference between the two continents is surprising and deserves some attempt to understand the situation and improve it."

Indeed, there are very few publications by United States authors dealing with detailed or high-resolution applications of gravimetry of any type; use of gravimetric methods has been restricted to the familiar large-scale, reconnaissance-type surveys. However, as indicated by Professor Neumann, high-resolution gravity methods, microgravimetry, are used extensively in Europe (as well as in Russia) for small-scale geotechnical applications.

2. The term "microgravimetry" refers to geophysical investigations involving relative measurements of the acceleration of gravity that require measurement accuracy and precision and instrument sensitivity in the μGal range (1 μGal = 10^{-6} Gal = 10^{-6} cm/s^2 $\approx$ 10^{-9} times the normal gravitational acceleration). As used in this study, microgravimetry also connotes the scale of the survey, i.e., a

significant scaling down in sizes and depths of the geologic structures or features of interest as well as a corresponding decrease in the required profile and grid spacing. For geotechnical applications, delineation of features with characteristic dimensions of 1 m or less is often desirable, while the maximum depth of interest may typically be 100 m or less. Prior to 1969, when the first LaCoste & Romberg Model-D gravity meter was completed, a true "microgal" gravity instrument (microgravimeter) did not exist. The best meters previously available had a sensitivity of 10 µGal at best. The Model-D meter, however, has a sensitivity of about 1 to 2 µGal and can determine gravity differences over a traverse with a precision approaching 2 µGal, but the error in the determination of gravity differences along a traverse is probably about 5 µGal (Lambert and Beaumont, 1977; McConnell et al., 1974; Neumann, 1973b).* Many attempts to apply gravimetry to geotechnical and shallow structural problems have been disappointing in that the anomalies due to small structures of interest could not be extracted from the data, i.e., only anomalies due to very large or very shallow structures (or some fortuitous combination of the two factors) could be resolved. With a microgravimeter such as the Model-D, the prospect is much improved, since anomalies as much as an order of magnitude smaller than previously detectable should now be detectable on a practical basis.

Applications of Microgravimetry

3. The full scope of possible applications of microgravimetry is just beginning to be realized. For conventional site investigations, microgravimetry should be most effective for the detection of two- and three-dimensional anomalies or troublesome conditions such as bedrock surface irregularities, faults, fracture zones, cavities, and buried

---

* All comments concerning the LaCoste & Romberg Model-D meter in this report refer to the meter equipped with electronic readout. This option makes use of an eyepiece unnecessary during the course of a microgravimetric survey and increases the precision of the reading.

channels. A site with essentially uniform horizontal layering (one-dimensional features), on the other hand, would produce no gravity anom-alies, and the definition of the subsurface by geophysical surveys would require the application of other methods (such as seismic refraction and electrical resistivity methods). Thus, microgravimetry should be viewed as only one of the geophysical techniques available for adequate site definition. However, use of complementary geophysical methods at a site, accompanied by selective drilling, can still achieve the required site definition at considerably less cost than a comprehensive drilling program along.

4. In addition to site investigations, microgravimetry has other potential applications, some of which are perhaps not obvious:

<u>a</u>. Monitoring of seasonal groundwater level fluctuations and aquifer porosity estimations.

<u>b</u>. Detection of vertical tectonic movements and earthquake mechanism studies.

<u>c</u>. Monitoring crustal movements due to reservoir loading, underground fluid injection or withdrawal, etc.

<u>d</u>. Initial grout mass requirement estimation and monitoring grout intake and movement.

Usefulness of Gravity Gradients

5. The gravity method involves the measurement of the vertical component of the gravitational attraction at the surface. The measure-ment of the first vertical and horizontal derivatives (gradients) of the vertical component of the gravitational attraction can be of con-siderable fundamental and practical importance. Measurement of the gradients would offer two particular advantages over measurement of just gravity alone:

<u>a</u>. The gradient profiles have diagnostic properties that, in many cases, make subsurface structure identification more straightforward.

<u>b</u>. The gradients selectively filter out the effects of deeper-seated structures and enhance anomalies caused by shallow structures of interest in geotechnical investigations.

6

6. Practical field measurement of gravity gradients has not been feasible in the past due to poor gravimeter sensitivity and precision. The availability of microgravimeters should make practical field gravity gradient measurements realizable.

Previous Work and State of the Art

7. One of the first reported high-resolution gravity surveys was for chromite bodies in Cuba (Hammer, 1953; Hammer et al., 1945), where a probable instrument error of 20 µGal was reported and anomalies as small as 50 µGal were sought. This is typical of the state of the art through the mid-1960's. The use of gravity survey in ore prospecting is described in the text by Parasnis (1966). Detection of cavities (natural or man-made) represents one of the most often reported applications of detailed gravity investigations, with the earliest known report appearing in 1963 (Colley). Since that time, several reports have appeared on cavity detection by gravimetric methods (Arzi, 1975; Chico, 1964; Fajklewicz, 1976; Neumann, 1967, 1972, 1973b, 1974, 1977; Speed, 1970). High-resolution gravimetry has also been applied to geotechnical engineering problems, such as delineating fracture zones, estimating aquifer porosity, estimating depth to bedrock, delineating buried river channels, and verification of bedrock soundness (Arzi, 1975; Carmichael and Henry, 1977; Domenico, 1967; Eaton et al., 1964; Hall and Hajnal, 1962; Wolters, 1973), with varying degrees of success.

8. The term "micro-gravity" or "microgravimetry" first began to appear in the literature in the early 1970's (Boubakar, 1973; Cabrera, 1973; Neumann, 1972) and emphasizes that measurement accuracy, precision, and instrument sensitivity in the µGal range are required for certain applications of gravimetry. The term "nanogravimetry" has also been proposed (Lambert and Beaumont, 1977), emphasizing the fact that in SI units changes in gravity of as small as 10 nm/s^2 or 10^{-9} times the acceleration of gravity are of interest. However, as indicated earlier, the term microgravimetry as used herein also connotes the smaller scale of the survey. Correspondingly, there is a more rigorous demand placed on

the determination of station locations and elevations, as well as on data reduction techniques, facts which have not been adequately appreciated by some investigators.

9. The value of the direct measurement of profiles of the vertical gradient for delineation of geologic structures was recognized by Evjen (1936), but he concluded that fluctuations in the vertical gradient due to shallower irregularities would be too large and that existing gravity instruments did not have the required sensitivity and accuracy required for the measurements. These conclusions were partially valid in 1936; however, the availability of extremely sensitive "microgal" gravity meters within the past 10 years may make vertical gravity-gradient measurements utilizing tower structures with gravity measurements at two or more elevations feasible on a routine basis. Also, the mapping of shallow irregularities mentioned by Evjen has become a major objective of microgravimetry and vertical gradient measurements.

10. Practical measurement* of the vertical gradient presents considerable difficulties (Fajklewicz, 1976; Hammer and Anzoleaga, 1975; Janle et al., 1971; Neumann, 1973a; Thyssen-Bornemisza and Stackler, 1956; Thyssen-Bornemisza et al., 1972). Primarily, the problems reduce to two: (a) designing a stable platform or tower, which minimizes the effect of wind- or ground-motion-induced vibrations on the gravity meter; and (b) a tradeoff between keeping tower height small ($\sim$1 to 4 m) to allow practical field implementation, the need for greater separation to decrease the probable error of the difference between the two measurements, and the need to approximate the true gradient (Neumann, 1973a). Since measurement of the horizontal gradient just involves measurements on the surface, implementation of procedures such as proposed by Hammer and Anzoleaga (1975) involving measurements at the corners of a triangle or the double-track profiling concept of Thyssen-Bornemisza (1965) should pose no particular problems. The horizontal gradient measurements

---

* In this study, measurement of gravity gradients refers to making finite difference approximations to the true gradients by making g_z measurements at the surface and a distance above the surface (along the plumb line), using a tower or tripod structure, and then dividing by the vertical separation.

do require station spacings considerably smaller (3 to 100 m) than used
in standard gravity surveys; however, since such small station spacings
will be used routinely in microgravity surveys, the horizontal gradient
data will be readily available.

Purpose and Scope

11. The purpose of this project is to investigate the possible
applications of microgravimetric techniques to the broad range of geo-
technical problems of interest to the Corps of Engineers and to assess
the feasibility and desirability of developing complete in-house
capability for application of microgravimetry. Part II of this report
discusses pertinent aspects of the theory of gravity fields (potential
theory) and the concepts of regional and residual gravity fields.
Part III presents field procedures, corrections to the field data, and
requirements for data reduction and anomaly interpretation. Part IV
addresses the important question of the detectability limits of struc-
tures of interest. Part V considers the application of microgravimetry
to geotechnical site investigations, and Part VI presents the results of
a field study of gravity-gradient measurement techniques. Part VII
assesses the use of microgravimetric techniques for the detection of sur-
face elevation changes due to reservoir loading, underground fluid injec-
tion or withdrawal, and earthquakes. Part VIII discusses the use of the
microgravimeter as a tidal recording instrument and long-period vertical
seismometer, and Part IX presents the summary and conclusions.

PART II: ELEMENTS OF POTENTIAL THEORY

Gravitational Force Field

12. The gravitational potential field of the earth is due to the distribution of mass within the earth. Our knowledge of the potential field (U) comes from measurements of components, primarily the vertical component, of the gravitational force field ($\vec{g}$) on or above the surface of the earth. The field $\vec{g}$ is defined as the force $\vec{F}$ acting on a unit mass m at a point due to the mass distribution in the earth. The relation of the force field to the potential field is given by

$$\vec{g} = \frac{\vec{F}}{m} = \frac{\gamma M}{r^2} \left(\frac{\vec{r}}{r} \right) = -\nabla U(\vec{r}) \tag{1}$$

where

γ = universal gravitational constant*

M = mass of the earth

$\vec{r}$ = position vector from the center of the earth to the measuring point (with length r)

∇ = gradient operator**

The potential U is a function of position only, and the space derivatives of U in various directions give the components of $\vec{g}$ in those directions. For local problems, where the curvature of the earth can be neglected, a Cartesian coordinate system can be used. In particular,

$$g_z = \frac{\partial U}{\partial z} \tag{2}$$

gives the vertical component of the gravitational force field, where the

---

* $\gamma = 6.67 \times 10^{-11}$ m^3/kg-s^2.

** $\nabla = \hat{i}\frac{\partial}{\partial x} + \hat{j}\frac{\partial}{\partial y} + \hat{k}\frac{\partial}{\partial z}$ in Cartesian coordinates, where $\hat{i}$, $\hat{j}$, and $\hat{k}$ are unit vectors along x, y, and z directions.

z-axis at a point is taken as vertically downward. That $\vec{g}$ is derivable from a scalar potential implies that the gravity field is a conservative field and likewise that U is a harmonic function satisfying Laplace's equation in source-free (mass-free) space:

$$\nabla^2 U = 0*$$

(3)

The vertical component of gravity also satisfies Laplace's equation in source-free regions:

$$\nabla^2 g_z = 0$$

(4)

From Equations 2, 3, and 4:

$$\partial^2 U/\partial z^2 = \partial g_z/\partial z = -(\partial^2 U/\partial x^2 + \partial^2 U/\partial y^2)$$

(5)

and

$$\partial^3 U/\partial z^3 = \partial^2 g_z/\partial z^2 = -(\partial^2 g_z/\partial x^2 + \partial^2 g_z/\partial y^2)$$

(6)

Thus, it is seen that the vertical gravity gradient $(\partial g_z/\partial z)$ is equal to the second vertical derivative of the potential field. In the following text, the directional derivatives ("gradients") of g_z along the axes of a Cartesian coordinate system (z-axis vertically downward) are defined by the following notation:

$$g_{z,z} \equiv \frac{\partial^2 U}{\partial z^2} \; ; \; g_{z,x} = \frac{\partial^2 U}{\partial x \partial z} \; ; \; g_{z,y} = \frac{\partial^2 U}{\partial y \partial z}$$

(7)

---

* $\nabla^2 = \dfrac{\partial^2}{\partial x^2} + \dfrac{\partial^2}{\partial y^2} + \dfrac{\partial^2}{\partial z^2}$ in Cartesian coordinates.

Newtonian Potential and Consideration
of Simple Geometries

13. The Newtonian potential at a point $P(x,y,z)$ due to a generalized mass distribution with density $\rho(\epsilon,\eta,\zeta)$ in a volume ν is given by

$$U(x,y,z) = \gamma \int_\nu \frac{\rho(\epsilon,\eta,\zeta)}{r(x,y,z;\epsilon,\eta,\zeta)} \, d\nu \tag{8}$$

where the integration is over the volume ν, $r = \left[(\epsilon-x)^2+(\eta-y)^2+(\zeta-z)^2\right]^{1/2}$ is the distance from the mass element $d\nu(=d\epsilon d\eta d\zeta)$ at $Q(\epsilon,\eta,\zeta)$ to the point $P(x,y,z)$, and P is outside ν (Figure 1a). The vertical component of the gravitational attraction is then given by (dropping the arguments of ρ and r)

$$g_z = \frac{\partial U}{\partial z} = \gamma \int_\nu \frac{\rho(\zeta-z)}{r^3} \, d\nu \tag{9}$$

and the gravity gradients by the expressions

$$g_{z,x} = 3\gamma \int_\nu \frac{\rho(\zeta-z)(\epsilon-x)}{r^5} \, d\nu \tag{10}$$

$$g_{z,y} = 3\gamma \int_\nu \frac{\rho(\zeta-z(\eta-y)}{r^5} \, d\nu \tag{11}$$

$$g_{z,z} = \gamma \int_\nu \frac{\rho\left[2(\zeta-z)^2 - (\epsilon-x)^2 - (\eta-y)^2\right]}{r^5} d\nu \tag{12}$$

14. It is frequently possible to approximate many real geologic structures by models with simple geometries. The gravity fields of the

a. COORDINATE SYSTEM

b. GEOMETRY OF SPHERICAL MODEL

c. HORIZONTAL CYLINDRICAL MODEL GEOMETRY
MODEL GEOMETRY

d. TRUNCATED PLATE MODEL GEOMETRY

Figure 1.   Geometries of three simple models

13

models can be studied by applying Equations 9-12. For simple
three-dimensional models such as the sphere and two-dimensional models
such as the horizontal cylinder (infinite in length) and polygonal
cross-section models (infinite in length), the integrals 9-12 can be
evaluated easily in closed form.

15. Consider a homogeneous <u>sphere</u> of radius R and density ρ
in a massless half-space. Its center is at depth ζ, and the z-axis
passes through the center as shown in Figure 1b. For this case, Equations 9-12 reduce to

$$g_z = \frac{4}{3}\pi\gamma\rho R^3 \frac{\zeta}{(x^2 + \zeta^2)^{3/2}} \tag{13}$$

$$g_{z,x} = g_{z,y} = -\frac{4}{3}\pi\gamma\rho R^3 \frac{3x\zeta}{(x^2 + \zeta^2)^{5/2}} \tag{14}$$

$$g_{z,z} = \frac{4}{3}\pi\gamma\rho R^3 \frac{2\zeta^2 - x^2}{(x^2 + \zeta^2)^{5/2}} \tag{15}$$

for the points P on the x-axis. This solution is symmetric about the
z-axis.

16. A two-dimensional geometry is one with a constant cross
section and infinite extent in, for example, the y-direction. Figure 1c
illustrates the simplest of this type of model, a <u>horizontal cylinder</u>
with uniform density ρ, radius R, and axis perpendicular to and
passing through the z-axis at depth ζ. Equations 9-12 simplify to

$$g_z = 2\pi\gamma\rho R^2 \frac{\zeta}{x^2 + \zeta^2} \tag{16}$$

$$g_{z,x} = -2\pi\gamma\rho R^2 \frac{2x\zeta}{(x^2 + \zeta^2)^2} \tag{17}$$

$$g_{z,z} = 2\pi\gamma\rho R^2 \frac{\zeta^2 - x^2}{(x^2 + \zeta^2)^2} \qquad (18)$$

and $g_{z,y} = 0$, for points P on the x-axis.

17. Figure 1d illustrates a particular case of the class of two-dimensional models with a polygonal cross section: a __truncated__ __plate__ that extends to infinity in the positive x-direction as well as the positive and negative y-directions. For a uniform density ρ and slope angle α with respect to the horizontal, Equations 9-12 yield

$$g_z = 2\gamma\rho\left\{\zeta_2\phi_2 - \zeta_1\phi_1 - (C-x)\left[\sin^2\alpha \ \ell n\left(\frac{r_2}{r_1}\right)\right.\right.$$

$$\left.\left. + (\phi_2-\phi_1) \sin\alpha \cos\alpha\right]\right\} \qquad (19)$$

$$g_{z,x} = 2\gamma\rho\left[\sin^2\alpha \ \ell n\left(\frac{r_2}{r_1}\right)+ (\phi_2-\phi_1) \sin\alpha \cos\alpha\right] \qquad (20)$$

$$g_{z,z} = 2\gamma\rho\left[\sin\alpha \cos\alpha \ \ell n\left(\frac{r_2}{r_1}\right)- (\phi_2-\phi_1) \sin^2\alpha\right] \qquad (21)$$

for points P on the x-axis, where α , ϕ_1 , ϕ_2 , r_1 , r_2 , and C are defined in Figure 1d. Details of this derivation as well as many others of importance can be found in references such as Pick et al. (1973), Geldart et al. (1966), and Telford et al. (1976).

18. It is possible to __approximate__ many real subsurface struc-
tures with the three simple geometries (or some combination of the three) presented thus far. The discussion has considered only isolated models in massless space. In the real earth, the gravity field due to subsurface structures will be superimposed on the gravity field of the whole earth. For the case in which the earth is homogeneous with constant density (horizontally uniform) around the structure, it is more fitting to speak of the __density__ __contrast__ between the structure and the surrounding earth, and it is possible in principle to "subtract out" the contribution of the whole earth (the regional field) leaving just

15

the field due   structure (the residual or anomaly field). Similar-
ly, models used to approximate the structures can be assigned a density
contrast. This concept will be discussed later.

Relation Between Gravity Gradients for Two-Dimensional Problems

19. The gravity gradients are components of the same physical
field, and for simple geometries, unique relations exist between the
gradients. For two-dimensional problems such as illustrated in
Figures 1c and 1d, the gravity gradients on the boundary $z = 0$,
$g_{z,x}(x,0)$ and $g_{z,z}(x,0)$, are related by a Hilbert transform (Sneddon,
1972). That is,

$$g_{z,z}(x,0) = \frac{1}{\pi} \int_{-\infty}^{\infty} \frac{g_{z,x}(\zeta,0)}{\zeta - x} \, d\zeta \qquad (22)$$

where x is real (the profile point at which $g_{z,z}$ is to be calculated)
and the integral is to be interpreted in the sense of its Cauchy princi-
pal value.* The utility of this expression is that it allows the vert-
ical gradient to be calculated from horizontal gradient profiles or
conversely via the inverse transform. Thus, if it proves possible to
reliably determine horizontal gravity-gradient profiles in the field, the
vertical gradient profile can be obtained with requiring the use of a
tripod or tower in the field. A computer program has been written as
part of a companion project (see Preface) to numerically evaluate the
Hilbert transform for gravity data sampled at discrete intervals.

---

* I.e., the integral is interpreted in the sense

$$\lim_{a \to 0} \left[\int_{-\infty}^{x-a} + \int_{x+a}^{\infty} \right] \frac{g_{z,x}(\zeta,0)}{\zeta - x} \, d\zeta$$

16

20. Solution of problems or interpretation of data in gravi-
metry generally follows one of two approaches. The direct problem
involves specification or assumption of a geometry, size, depth of
burial, and density contrast and calculation of the gravity anomaly
caused by the model; such a solution is unique, i.e., there is no other
solution to the problem as posed (Equations 13-21 are examples of
solutions to the direct problem). The inverse problem involves deducing
or calculating the geometry, size, depth of burial, and density con-
trast from an observed gravity anomaly profile or contour plot. A solu-
tion to the inverse problem is inherently nonunique, i.e., there is
more than one possible structure that could produce the observed gravity
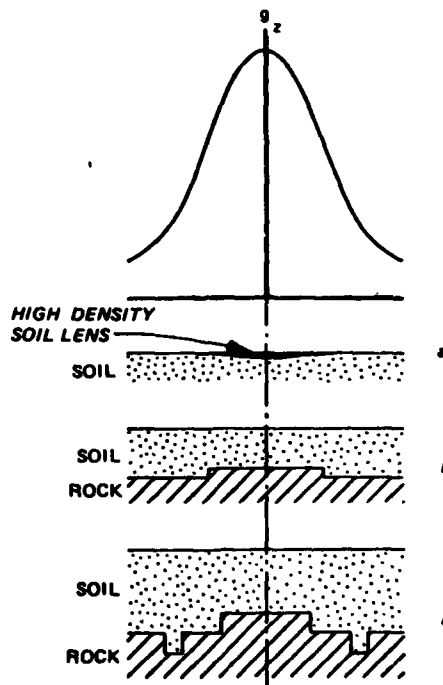anomaly (Figure 2).

Figure 2. Three hypothetical structures or density
distributions each producing the same gravity anomaly:
(a) surface or very shallow soil lens; (b) bedrock
high or ridge; (c) top of rock irregularities
beneath soil cover (Jung, 1961)

17

21. Utilization of solutions of the direct problem in gravimetry for the interpretation of observed gravity data is generally by iteration and comparison. The gravity profile plot or contour plot will sometimes suggest a class of possible structures responsible for the anomaly. For the class of possible structures, a model (geometry, size, depth of burial, and density contrast) will be selected that is generally consistent with the observed anomaly magnitude and width (wavelength).* The calculated gravity anomaly for the assumed model is then compared with the observed anomaly; the assumed parameters are then iteratively adjusted until a "good fit" is obtained. The result of this iterative calculation is one possible causative structure; however, other models can be postulated that will give an equally "good fit" to the observed data. All available information concerning geological conditions and structural style in the area and known subsurface conditions at the site should be used to constrain the iteration process and to guide the selection of a possible causative structure. In principle, sets of characteristic curves can be constructed similar to the familiar master resistivity depth sounding curves such that the observed gravity data can be quickly fitted to a curve for a given assumed geometry to yield size, depth of burial, and density contrast (Grant and West, 1965; Neumann, 1973c).

22. The general solution of the inverse problem of gravimetry is not only nonunique but very complex in nature. Two properties of a causative anomalous structure, however, can be readily deduced: (a) the location of the structure in plan, and (b) the mass excess or deficiency. Both of these properties are of considerable importance in geotechnical applications of microgravimetry. Frequently the location of an anomaly in plan is all that is really required, since the drilling option is readily available to verify and evaluate anomalies. The estimation of mass excess or deficiency due to an anomalous subsurface condition or structure is useful, for example, in grout mass requirement estimation, in verifying the effectiveness of a remedial

---

* The relation of anomaly magnitude and wavelength to the parameters describing a structure is discussed in Part IV.

18

grouting program, or in estimating in situ bulk densities of anomalous zones. Determination of depth to an anomalous structure is commonly approached via downward continuation* of the observed gravity field (Grant and West, 1965; Telford et al., 1976), although there are simple _maximum_ depth rules that will be discussed later. Oldenburg (1974) discusses the solution of the inverse gravity problem, but in general the subject is beyond the scope of this study.

Regional-Residual Field Separation

23. The gravitational field is linear, and hence the principle of superposition is valid. Thus, the gravitational field measured on the surface of the earth can be considered the simple sum of components caused by many mass sources having a wide range of spatial wavelengths. In practice, for most exploration applications, the measured field can be considered to be composed of a regional and a residual component. The regional field will have long spatial wavelengths and will presumably be caused by deep-seated structures in the earth (relative to the structures of interest). The residual field is just what is left after subtracting the regional field from the observed field, and presumably includes components caused by structures of interest in the exploration program. Clearly, the definition of what constitutes the residual and regional fields depends on the objectives and scale of the survey (Telford et al., 1976), i.e., the residual field in a petroleum exploration survey might correspond to the regional field in a survey for geotechnical engineering applications.

24. In a microgravimetric survey for geotechnical applications, the objectives are the detection and definition of shallow geologic structures. The shallow geologic structures will give rise to short wavelength (high spatial frequencies) anomalies. In contrast, the regional field will vary slowly in space (long wavelength) and can be

---

* Downward continuation is an analytical method of calculating values of the gravity field on a horizontal plane below the surface from the observed gravity field values on the surface.

approximated by a low order polynomial surface. For the common case
where the regional is approximately a simple inclined plane over the
survey area, the regional component can be determined by visual inspec-
tion of the gravity data. Even though the regional field in a micro-
gravimetric survey can often be determined by simple inspection,
automated procedures, such as ring and center-point methods (Nettleton,
1971; Telford et al., 1976) and polynomial surface fitting methods
(Coons et al., 1967; Nettleton, 1971), can be utilized, and the results
are usually comparable. The concepts of the regional-residual
separation process by the inspection or graphical method are illustrated
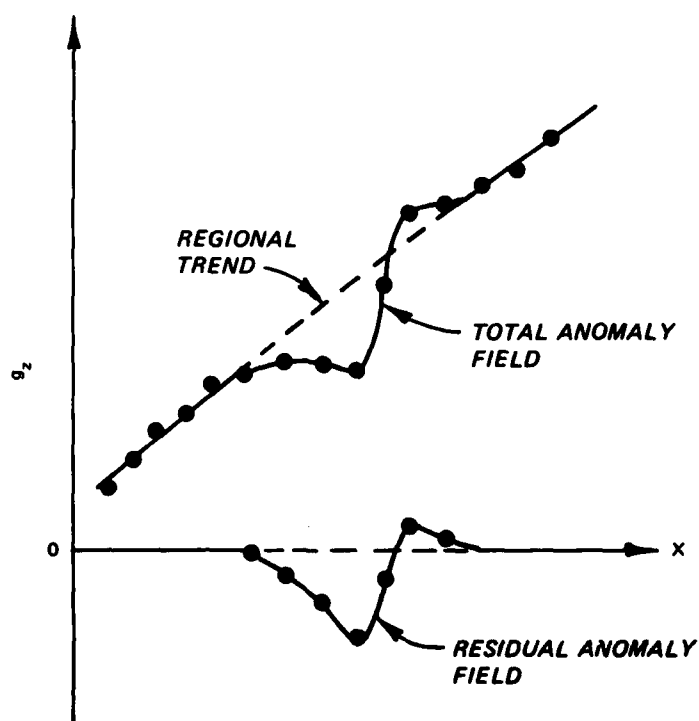in Figure 3.

Figure 3. Graphical method of regional-residual
separation

Mass Estimation and Maximum Depth Rules

25. From the residual gravity anomaly map, it is possible to compute the mass excess or deficiency causing a given gravity anomaly. For a rectangular grid of residual gravity values, with grid spacings Δx and Δy, the mass anomaly ΔM is given by

$$\Delta M = \frac{1}{2\pi\gamma} \sum_i \overline{\Delta g}_{zi} \, \Delta x \, \Delta y \tag{23}$$

where $\overline{\Delta g}_{zi}$ is the average gravity anomaly value in the ith rectangular grid element. Clearly the summation must be carried out to regions of the map where $\overline{\Delta g}_{zi} \to 0$ if the result is to be an accurate representation of the true ΔM. Details of the derivation of this equation are given in Telford et al. (1976).

26. If we assume some simple model and density contrast for a structure causing a residual gravity anomaly, it is usually possible to calculate the depth to the structure based on the assumption. Without making an assumption regarding the anomalous structure, however, the best that can be done is to estimate the maximum depth at which the structure could be located. Parasnis (1966) summarizes a number of these maximum depth rules, where the only assumption regarding the structure is that its density contrast must be either entirely negative* or entirely positive. If $\left(\Delta g_z\right)_{max}$ and $\left(\Delta g_{z,x}\right)_{max}$ are the maximum values of the residual gravity anomaly and the horizontal gravity gradient, respectively, the maximum depth d to the top of the anomalous structure is given by

$$d \lesssim \frac{0.86 \left(\Delta g_z\right)_{max}}{\left|\left(\Delta g_{z,x}\right)_{max}\right|} \tag{24}$$

---

* An air-filled cavity is an obvious example of a subsurface structure with a negative density contrast.

If the anomaly is apparently due to a two-dimensional structure, the numerical factor in Equation 24 can be replaced by 0.65. If the anomaly is only partially mapped, such that the maximum values cannot be reliably determined, then for any surface position (x,y)

$$d \lesssim \frac{1.50 \ \Delta g_z(x,y)}{|\Delta g_{z,x}(x,y)|} \tag{25}$$

Similarly, if the structure is apparently two-dimensional, the numerical factor in Equation 25 can be replaced by 1.00.

PART III: MICROGRAVIMETRIC SURVEYS -
REQUIREMENTS AND PROCEDURES

Gravity Meter Sensitivity, Accuracy, and Precision

27. The sensitivity, accuracy, and precision of the LaCoste &
Romberg Model-D "Microgal" gravimeter was discussed in Part I. For
purposes of this study, accuracy refers to the closeness of a measured
value to the "actual" or "real" value of the physical quantity, whereas
the term precision refers to the closeness with which a series of
measurements of the same thing agree with one another. Thus, accuracy
includes precision, but the converse is not necessarily true. That is,
an accurate instrument must necessarily be precise, but a precise
instrument is not necessarily accurate. Accuracy depends on all the
random, systematic, and accidental errors that can affect a measurement.
Thus, the possible error is a measure of the accuracy. Sensitivity
refers to the detectability limit or threshold of an instrument, i.e.,
the smallest change in a quantity that can be detected by an instru-
ment. For example, the LaCoste & Romberg Model-D "Microgal" gravity
meter has the smallest divisions of approximately 1 µGal size such that
the g_z value can be estimated to a fraction of 1 µGal; the sensi-
tivity is, however, more than likely between 1 and 2 µGal. The preci-
sion of a carefully repeated set of measurements with the "microgal"
meter equipped with electronic readout is 2 µGal; the accuracy of the
instrument for a single relative measurement of gravity under ideal
operating conditions is considered to be $\pm$ 2 µGal (McConnell et al.,
1974; Neumann, 1973b). Under field conditions involving transport,
long time periods, and large gravity ranges, the accuracy and precision
might reasonably be expected to lie in the range of 3 to 6 µGal. As
is well known, measures of the precision of a set of measurements, such
as the "mean square error of the arithmetic mean," decrease with the
number of measurements. Further, if it can be demonstrated that varia-
tions of the gravimeter readings are normally distributed, then the
arithmetic mean is an unbiased estimator of the actual value, and it is

23

possible to make probability statements on the actual value. Torge (1971), for example, showed that measurements with two LaCoste & Romberg meters appeared to be normally distributed. Thus, even though measures of the precision of a group of measurements can be reduced well below the probable error or accuracy of a single measurement, it does not necessarily imply that measurement accuracy has been correspondingly improved.

28. In any event, gravity anomalies with magnitudes in the 5-to 10-µGal range should be detectable with the Model-D gravimeter (using carefully repeated measurements and averaging to improve the signal-to-noise ratio), while an anomaly ≥ 10 µGal should be routinely detectable. Use of the Model-D gravimeter with electronic readout is considered essential for the general success of a microgravimetric program. Other standard gravimeters, such as the LaCoste & Romberg Model G and the Worden Master, can be used for microgravimetric surveys, but the minimum detectable anomalies would be larger by a factor of 5 to 10. For the comparison, the LaCoste & Romberg Model-G, equipped with electronic readout, is capable of anomaly detection in the 20-to 30-µGal range, and the survey reported by Hammer et al. (1945) using the Gulf gravimeter illustrated a 50-µGal anomaly over a known ore body with an instrument accuracy and precision estimated at about 20 µGal.

Field Procedures

29. Microgravimetric surveys are of two types: (a) profile surveys, where gravity measurements are made along a profile line that is generally perpendicular to the presumed strike of a linear-type subsurface structure, such as a fault, anticline/syncline, and buried river channel; and (b) areal grid surveys, where gravity measurements are made at stations on a grid over an area. Station locations and relative elevations must be determined by a site-leveling survey; requirements for this topographic survey will be discussed later. The field procedures used for the surveys are dictated by considerations of survey objectives and subsequent corrections which must be made to the

measured data. The measurements in a microgravity survey are normally made relative to a local reference station, and there is usually no attempt to tie the values to an absolute gravity determination. When the regional-residual separation is made, each gravity measurement will be positive or negative relative to the regional gravity field.

30. In microgravimetric surveys, the quality of each individual measurement is of utmost importance. The meter must be handled carefully, and the reading procedure standardized. The general sequence for obtaining a measurement is as follows:

<u>a</u>. Place baseplate over or immediately beside the station survey marker and approximately level the baseplate.

<u>b</u>. Place gravity meter on baseplate and very carefully and accurately level the instrument (avoid direct sunlight on the top of the meter).

<u>c</u>. Unclamp the gravity meter and carefully make measurement, always making the final approach to null or the reading line from the same direction to avoid backlash.

<u>d</u>. Recheck level bubbles prior to recording meter reading.

There is not a <u>best</u> method for placing the baseplate on the ground surface and making the instrument level adjustment, but whatever procedure is followed, the elevation of the sensitive element of the gravimeter above the surveyed surface point should <u>either</u> remain essentially constant during the gravity survey or be measured to the same or better accuracy as required for the topographic survey (Figure 4). The data that must be recorded for each gravity station are: (a) station location, (b) station elevation, (c) instrument height above survey point, (d) meter reading, (e) time of reading, and (f) general comments regarding the "noise" affecting the reading and the surroundings of the station.

31. For a microgravimetric survey of a relatively small site (0.25 km^2 or less), generally one station will be designated as the <u>base</u> <u>station</u>. The base station gravity reading will be obtained at the beginning and end of each work day, before and after "breaks" in the survey, and at least once each hour (on the average) during the course of the survey. The multiple measurements at the base station are used
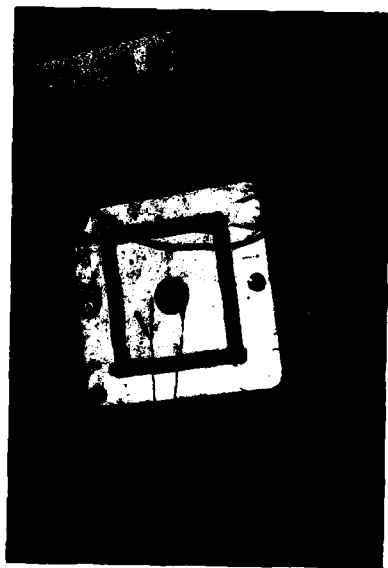
a. Flat leveling baseplate in place over survey marker
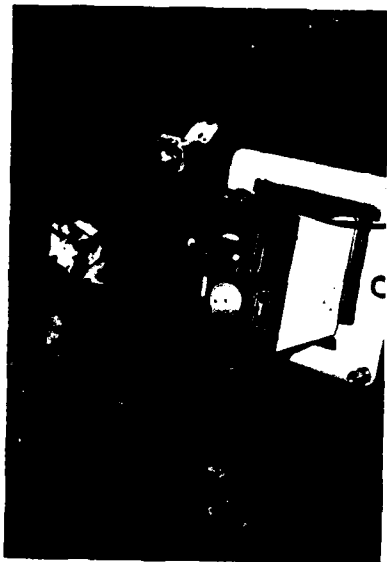
b. Model-D gravimeter in place on flat baseplate
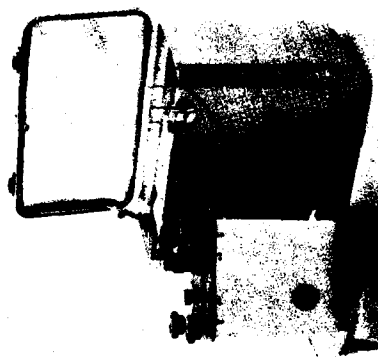
c. Model-D gravimeter in place on concave leveling baseplate

Figure 4. Gravimeter baseplates

26

to correct for changes in gravity with time at the site and for drift in the gravity meter itself. A base station gravity measurement should be a high-quality determination. A good procedure is to make two or three readings for each base station occupation within a 5- to 10-min period and require agreement to better them 10 µGal for the set of readings (except during periods of rapid earth tide change,* the readings should agree to within 5 µGal). Following this procedure will also ensure that the dependence on clamp history,** which can be significant for some gravity meters, does not introduce unacceptable errors. During routine station occupation and measurement (sequential clamping for transport and unclamping for measurement) with no more than a 15-min cycle time, no special procedures related to the clamp history need be considered. However, anytime the meter is left clamped or unclamped for an extended period of time, the base station should be reoccupied and the above procedure followed to obtain a sequence of three measurements agreeing within 10 µGal.

32. Stations occupied between two successive base station occupations make up a _program_. Programs should be planned to minimize the distance between the last station and the base station if possible; and _long_ in-line programs should be avoided (short looping or "zigzag" programs are preferable). A program should include approximately 20 percent reoccupation of stations occupied during previous programs. After correction for drift, reoccupied station measurements should agree with each other to within 5 µGal, or a third measurement should be made during a subsequent program. The occurrence of either of the following necessitates a return to the base station: (a) accidental exposure of the level bubbles to direct sunlight, or (b) rough handling of the gravity meter such as knocking it over or dropping it. Following the base

---

* Changing gravitational attraction due to changing relative positions of the earth and moon is discussed in Part VIII.
** Gravimeters have clamping devices to protect delicate components from damage during transport. Some gravimeters exhibit an observable dependence on clamp history, e.g., the readings will vary (recover) for several minutes during first use after being clamped overnight.

station reoccupation as suggested, the last occupied station should also be reoccupied prior to continuing the program.

Normal Gravity Variations and Data Corrections

33. The gravitational attraction on the earth's surface varies because of location, elevation, and time in addition to variations caused by subsurface geology. These normal variations in gravity and the procedures for correcting gravity field data for the variations are discussed thoroughly in standard references, such as Grant and West (1965), Pick et al. (1973), and Telford et al. (1976). Thus, discussion of data corrections will be brief, with elaboration only of points of particular relevance to microgravimetric surveys. Certain aspects of the data correction process for microgravimetric surveys are simpler than those for larger scale gravity surveys, while some aspects require greater care and accuracy.

34. Corrections to gravity survey data are required in order to compensate for normal gravity variations over the survey area and over the time span required for the survey. In this manner, the corrected gravity values presumably are due solely to the subsurface geologic structure of interest plus "regional components." Normal gravity variations and compensating corrections are discussed below:

    a. Meter factor. The meter factor is the value that converts the meter readings to values in mGal. For the Model-D, a single value can be used over the complete 200-mGal range. While not a correction as such, conversion to mGal values is the first step in data processing.

    b. Corrections for time variations. Gravity values over the survey area will change with time because of the gravity tide and instrument drift. The usual procedure for accomplishing this correction is to reoccupy a base station frequently. Then, by assuming that gravity values at all stations in the survey area vary in the same manner as the base station, both tidal and drift effects can be corrected. This is a good assumption for microgravity surveys. Figure 5 illustrates a drift curve. Between occupations of the base station, linear drift is assumed. The correction is used to compensate for the drift at each station at the time of the station measurement. Thus, if the gravity value is increasing at the

28
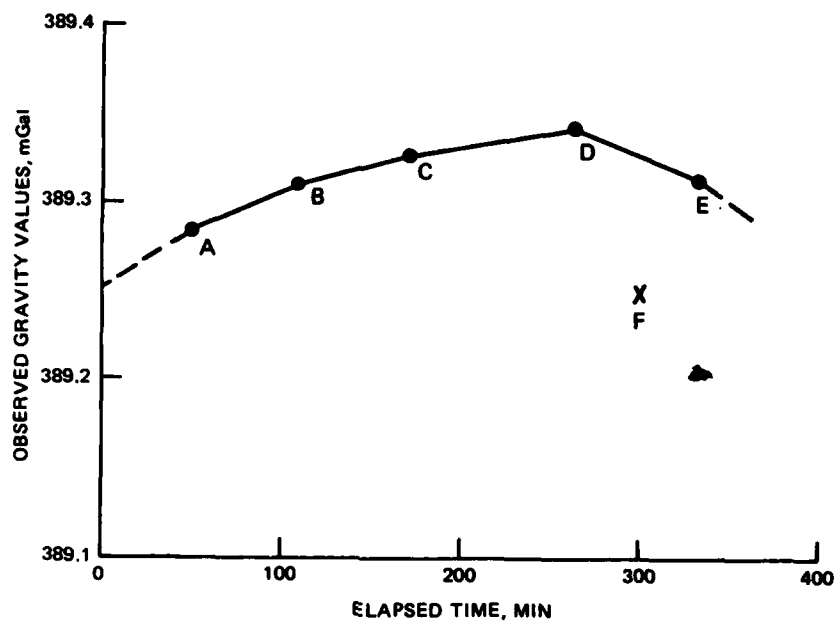
a. DRIFT CURVE FOR PORTION OF MICROGRAVITY SURVEY.
   INCLUDES INSTRUMENT DRIFT AND TIDAL VARIATION.

DRIFT RATES

SEGMENT	R(μGal /MIN)
AB	0.43
BC	0.30
CD	0.18
DE	-0.44

DRIFT CORRECTION FOR STATION F

STATION	TIME, MIN	FIELD READING, mGal	DRIFT CORRECTED READING, g_{obs}, mGal
D (BASE)	263	389.344	400.000
F	300	389.250	399.922*
E (BASE)	334	389.313	400.000

$$*g(F)_{obs} = (400.00 - 389.344) + 389.250 - R_{DE}\Delta T$$
$$= 399.906 - (-0.00044) (37)$$
$$= 399.922 \text{ mGal}$$

b. EXAMPLE DRIFT CORRECTION PROCEDURE.

Figure 5.   Field base station drift curve and drift
            correction procedure

base station, the correction is subtracted from the station gravity value. Figure 5 also shows the procedure for making the correction for a typical case. Note that a reference value of 400.000 mGal is used for the base station in the sample drift correction in Figure 5; the first reading taken at the base station on the first day of the survey, for example, could also be used for the reference value. This example illustrates the relative nature of the values measured during a microgravity survey. It is desirable to produce a theoretical tidal curve (Longman, 1959) for the survey site in order to have an idea of the magnitude and rate of variation to be expected at the site during the survey period. The use of theoretical tidal curves and gravity meter recorded tidal curves is illustrated in Part V. Observed gravity values corrected for drift will be denoted g_{zobs}.

c. <u>Latitude correction</u>. Gravity on the geoid (sea level equipotential surface) varies with geocentric latitude (ϕ), according to the 1967 Geodetic Reference System formula:

$$g_z(\phi) = 978.01385(1 + 0.005278895 \sin^2 \phi$$
$$- 0.000023462 \sin^4 \phi) \qquad (26)$$

This equation accounts for the spheroidal shape (flattened at the poles) of the geoid and centrifugal acceleration. For microgravimetric surveys, it is usually sufficient to assign a reference latitude to the base station and then to use the following formula to compute latitude corrections for all other stations:

$$\Delta g_{zL} = \pm 0.81 \cdot \sin 2\phi \cdot \Delta L \ \mu Gal \qquad (27)$$

where ΔL is the north-south distance in metres from the base or reference station, and ϕ is the reference latitude. The positive sign is used if the station value to be corrected is south of the base station, and the negative sign is used if the station value to be corrected is north of the base station.

d. <u>Free air correction</u>. Two corrections are necessary to account for elevation differences between stations in a microgravity survey. The free air correction compensates for the fact that the gravitational attraction varies because of changing distance from the center of the earth. The <u>normal</u> free air vertical gravity gradient

(0.30855 mGal/m) is essentially constant and can be used for all stations in a microgravity survey. Since the results of a microgravity survey are entirely relative, any reference elevation (the elevation of the base station or even the geoidal or zero mean sea level elevation) can be used and only station elevations relative to this reference elevation are needed. The free air correction formula is

$$\Delta g_{zFA} = \pm 308.55 \ \Delta h \ \mu Gal \qquad (28)$$

where Δh is the difference in elevation in metres between the station to be corrected and the reference elevation; the positive sign is to be used if the station is higher in elevation than the reference elevation, and vice versa.

e. <u>Bouguer correction</u>. The Bouguer correction is an elevation correction which compensates for the fact that gravity values in a survey are affected by differing masses of material beneath the stations due solely to elevation variations. For the Bouguer correction a reference elevation is chosen (preferably the same as used for the free air correction), and the material between the ground surface at each station and the reference elevation is approximated by an infinite horizontal slab with density equal to that of the material beneath the station. The correction is calculated using the Bouguer slab formula:

$$\Delta g_{zB} = \mp 41.91 \ \rho \Delta h \ \mu Gal \qquad (29)$$

where ρ is the slab density in g/cm^3, and Δh is the elevation difference in metres between the station to be corrected and the reference elevation. The negative sign is used if the station is above the reference elevation, and vice versa. The appropriate density for the Bouguer correction in a microgravity survey can frequently be determined by direct density measurement.

f. <u>Terrain correction</u>. The Bouguer correction does not compensate for the effects on a station gravity value due to topographic variations within and around the microgravity survey site. To compensate for the reduced gravity values at stations due to either "hills" or "valleys" in the vicinity, terrain corrections must be

31

determined and added to the station gravity values.*
For a microgravity survey, the correction for terrain effects within 50 m of a station can be significant and must be carefully considered. The effects due to more distant terrain features (∿1 km or more distant), while possibly quite large in magnitude (caused by large mountains or valleys), will influence each station value in a small-scale microgravity survey to an equal extent; hence, since the gravity values are all relative, these more distant terrain feature corrections need not be considered. A terrain template (Figure 6) is used to determine the terrain correction for microgravity survey results. The template is centered on a gravity station location on a site topographic map (template drawn to the same scale as the map), and the average elevation difference (relative to the station) <u>irrespective of sign</u> is determined for each compartment in the template. Then for these elevation differences, the terrain corrections can be determined from the curves for each compartment in Figure 7. Note that Figure 7 is for a terrain density of 2.00 g/cm^3; for other terrain densities, the values can be proportionately adjusted. The total terrain correction Δg_{zT} for the gravity station is the sum of the corrections for all compartments. This procedure is repeated for each gravity station location. With suitably digitized elevation values over the survey site, the terrain correction calculations can be performed by a computer program.

g. <u>Bouguer anomaly</u>. When the observed gravity value at a station is corrected as described in <u>a</u> through <u>f</u> above, the result is called the Bouguer anomaly for the station. The Bouguer anomaly g_{zB} can be expressed as

$$g_{zB} = g_{zobs} + \Delta g_{zLC} + \Delta g_{zFAC} + \Delta g_{zBC} + \Delta g_{zTC}$$

$$= g_{zobs} \pm 0.81 \cdot \sin 2\phi \cdot \Delta L \pm 308.55 \, \Delta h \qquad (30)$$

$$\mp 41.91 \, \rho \Delta h + \Delta g_{zTC}$$

---

* <u>Compensation</u> for the effect on the gravitational attraction at a station due to nearby "hills" and "valleys" is accomplished by <u>adding</u> a terrain correction in both cases. This can be visualized by considering the "hill" as a positive mass and the "valley" as a "negative" mass, both of which decrease the gravitational attraction at the station compared with the value it would have if the "hill" and "valley" were not present.
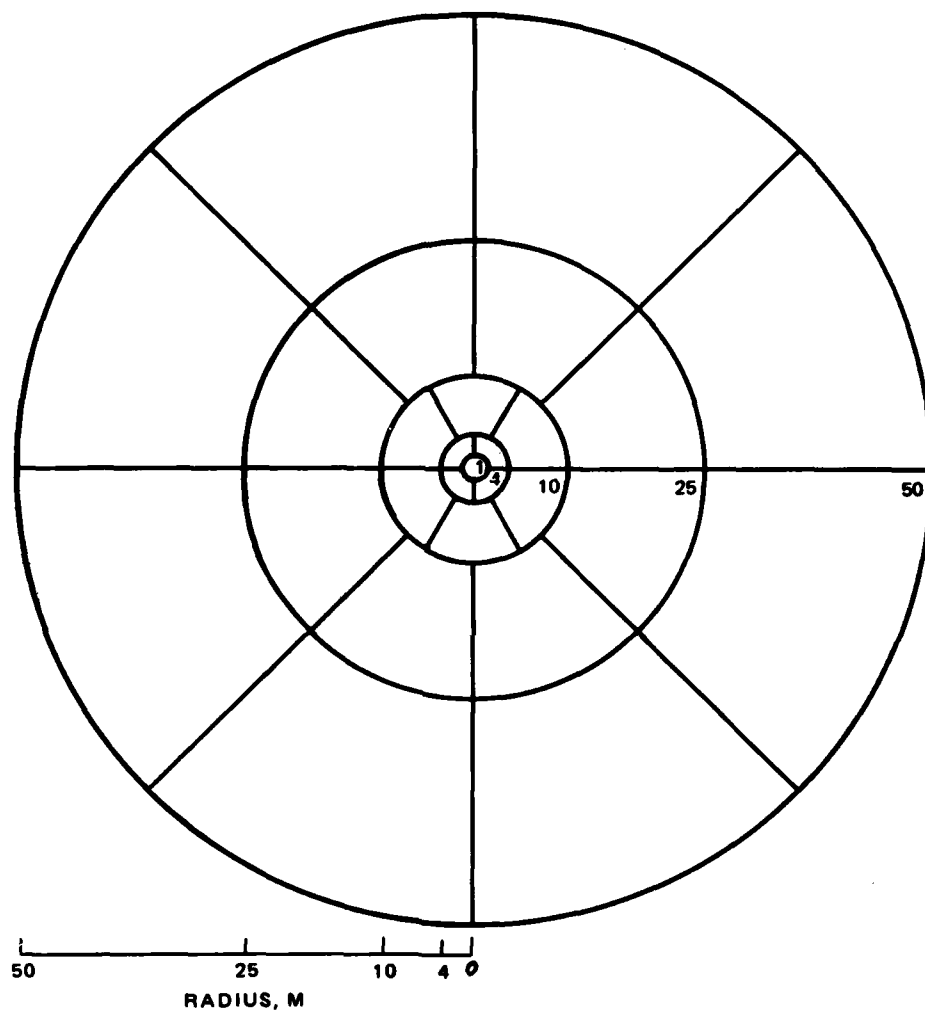
RADIUS, M

Figure 6.   Terrain correction template (0 to 50 m) for microgravity
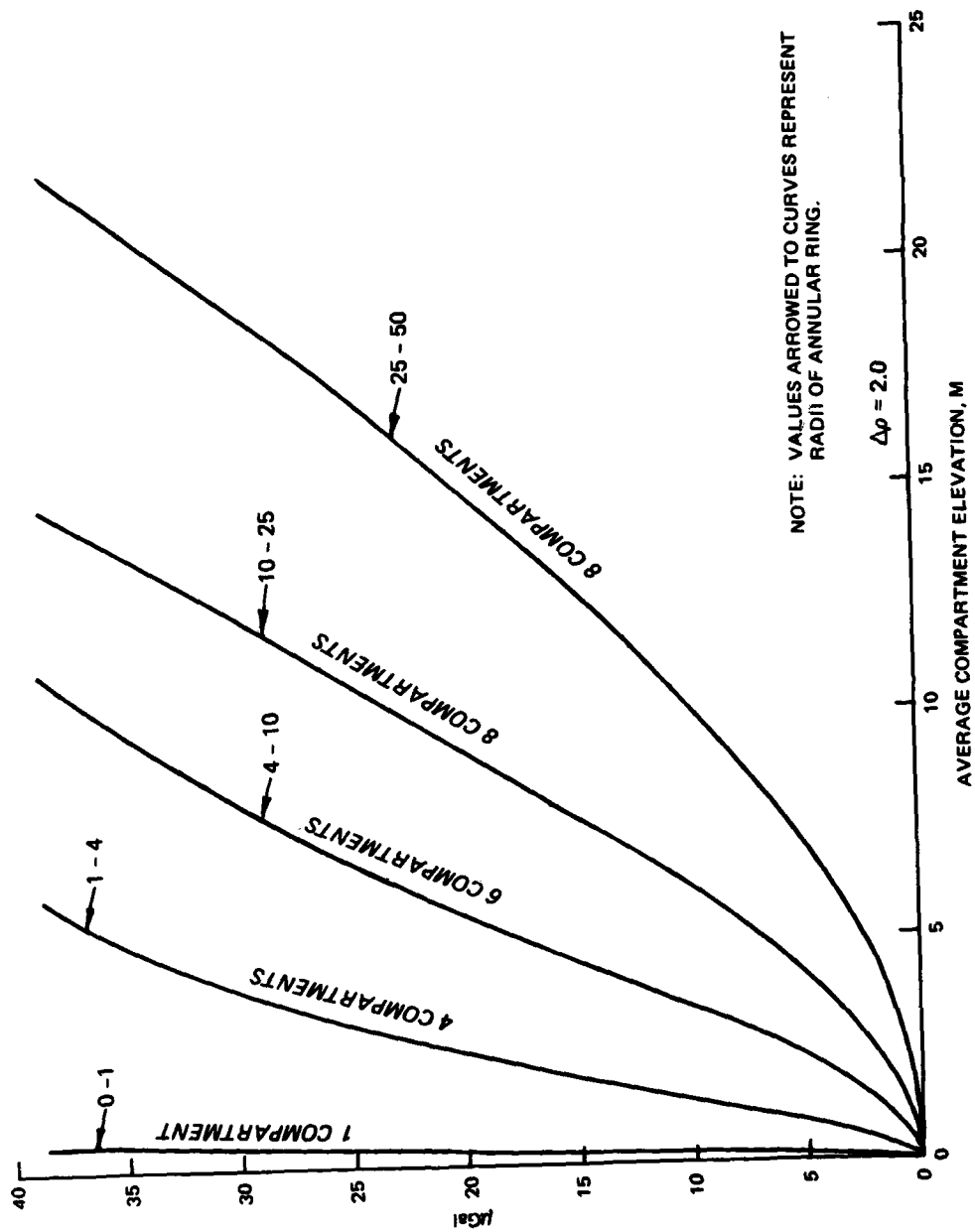surveys (drawn to same scale as site topographic map)

Figure 7. Terrain correction curves for template in Figure 6

34

The selection of signs for the correction terms is
described in a through f above. Anomaly values deter-
mined by Equation 30 are still completely relative. A
Bouguer anomaly contour map of the site can now be
examined to determine the regional field component g_{zR}
by the methods presented in Part II. Sometimes, for a
microgravity survey, the surveyed area is too small to
allow the regional component to be determined, or the
regional component can properly be assumed to be a
constant over the area; in this case, a reference station
value (commonly the base station value) will be selected
and is also denoted g_{zR} . If the regional or reference
gravity value is then subtracted from each Bouguer
anomaly value,

$$\Delta g_z = g_{zB} - g_{zR} \qquad (31)$$

the result Δg_z is called the residual Bouguer gravity
anomaly or simply the residual anomaly.

Accuracy Requirements

35. Equations 27-30 allow requirements for survey accuracy to be
stated concerning a desired maximum error level for the results. As
stated previously, under field conditions the precision and accuracy of
a set of microgravity measurements can be expected to be in the range
of 3 to 6 µGal. Since the definition of gravity anomalies in the 5-to
10-µGal range is desired, it is necessary that errors introduced by the
gravity data corrections be kept well below these ranges of values.

36. Errors in determination of relative north-south distances in
a site survey can introduce errors in corrected gravity values. From
Equation 27, it can be seen that determination of relative north-south
distances to within 1 m or better will keep errors in the latitute cor-
rection well below 1 µGal, and this certainly does not place stringent
requirement at all on determining station locations. If relative eleva-
tions over the site are determined to an accuracy of ± 0.3 cm (± 0.01 ft),
errors in the free air correction (Equation 28) will be less than
± 1 µGal. For a given value of density ρ , the errors introduced in the

Bouguer corrections (Equation 29) by errors in Δh are much less than for the free air correction. If the Bouguer slab density is estimated or determined within ± 0.02 g/cm^3, errors in the Bouguer correction will be less than ± 1 µGal. The error in the Bouguer correction due to the product $\rho \Delta h$ (which depends not only on the individual errors but also on the absolute values of ρ and Δh) should be of the order of ± 1 µGal or less if ρ is determined within ± 0.02 g/cm^3 and Δh is determined within ± 0.3 cm. Note in Figure 7 that possible errors due to the terrain correction can be significant for the inner template zone (0-1 m radius about station); however, it is usually possible to select station locations which are relatively level or even to "hand level" for a 1-m distance about the station. If this is possible, and for the type site elevation surveys discussed above (to accuracy of ± 0.003 m on a 3- to 6-m grid), the errors introduced by the terrain correction (or lack thereof) should easily be kept less than ± 5 µGal and an error level of ± 1 µGal should be achievable with extreme care. If the error levels mentioned above are achieved (i.e., probable error introduced in Equation 30 by the readings and their corrections kept below ± 5 µGal), then anomalies in the 5-to 10-µGal range should be detectable.

Corrections to Vertical Gradient Measurements

37. Since the determination of the vertical gravity gradient involves the difference in two values of the vertical component of gravity with only a vertical separation, the required corrections to the field data are minimized. Further, since it is possible to make the vertical gradient determination in a time span of about 5 to 10 min, consideration of instrument drift and tidal gravity variation is not necessary. The only required correction is for topography in the vicinity of the station. Procedures for making the topography or terrain correction are similar to standard techniques in gravity surveying except that two stations separated by Δz must be considered for each vertical gradient topographic correction. Details of the topographic correction procedure are discussed by Fajklewicz (1976) and Janle et al. (1971). Although

36

the topographic correction is all that is required for the vertical gradient measurement, it is important to note that the g_z measurements at the bottom stations give a standard gravity survey (which would require all the standard corrections). There is considerable value and advantage in having simultaneously-determined gravity and vertical gradient values (Thyssen-Bornemisza et al., 1972).

PART IV: DETECTABILITY CONSIDERATIONS FOR SIMPLE STRUCTURES

Concepts of Detectability and Resolution

38. In consideration of any geophysical exploration method, questions regarding the detectability and resolution limits of the method inevitably arise. From a cursory examination of Equations 13-21 for a given structure model, the gravity anomaly produced by the structure will depend jointly on size, depth of burial, and density contrast. Thus, the general procedure for establishing detectability limits is to examine the gravity anomalies produced by typical idealized models for a wide range of sizes, depths of burial, and density contrasts. Then, considering survey procedures and gravimeter sensitivity, accuracy, and precision, detectability thresholds can be assigned such that for a given model all combinations of parameters resulting in a gravity value above the threshold can, in principle, be detected gravimetrically.

39. For more than one subsurface structure in the same vicinity, the question of resolution must be addressed. That is, for certain combinations of depths and separations of the structures, separate gravity anomalies will not be observed, but the individual gravity anomalies will superpose to present a total anomaly, which may give no hint as to the multiple sources. The problem of multiple-structure resolution can be illustrated by simple examples. Consider the problem of the resolution of two horizontal cylinders by a gravity survey, as illustrated in Figure 8a. The gravity anomaly along the surface can be expressed (using Equation 16)

$$\Delta g_z(x) = 2\pi\gamma\Delta\rho R^2 \left[\frac{z_o}{\left(x - \frac{d}{2}\right)^2 + \left(z_o\right)^2} + \frac{z_o}{\left(x + \frac{d}{2}\right)^2 + \left(z_o\right)^2} \right] \qquad (32)$$

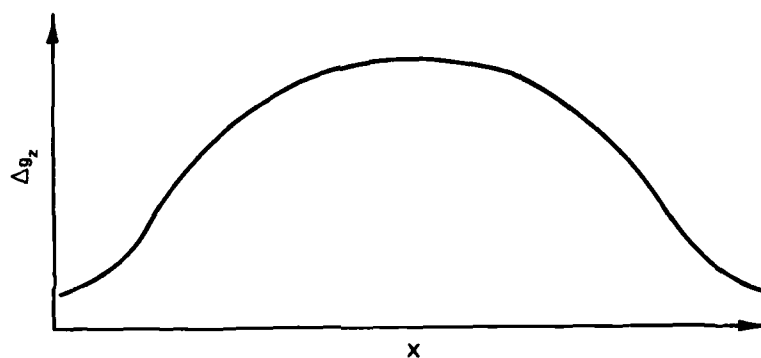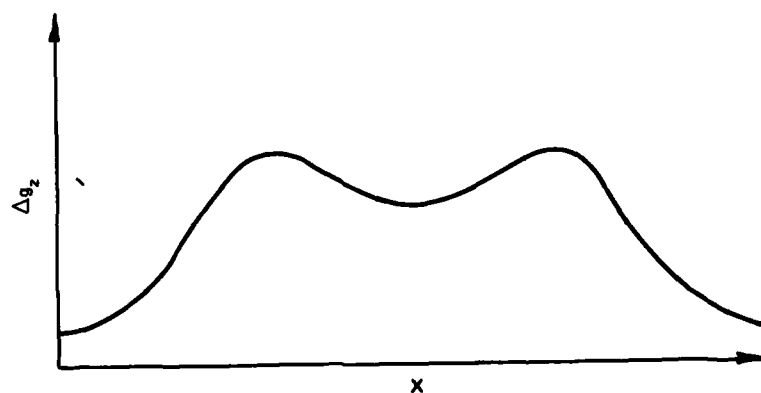where

Δρ = density contrast of the cylinders

R = radius of the cylinders

38
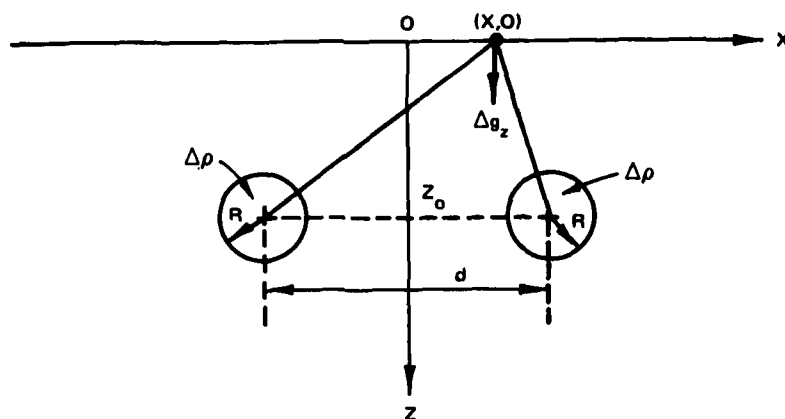
a. GEOMETRY FOR DISCUSSION OF RESOLUTION OF TWO HORIZONTAL
CYLINDRICAL STRUCTURES BY A GRAVITY SURVEY.

b. STRUCTURES NOT RESOLVED BY GRAVITY SURVEY.

c. TWO STRUCTURES RESOLVED BY GRAVITY SURVEY.

Figure 8.   Structural resolution by gravity surveys

39

z_o = depth to the centers of the cylinders

d = separation of the centers

x = position along the surface

If the gravity anomaly profile is like Figure 8b, the structures are not resolved; whereas if the profile is like Figure 8c, the structures are said to be resolved. Examination of the second partial derivatives of Equation 32 with respect to z_o and d results in the following reciprocal relations for theoretical resolution of the structures:

$$d_{minimum} = \frac{2}{\sqrt{3}} z_o \tag{33}$$

$$z_{o_{maximum}} = \frac{\sqrt{3}}{2} d \tag{34}$$

where $d_{minimum}$ is the minimum separation for which the two structures are just resolved for a given depth z_o , and $z_{o_{maximum}}$ is the maximum depth for which the structures can just be resolved for a given separation d .

40. In a similar manner, the question of resolution of the two structures can be examined for the case of a vertical gradient survey using Equation 18. For the vertical gradient survey, the reciprocal relations are

$$z_{o_{maximum}}' = \frac{\sqrt{3 + \sqrt{8}}}{2} d' \tag{35}$$

$$d'_{minimum} = \frac{2}{\sqrt{3 + \sqrt{8}}} z_o' \tag{36}$$

40

where $z_o'_{maximum}$ and $d'_{minimum}$ are the maximum depth and minimum separation, respectively, for which the structures can just be resolved. A comparison of Equations 34 and 35 shows that for a given separation of the two structures the maximum depth for theoretical resolution is about 39 percent greater for the case of the vertical gradient survey. Similarly, the minimum separation, for a given depth, for theoretical resolution is about 28 percent less for the case of the vertical gradient survey. Therefore, vertical gradient surveys offer definite advantages in resolving anomalies due to multiple structures.

41. Figure 9 illustrates structural resolution for a specific case for both gravity anomaly and vertical gradient* profiles. The structures in this case are spheres with centers at a depth of 5 m, and curves are shown for structure separations of 5 and 7.5 m. Each sphere is assumed to cause a 50-μGal gravity anomaly by itself. Figure 9a for the gravity anomaly profiles indicates theoretical resolution only for the larger structure separation, while Figure 9b for the vertical gradient profiles indicates theoretical resolution for both structure separations. It is emphasized that these conclusions are for theoretical resolutions. If more realistic conditions are considered, practical resolution would probably be achieved only for the vertical gradient survey over the structures with the larger separation.

Detectability Thresholds

42. On the basis of the discussion of sensitivity, accuracy, precision, and errors in Part III, a probable measurement error of 5 μGal seems reasonable, and this would define a background noise level.** To

---

* The unit for the gravity gradients is the Eötvos (E), where 1E = 0.1 μGal/m.
** This background noise level does not include the "lithological noise" component, which is completely site-dependent. Lithological noise is here defined as gravity variations due to very shallow, erratic density variations (usually in soil) at a site.
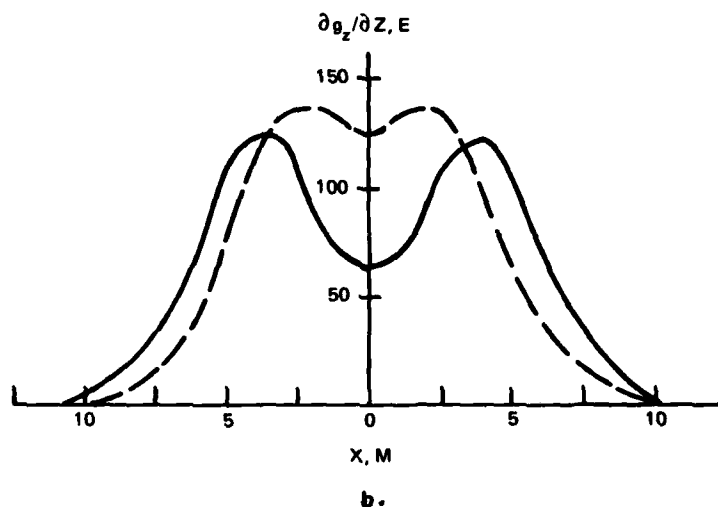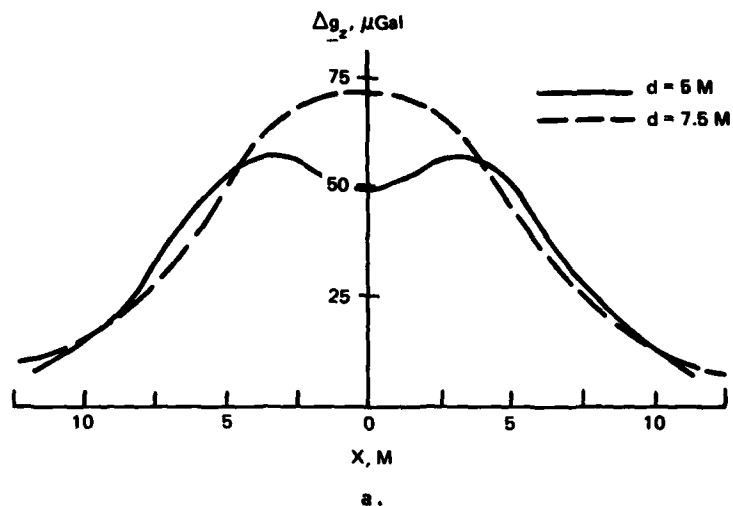
Figure 9. Comparison of Δg_z and $\partial g_z / \partial z$ for
two spheres buried at depth $z_0 = 5$ m and separated
by distances of 5 and 7.5 m (center-to-center
distance). Each sphere represents a maximum
gravity anomaly of 50 μGal

be detected, a gravity anomaly would have to be greater than this noise
level. Thus, assigning a detectability threshold of 10 μGal for anomaly
detection by microgravity surveys should be sufficiently conservative.
Due to the nature of the proposed vertical gradient measurement process,

i.e., a rapid "up and down" measurement sequence between a surface station and a station Δz vertically above it, the only corrections necessary are for nearby topography. Thus, the probable error for a Δg_z determined in this manner should be close to the accuracy for a single measurement, 2 μGal (Neumann, 1973a); for a Δz of 2 m, this corresponds to 10 E.* Using a similar criterion as for the gravity survey, the detectability threshold for a vertical gradient survey is taken as 20 E. The same threshold (20 E) will be used for any considerations of horizontal gradient surveys.

Gravity Anomalies of Simple Structures and Detectability
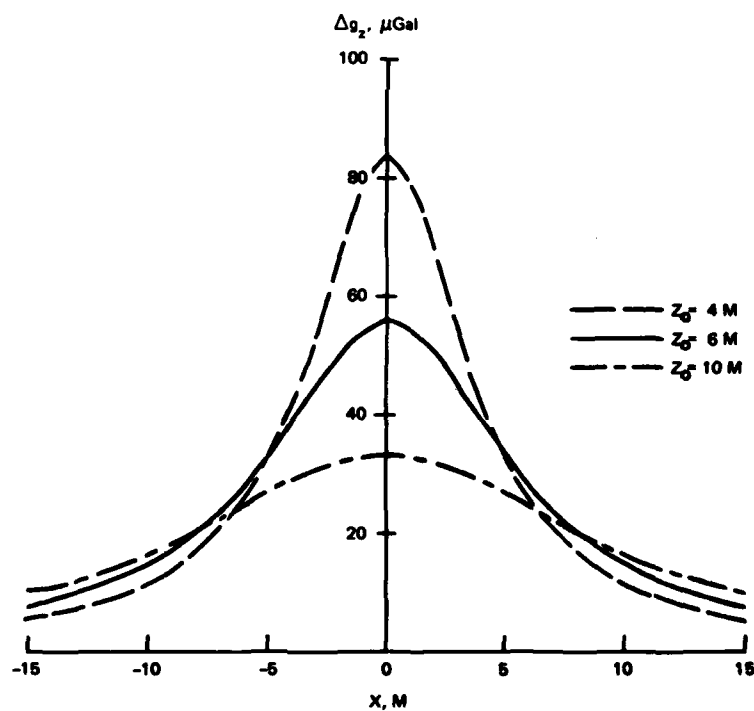
Typical anomaly profiles

43. The anomaly profiles over the three simple models analyzed in Part II will be illustrated with specific examples. Gravity anomaly profiles over a spherical model and a horizontal cylindrical model, where both models have a density contrast ($\Delta\rho$) of 2.0 g/cm^3, a radius (R) of 2 m, and depths (z_0) to center of 3, 4, and 6 m for the sphere and 4, 6, and 10 m for the cylinder, are presented in Figures 10a and b, respectively. Note the similarity in appearance of the profiles for the two structures. The differences become more apparent when profiles for the same depth to center are examined. For a depth to center of 6 m, the anomaly at $x = 0$ for the horizontal cylinder is larger by a factor of 4.5 than the anomaly for the sphere; also, the profile width at half maximum for the cylinder is larger by a factor of 1.3. For the anomaly profiles over a sphere, the depth to center is given by 1.3 $x_{1/2}$, where $x_{1/2}$ is one-half the profile width at half maximum; and for the horizontal cylinder, the depth to center is equal to $x_{1/2}$. Since the density contrast is a linear factor in the equations for the anomaly profiles, it is easy to visualize the effect of considering other

---

* Ten E is an accuracy estimate for the finite difference approximation ($\Delta g_z/\Delta z$) itself and does not refer to the accuracy with which the true (differential) gradient is approximated.

43
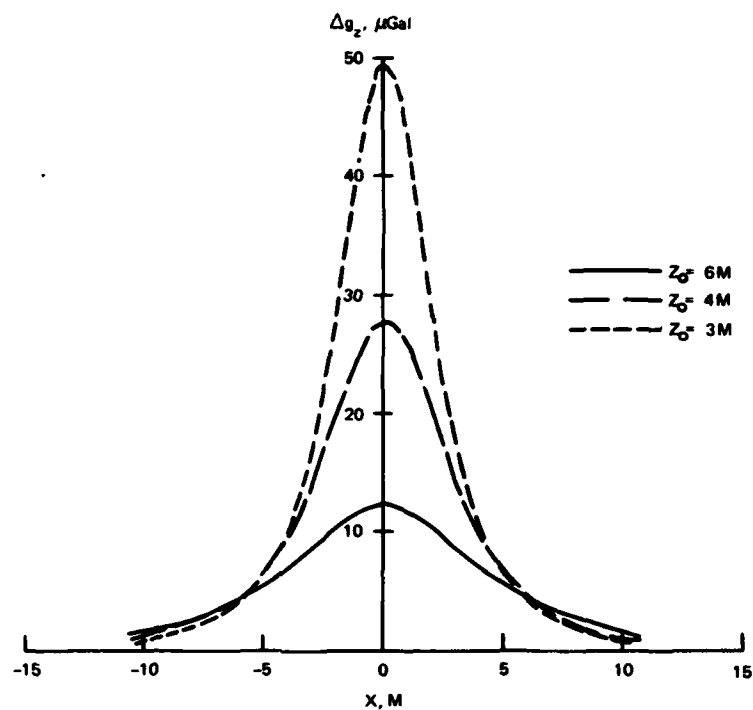
a. IDEALIZED SPHERICAL MODEL
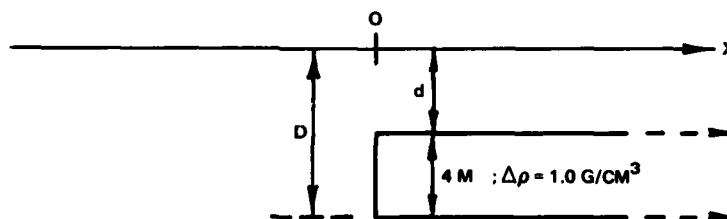

b. IDEALIZED HORIZONTAL CYLINDRICAL MODEL

Figure 10. Gravity anomaly profiles over idealized spherical and horizontal cylindrical models with $R = 2$ m and $\Delta\rho = 2.0$ g/cm^3

density contrasts: for a density contrast of 1.0 g/cm^3, gravity anomaly values will be reduced by one half for each profile location; for a density contrast of -2.0 g/cm^3, the profile curves are just the negative of those shown in Figure 10 (reflected in the x-axis).

44. Figure 11a illustrates a truncated plate model with a slope angle α of $\frac{\pi}{2}$ (Figure 1d), thickness of 4 m, and depths (d) to the top surface of 2, 4, and 10 m. Unlike the anomaly profiles for the sphere and horizontal cylinder, the truncated plate anomaly profile is asymmetrical (Figure 11b). For the three cases, as $x \to -\infty$, $\Delta g_z \to 0$, and as $x \to \infty$, $\Delta g_z \to 2\pi\gamma\Delta\rho T = 168$ µGal, where $T = 4$ m is the plate thickness (i.e., as $x \to \infty$, the gravity anomaly approaches a constant given by the Bouguer slab formula). The vertical face of the plate is located by the profile position where the maximum horizontal gravity gradient $g_{z,x}$ occurs (it is also the position where zero vertical gravity gradient $g_{z,z}$ occurs). The difference in slope at $x = 0$ for the three cases is the primary distinction. Figure 12 shows the manner in which a slope angle of less than $\frac{\pi}{2}$ affects the gravity profile. Dimensions of the models in Figure 12 are larger scale than those considered in Figures 10 and 11 and are appropriate for consideration, for example, when simulating one side of a buried river channel, of a fault with large throw, or of a stratigraphic truncation.

Detectability considerations

45. <u>Anomaly magnitude.</u> Detectability of a structure involves considerations of both the magnitude and wavelength of the gravity anomaly produced by the structure. The magnitude of a gravity anomaly is characterized by the maximum value (value at $x = 0$ for Figure 10). In practical field cases, determination of the anomaly magnitude may not be as straight-forward as indicated in Figure 10. For example, if a positive anomaly is surrounded by a nearly concentric negative anomaly region in a gravity contour map, it is possible that the process of defining the regional field for the site may result in the formation of a negative relative gravity anomaly region. Such a situation could result if the relative zero Δg_z value were selected at $\Delta g_z = 20$ µGal

a. GEOMETRY OF IDEALIZED TRUNCATED PLATE MODEL
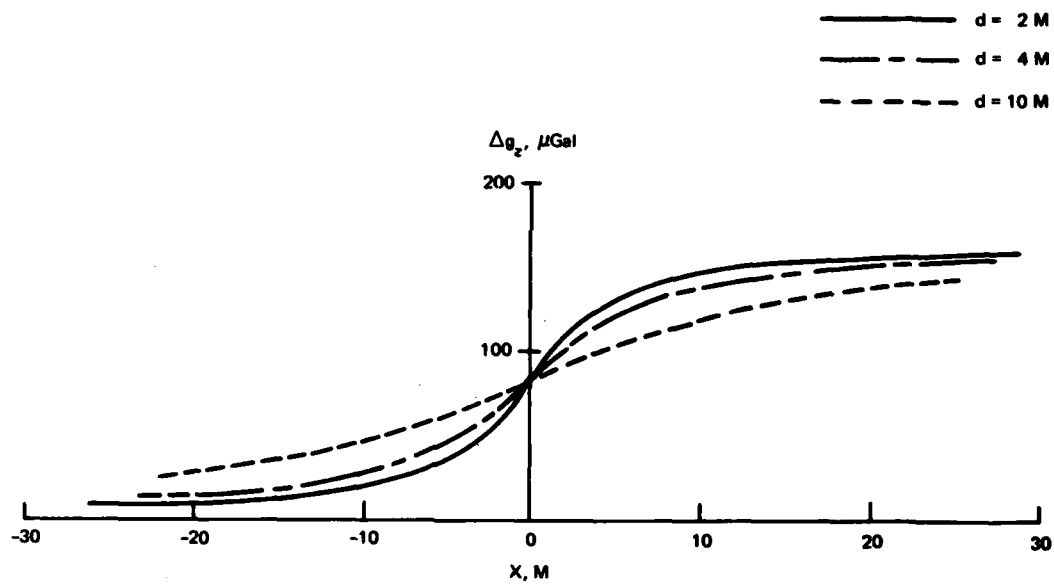
b. GRAVITY ANOMALY PROFILES

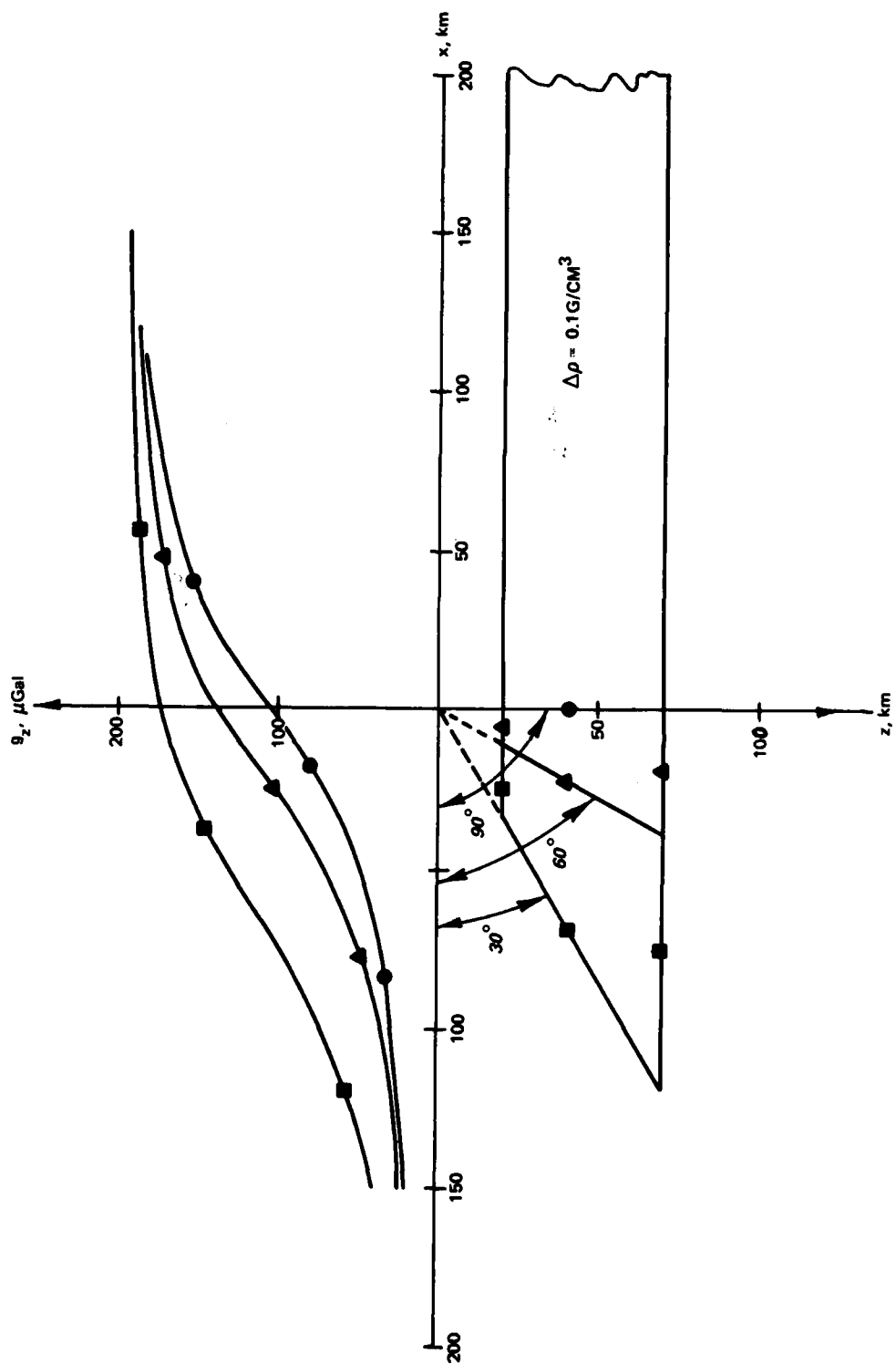Figure 11. Gravity anomaly profiles over idealized
truncated plate model

46

Figure 12. Gravity anomaly profiles over idealized truncated plate models with different dip angles

47

in Figure 10; in such a case, it is the total negative to positive anomaly value that, in effect, determines the detectability.

46. Figure 13 shows the maximum values (magnitudes) of the gravity anomalies produced by both the spherical and horizontal cylindrical models as a function of depth to the center for various radii ($\Delta\rho$ = 2.0 g/cm^3 for all curves). It is easy then to determine which combinations of radius and depth represent models detectable at the 10-μGal threshold. Figure 14 presents curves defining maximum depths (z_{max}) for a given radius R , for which the models cause a 10-μGal or greater anomaly and hence are theoretically detectable in a microgravity survey (solid curves). The dashed curves are included in Figure 14 to illustrate the increase in z_{max} , which would result if the detectability threshold could be decreased to 5 μGal. Determination of the optimum way to present the information in Figures 13 and 14 is difficult and in some respects is a "matter of taste" or preference. Figure 15, for example, illustrates the effect of both detectability threshold level and density contrast in determining the maximum depth at which a spherical model with a given radius can be detected. The curve for $\Delta\rho$ = 2.5 g/cm^3 would be appropriate for estimating the maximum depth at which an air-filled spherical cavity (of radius R) in good quality limestone can be detected (in this case $\Delta\rho$ is negative). Figure 16 (LaFehr, 1979) illustrates another presentation of the information in Figures 13a and 14 for a spherical model (cavity). Finally, Figure 17 (Arzi, 1975) illustrates rather nicely the interplay of radius and density contrast, for four selected depths, to produce identical anomaly profiles for simulated air- and water-filled cylindrical cavities in limestone.

47. For the truncated plate model, the anomaly magnitude is the total variation in value from large "negative" x-values to large "positive" x-values (in Figures 11 and 12, negative and positive x are defined relative to the projection of the truncated surface to z = 0). In practice, the magnitude is difficult to determine since the asymptotes are not usually well defined, particularly in microgravity surveys of small areal extent. A feature of the anomaly associated with the truncated plate is that for a given thickness and density contrast, the
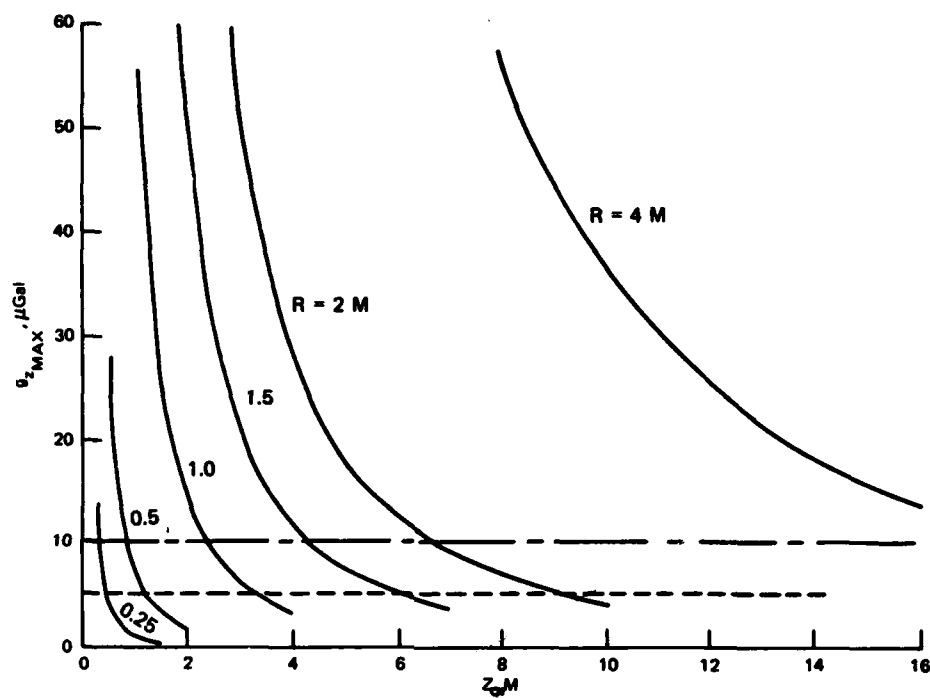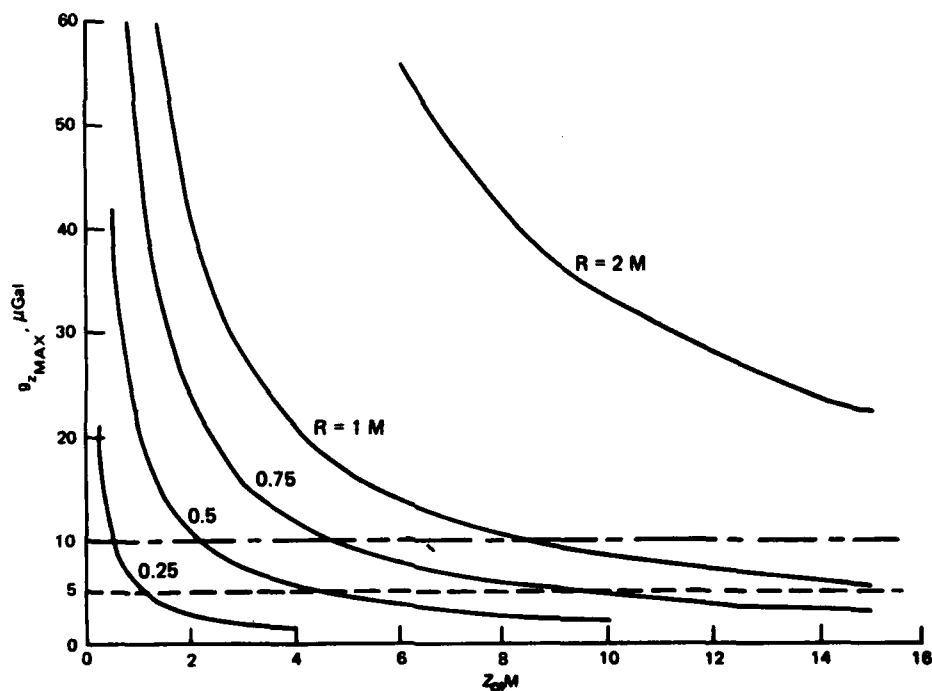
Figure 13. Maximum gravity anomalies produced by spherical and horizontal cylindrical models as a function of depth (z_o) for various radii (R); $\Delta\rho = 2.0$ g/cm^3
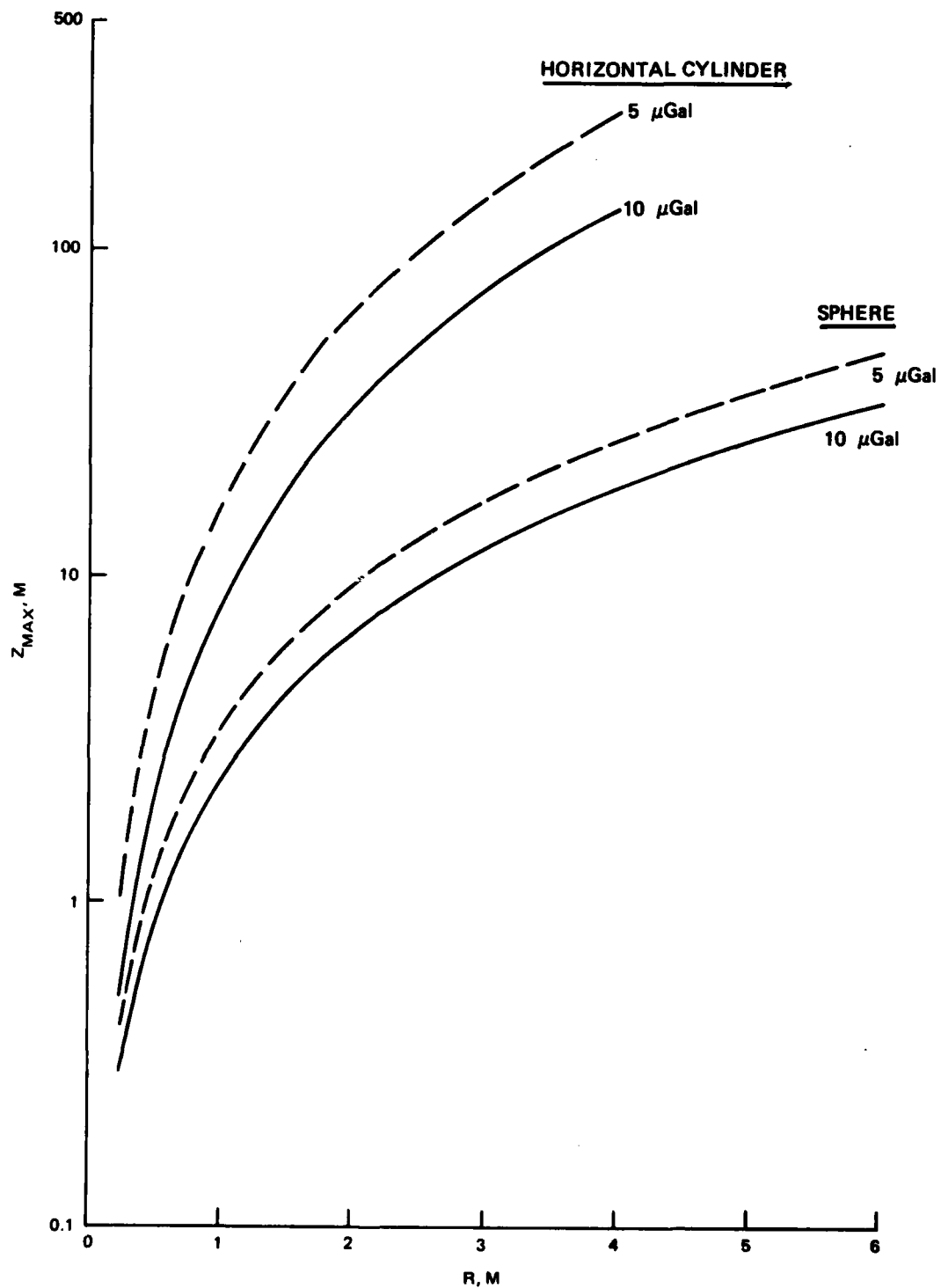
Figure 14. Maximum depth versus radius curves for which models produce
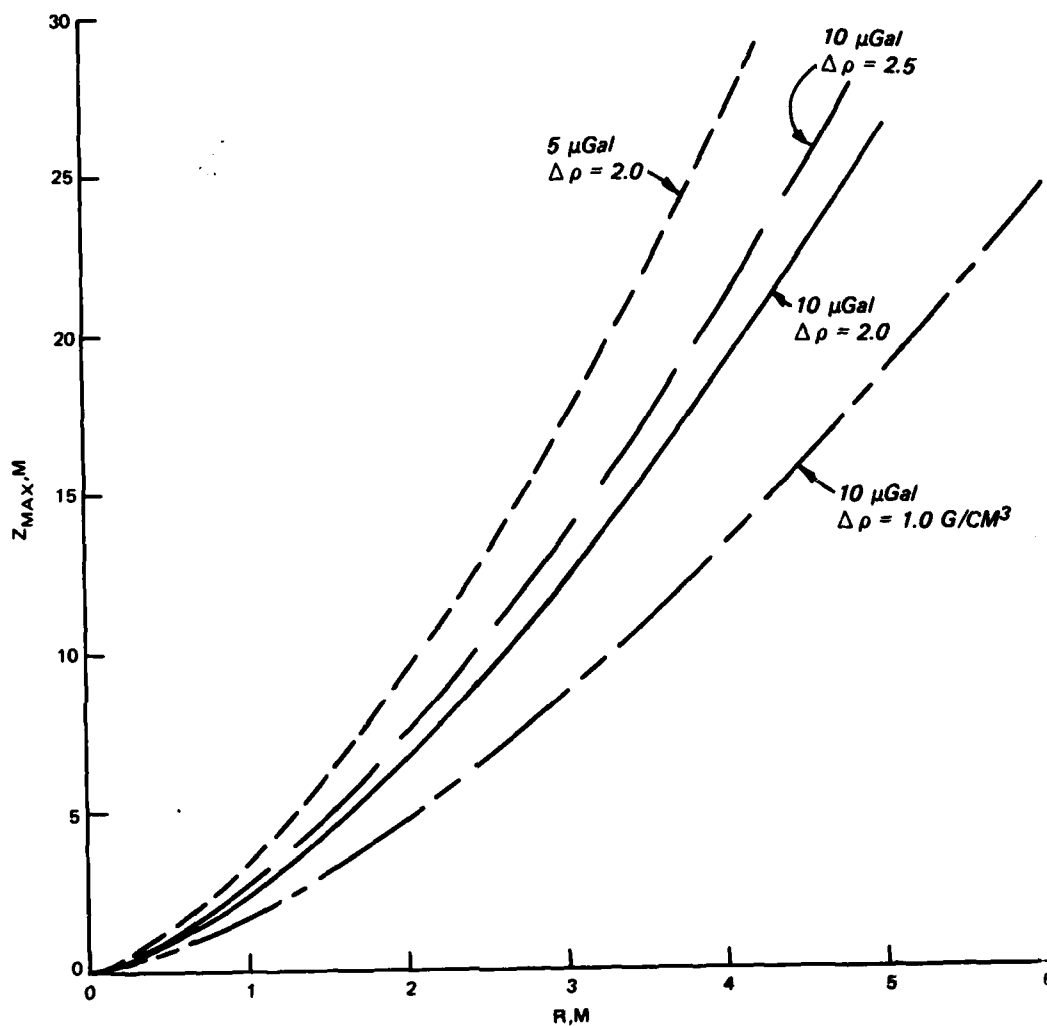≥ 5- and ≥ 10- μGal anomalies; $\Delta\rho = 2.0$ g/cm^3

50

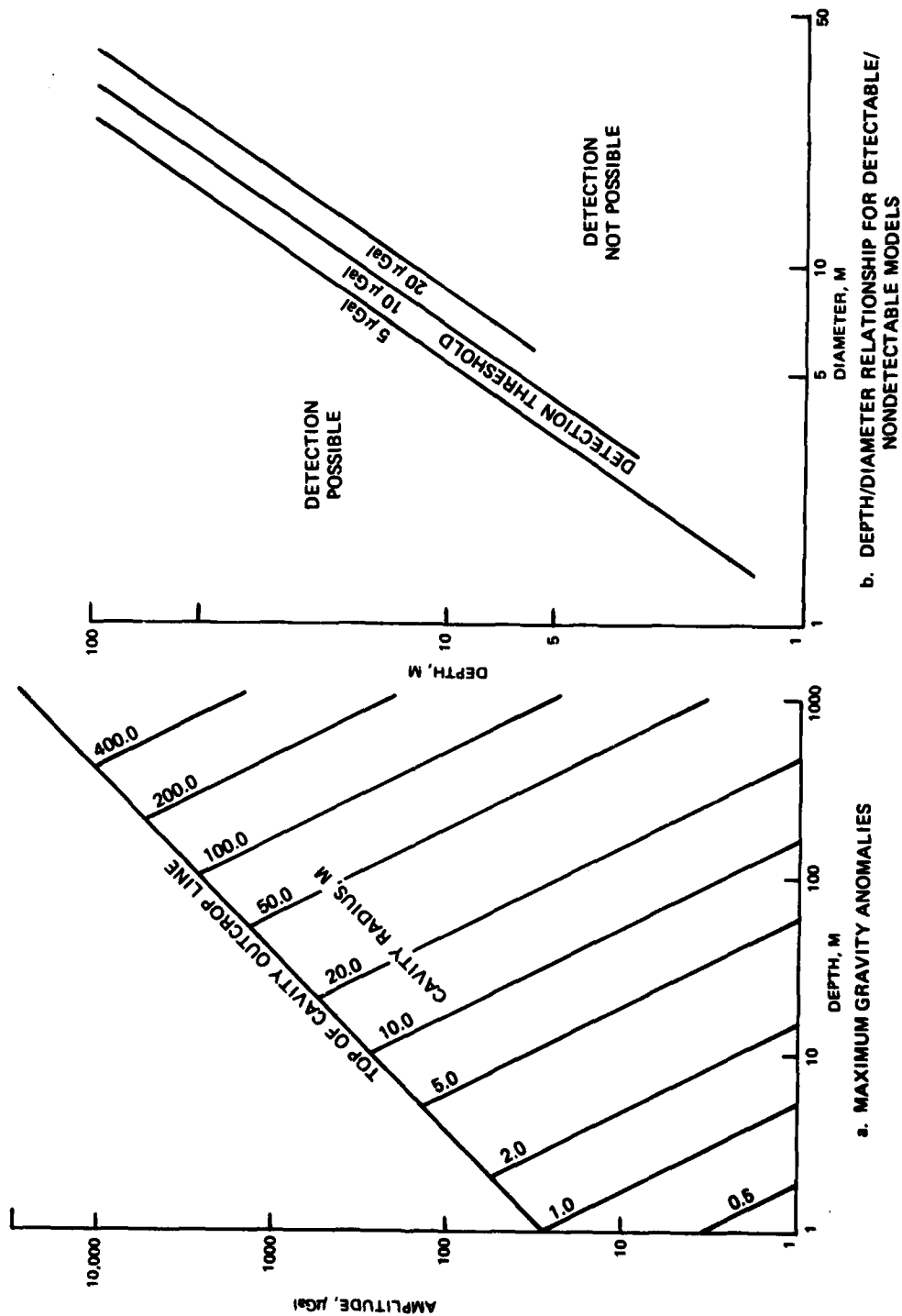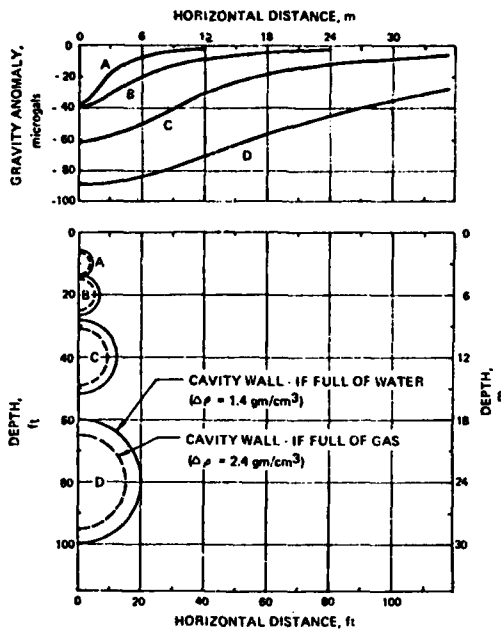Figure 15. Effect of detectability threshold level and density contrast on maximum depth for detection of spherical model

Figure 16. Maximum cavity anomalies and depth versus diameter relationship for detectability of spherical models; $\Delta\rho = 1.0$ g/cm^3 (from LaFehr, 1979)

52

HORIZONTAL DISTANCE, m

CAVITY WALL · IF FULL OF WATER
(Δρ = 1.4 gm/cm³)

CAVITY WALL · IF FULL OF GAS
(Δρ = 2.4 gm/cm³)

HORIZONTAL DISTANCE, ft

(Courtesy of Arzi, 1975; permission granted by
editor of Geophysical Prospecting)

Figure 17. Examples of long horizontal
cylindrical cavities (shown in trans-
verse sections) in a rock of 2.4 g/cm^3,
and the gravity anomalies that they
cause at the surface (shown above in
same section plane)

magnitude is independent of depth to the upper surface; however, as
shown in Figure 11b, the wavelength of the anomaly profile increases as
the depth to the upper surface increases. The magnitude of the anomaly
is linearly proportional to both the density contrast and the thickness
(Equation 29). The detectability of structures, such as illustrated
in Figures 11b and 12, is more dependent on wavelength (hence depth)
than on magnitude, since the magnitudes for density contrasts $\Delta\rho \sim$
1.0 g/cm^3, and thickness $T \gtrsim 1$ m will be quite large (in a microgravi-
metric sense). For sites with lateral changes in soil type, with
$\Delta\rho \sim 0.1$ g/cm^3, which can be approximated by truncated plates with

53

$T \stackrel{<}{\sim} 1$ m, the effect on microgravity surveys will be small and will be manifest in the form of lithological noise.

48. <u>Anomaly wavelength.</u> The wavelength of a gravity anomaly can affect detectability in two ways: (a) for short wavelengths, the discrete sampling of the anomaly in a survey may not be sufficient to adequately define the anomaly, and the anomaly would just add to the lithological noise; (b) for long wavelengths, the anomaly may be interpreted as part of the regional field and removed in the regional-residual separation. Figure 18 illustrates definitions of anomaly wavelength λ for a symmetrical and an assymmetrical anomaly. Sampling or station spacing should be less than one-half the anomaly wavelength in order to adequately define the anomaly. In other words, for a given station spacing S, the minimum wavelength (or maximum spatial frequency) anomaly that can be defined by the data is 2S. For the spherical structure of Figure 10a, station spacings <u>less than</u> 2.3, 3.1, or 4.6 m would be required to adequately define anomalies due to the structures at depths 3, 4, or 6 m, respectively. The corresponding station spacings required to adequately define the cylindrical structure anomalies of Figure 10b, for depths of 4, 6, and 10 m, would be <u>less than</u> 4, 6, and 10 m, respectively. Clearly, in practice, the selection of a station spacing becomes a trade-off between the minimum spacing that is econom-ically feasible and the maximum spacing that will adequately define the anomalies of interest in a survey. Station spacings of 3 to 10 m are typical for high-resolution microgravity surveys; while for some appli-cations, such as reconnaissance site surveys, station spacings of 15 to 30 m are used.

Gravity Gradient Profiles of Simple Structures

49. The advantages of gravity-gradient surveys for resolution of multiple structures have been discussed earlier. Two other features of gravity-gradient surveys are also advantageous: (a) for structures at shallow depths ($\stackrel{<}{\sim} 10$ m), the gradient anomalies have higher signal magnitude to probable error (noise) level ratios (S/N) than the gravity
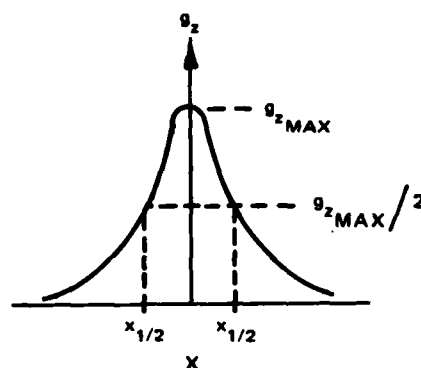
a. SYMMETRICAL PROFILE — $\lambda \equiv 2X_{1/2}$
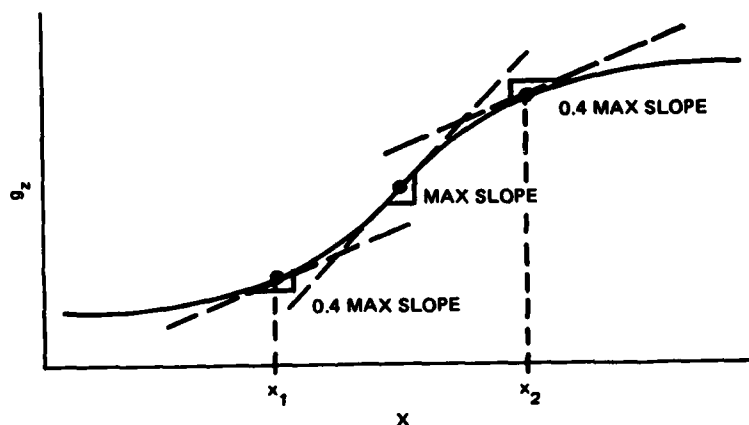
b. ASSYMMETRICAL PROFILE — $\lambda \equiv X_2 - X_1$ (FOLLOWING SUGGESTION OF GRANT AND WEST, 1965).

Figure 18. Definitions of anomaly wavelength

anomalies; (b) since the anomalies due to deep-seated structures (greater than depth of interest in a survey) will have long wavelengths ("regional-type" field), the gravity-gradient profiles will, in effect act as high-pass filters and accentuate anomalies due to shallow structures (shorter wavelengths).

55

50. Figures 19 and 20 illustrate schematically the shapes of the vertical $(g_{z,z})$ and horizontal $(g_{z,x})$ gravity-gradient profiles for the horizontal cylinder and truncated plate ($\alpha = \frac{\pi}{2}$), respectively. The gradient profiles for the sphere and cylinder are seen to exhibit more extrema than the gravity profiles. For the cylinder (Figure 19), $g_{z,z} = 0$ at $\frac{x}{z_0} = 1$, which yields the depth to center; also, at either of the extrema of $g_{z,x}$, $\frac{x}{z_0} = \frac{1}{\sqrt{3}}$. The gradient profiles for the truncated plate (Figure 20) are very diagnostic of the location of the vertical face; since, at that value of x, $g_{z,z} = 0$ (point of inflection) and $g_{z,x}$ has its maximum value. For a plate that is thin relative to the depth to the upper face, the x-distance between the maximum and minimum of the $g_{z,z}$ profile is equal to twice the depth to the plate.

51. A complete discussion of the nature of gradient profiles and detectabilities for simple structures is beyond the scope of this report. Theoretically, the gradient profiles offer the advantage of higher S/N than gravity profiles; however, some of this advantage is lost in practice, since in the field the true (differential) gradient is approximated in a finite difference sense. These concepts can be illustrated by a simple example (Neumann, 1973a). In Figure 21, plots of $\Delta(g_{z,z})$ and Δg_z over a sphere centered at depth $z_0 = 5$ m are presented for a case that produces a gravity anomaly with a magnitude 50 µGal. $\Delta(g_{z,z})$ refers to the theoretical vertical gradient produced by the spherical structure along $z = 0$, i.e., the anomalous vertical gradient (the normal free air gradient is not included). Also shown in Figure 21 is a plot of $\Delta(\Delta g_z'/\Delta h)$ over the sphere, where $\Delta(\Delta g_z'/\Delta h)$ refers to the anomalous vertical gradient measured by a tower structure, and $\Delta g_z'$ is the gravity difference between measuring points at $z = 0$ and $z = -2$ m (i.e., $\Delta h = 2$ m). The profiles are plotted to gravity and gravity-gradient scales, which are equivalent with respect to probable error levels, 5 µGal and 10 E, respectively. The magnitude of the theoretical vertical gradient is 20 times the probable error level, while the magnitude of the gravity anomaly is only 10 times the probable error level; the corresponding value for the case of the finite

56
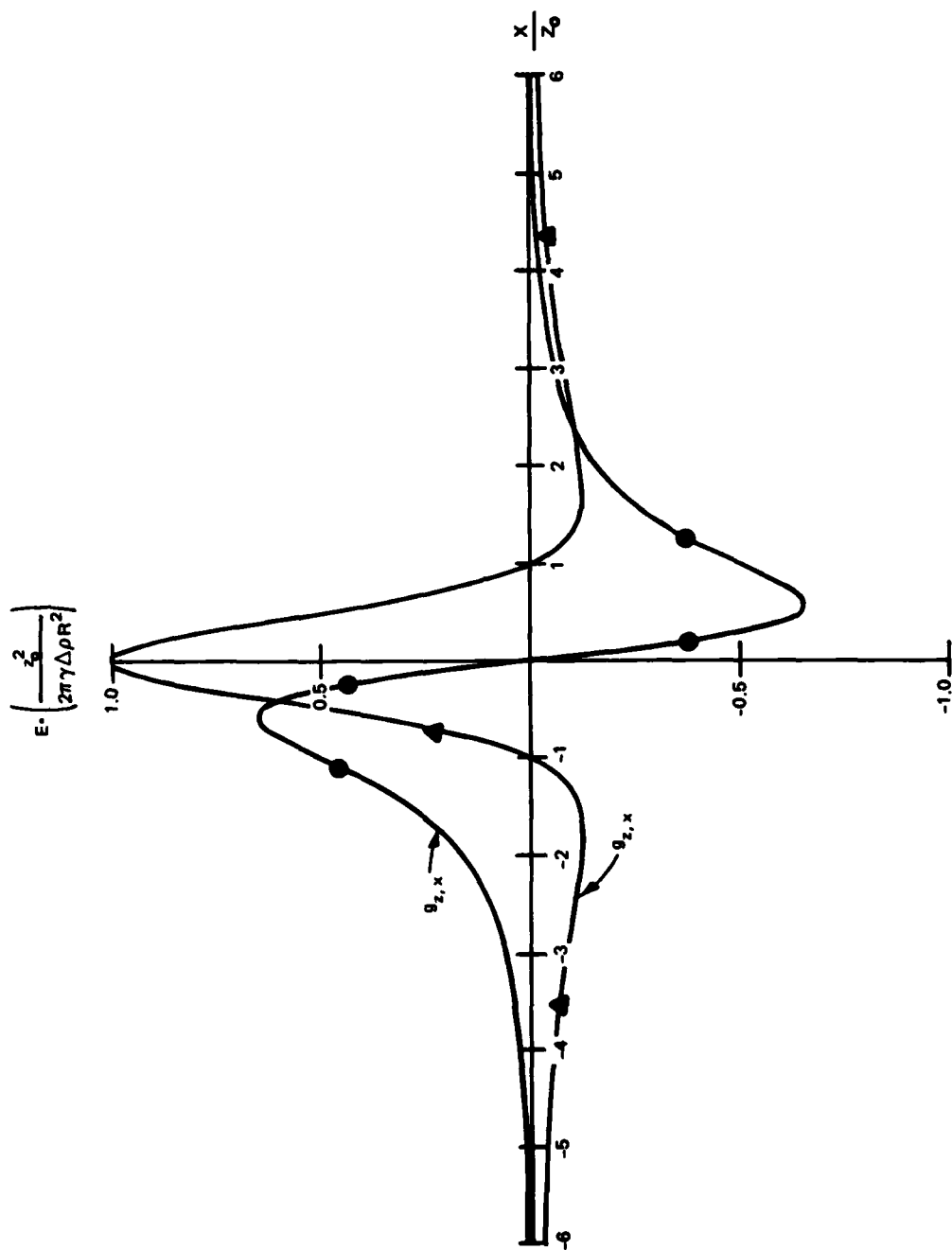
Figure 19. Gravity-gradient profiles for long horizontal cylindrical structure with radius R and depth to center z_0
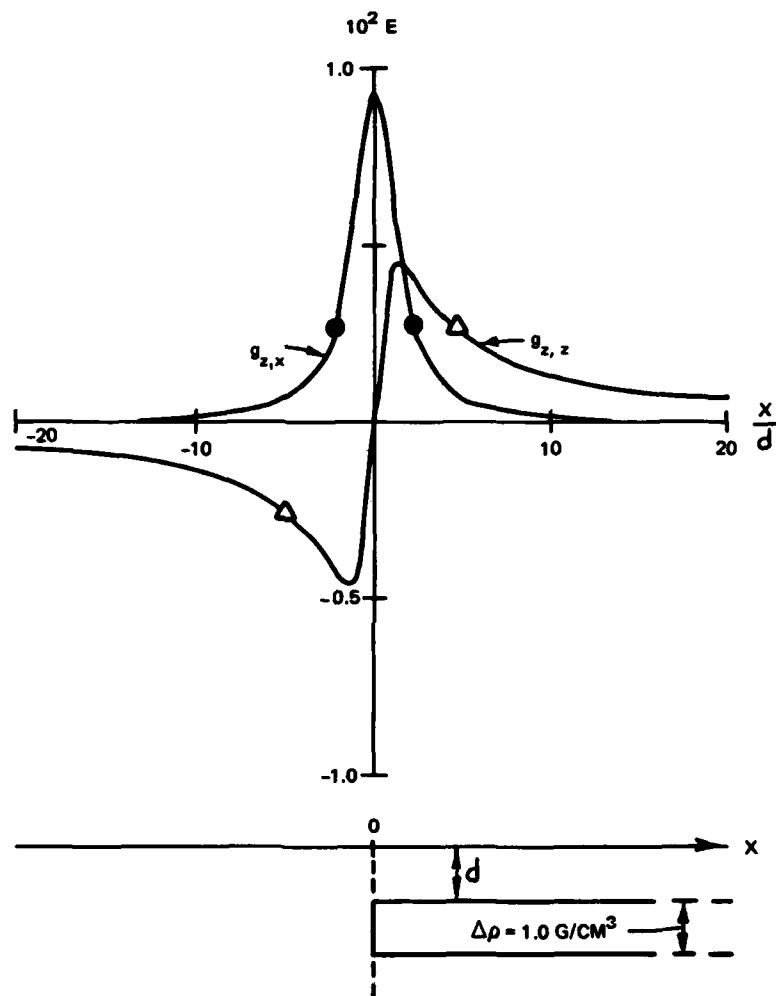
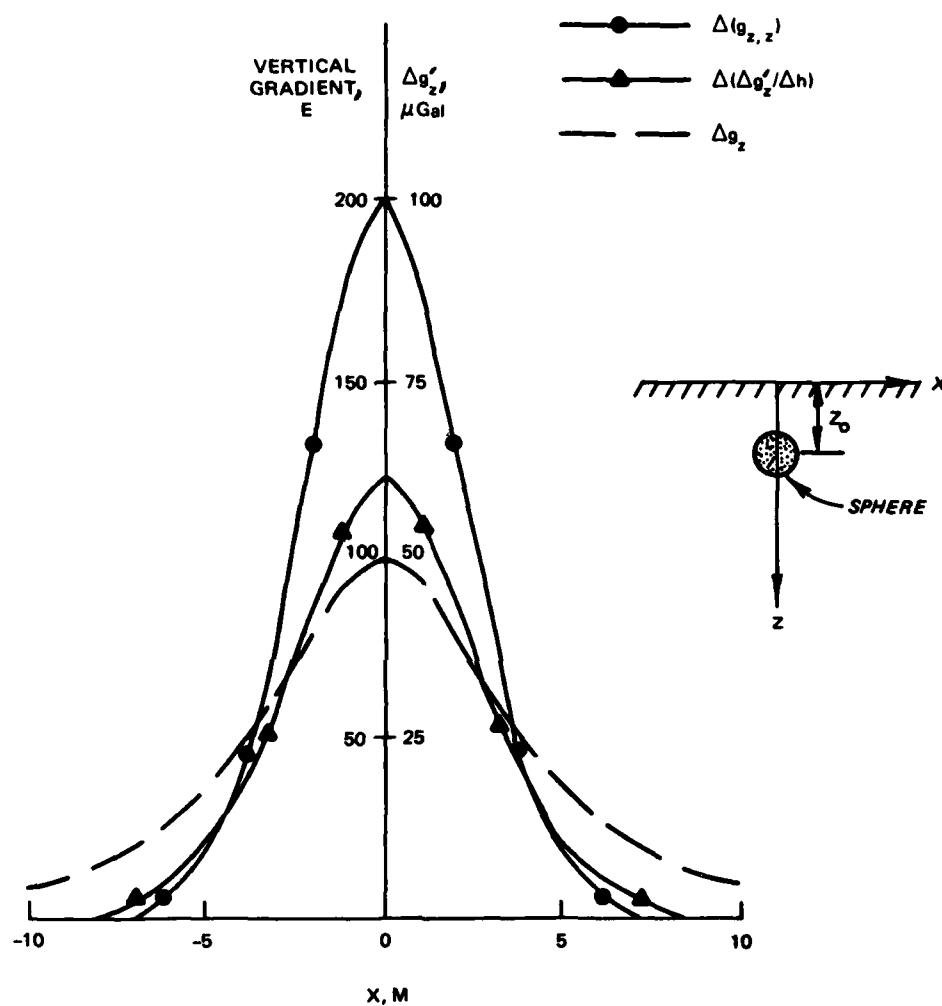Figure 20. Gravity-gradient profiles for truncated
plate geometry

58

Figure 21. Comparison of $\Delta(g_{z,z})$, $\Delta(\Delta g_z'/\Delta h)$, and Δg_z for $z_o = 5$ m, $\Delta h = -\Delta z = 2$ m (tower height), and $g_z(0,0) = 50$ μGal

difference (tower) vertical gradient is ~12.5. Although the S/N advantage of the vertical gradient profile is lessened in practice because of the finite difference measurement procedure, it still is considerably sharper than the gravity profile, and hence an improved resolution can still be achieved.

52. Another simple example serves to illustrate the filtering effect of the gradient profiles on long wavelength (regional) fields. Figure 22 presents individual and composite profiles of Δg_z and $\Delta(\Delta g_z'/\Delta h)$ over five shallow spheres, each producing a 50-μGal anomaly, and a deep-seated sphere producing a 500-μGal anomaly. Relative to the fields associated with the shallow spheres, the field of the large sphere can properly be considered a regional field (Figure 22a and c). In the composite Δg_z plot in Figure 22b, the anomalies due to the shallow spheres appear as just small perturbations on the large regional field. In contrast, on the composite $\Delta(\Delta g_z'/\Delta h)$ plot in Figure 22d, the individual gradient anomalies due to the shallow spheres are clearly defined against the regional gradient anomaly.
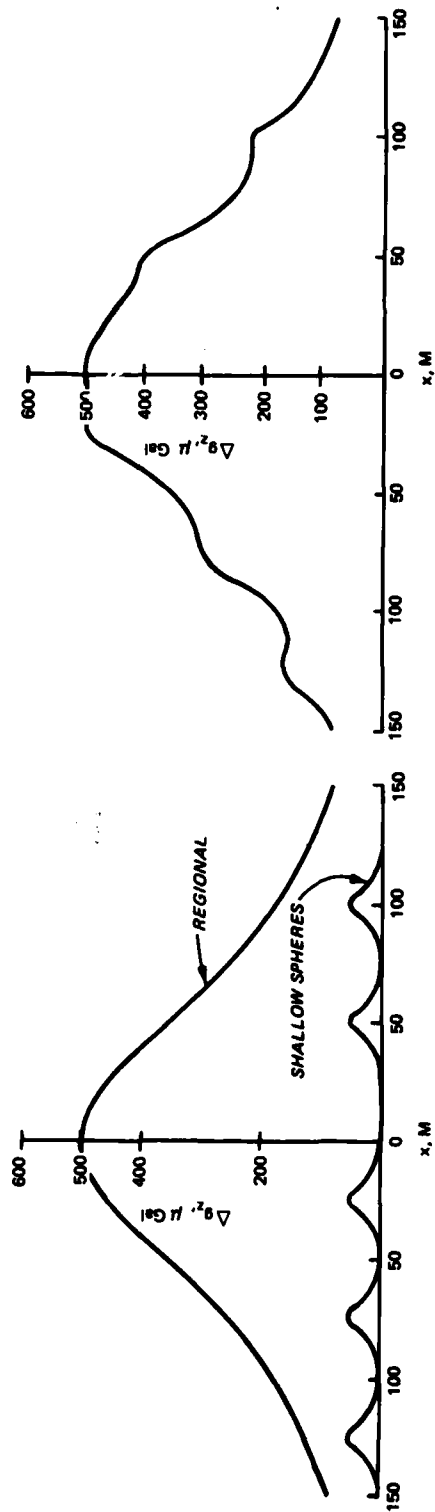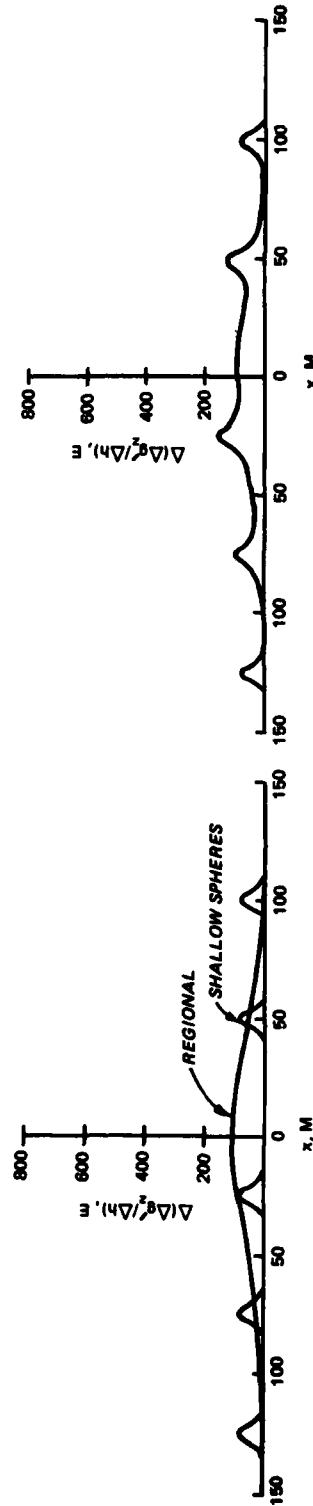
Figure 22. Hypothetical example showing Δg_z and $\Delta(\Delta g_z'/\Delta h)$ anomaly curves plotted to scales comparable as to expected error, assuming $\Delta h = 2$ m

61

PART V: MICROGRAVIMETRIC SITE INVESTIGATIONS FOR
CAVITIES AND OTHER ANOMALOUS CONDITIONS

Introduction

53. As noted in Part I, detection and delineation of subsurface
cavities is one of the most frequently cited applications of microgravi-
metry. Cavities may be either natural (such as solution cavities in
limestone, dolomites, or evaporites) or man-made (tunnels or mines) and
may be air-filled, water-filled, or filled with some secondary geologic
material. A potential field method, such as gravimetry (or magnetic
methods if the cavities represent a susceptibility contrast), is well
suited for the detection and delineation of the rather isolated anomalous
zones or trends represented by cavities, whereas cavities present a very
difficult objective for detection by other geophysical methods. Solu-
tion cavities are just part of the geologic complexity to be expected in
karst regions, and microgravimetry is an invaluable complement to other
geophysical, geologic, and direct methods for site investigations in
such areas. Three reported case histories involving cavity detection
are briefly discussed below, and the results of a microgravimetric site
survey conducted as part of this research effort at a natural cavity
site in Florida are presented in more detail.

Case Histories

Nuclear power plant site

54. Arzi (1975) presents the results of a high-resolution
microgravity survey conducted as part of a "bedrock soundness verifica-
tion" program for a nuclear power plant site. A LaCoste & Romberg
Model-G gravity meter was used,* and the gravimetry was performed with
"utmost care." The study consisted of four aspects: (a) two verifica-
tion or sensitivity checks; (b) a high-resolution survey over a 120- by

---

* The survey was performed in 1970, prior to the general availability
  of the Model-D.

80-m area around the containment building, using a station spacing of
4.6 m (15 ft) in the critical area beneath the containment vessel it-
self; (c) a reconnaissance survey over a 140- by 140-m area under a
proposed cooling tower location, using 15.2-m (50-ft) station spacings;
and (d) a limited remedial grouting verification survey.

55. Figure 23 illustrates one of Arzi's "sensitivity" demonstra-
tions, where a closely spaced (1.5-m) gravity profile reliably detects
a -40-µGal anomaly caused by a small pier excavation. A second "sensi-
tivity" or verification demonstration consisted of a 40-station survey
over an area suspected to have subsurface solution cavities (from photo-
geological examination). This survey revealed a localized anomaly of
about -100 µGal, which was verified by drilling as caused by a shallow
cavity (depth to center at 6.4 m). The high-resolution gravity survey
(4.6- to 7.6-m station spacing) under and around the proposed location
of the containment building, in conjunction with selective drilling,
allowed the foundation to be pronounced free of defects (cavities,
fractured zones, faults, etc.) in the depth range of concern ($\sim$ 50 m).
Terrain corrections proved extremely difficult to evaluate because of
vertical rock cuts in areas already excavated; however, the survey
demonstrates that survey results can be properly interpreted even in the
presence of terrain effects that cannot be completely or adequately
corrected.

56. The reconnaissance survey at the proposed cooling tower
site was conducted to detect solution defects in the foundation.
Figure 24 shows the Bouguer anomaly map (without terrain correction),
which indicates two isolated anomalous negative areas in the northeast
portion of the area. Subsequent drilling corroborated that the negative
anomalies were due to an extensive system of cavities up to 1 m in size
within 4.5 m of the surface. The drilling showed that the solution
features were limited to the area lying northeast of a line between A
and B in Figure 24, and none were found beyond the line to the southwest.
Subsequent to a remedial grouting program, a limited resurvey of the
northeastern portion of the area revealed that most of the grout had
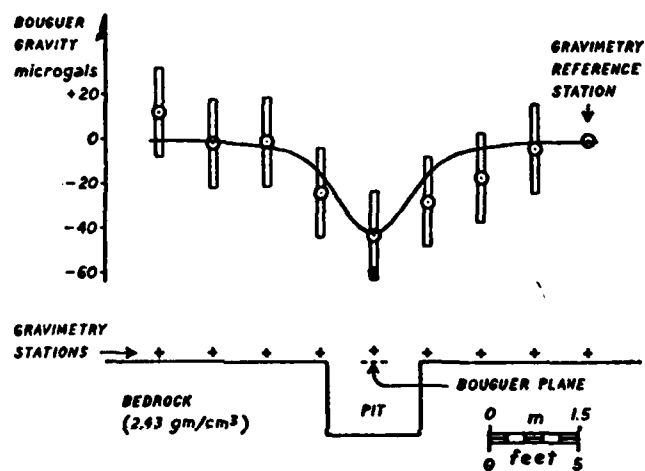
63

Figure 23.   Profiles of calculated anomaly (curve) and
observed Bouguer gravity (circles) over an excavation
(pit shaped as a vertical cylinder).   The $\pm$ 20-µGal
error bars represent four times the calculated probable
error on Bouguer gravity.   Excavation depth 1.2 m,
diameter 1.6 m, mass defect 6000 kg

64

migrated to the two anomalous zones and that the small eastern anomaly was completely eliminated.
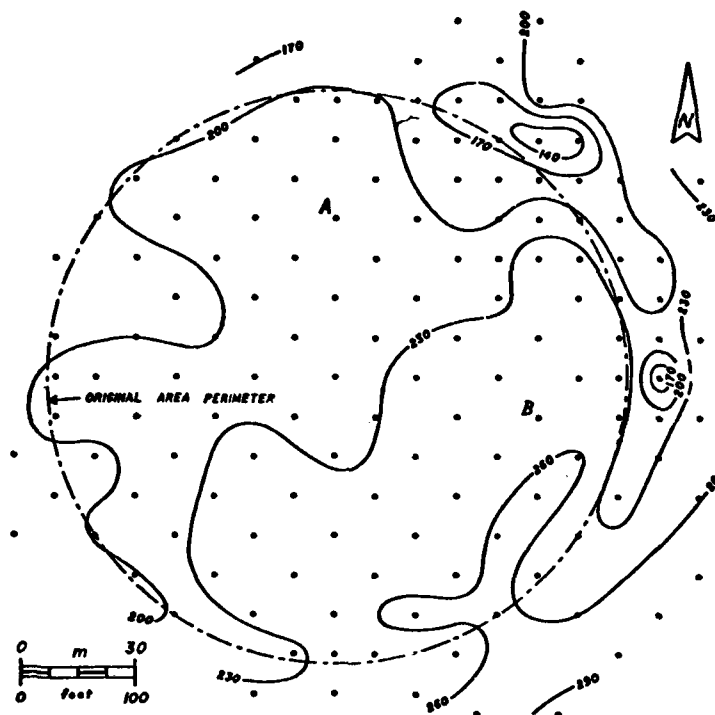
Figure 24. Isogal map, in microgals, of Bouguer gravity without terrain correction, over the cooling tower area (contour interval 30 μGal). All gravimetry stations marked with dots

57. Arzi (1975) concludes that the availability of true "micro-gal" gravimeters (such as the Model-D) could make microgravimetry a "leading geophysical method" for engineering applications. Also, he feels, on the basis of his experience that microgravimetry --

> "...is probably the least disturbing, and least disturbed, subsurface investigation on a construc-tion site, with a small involvement of personnel and equipment, which also makes for easier logis-tics and better adaptability in bad weather and immobilizing terrain."

Subsurface mine

58. A major geotechnical engineering problem in Europe is the
existence of numerous subsurface rock mines operated over the past
centuries and now abandoned, with no surface indication of the presence
of the mines (vertical entrances filled either by man or by natural
means) and no records of locations. The mines were commonly shallow
and followed no predictable exploitation pattern in general. These
mines now present a considerable threat to man's structures and a con-
siderable effort in money, manpower, and technology is being focused
on their location. Microgravimetry is one of the most successful and
frequently applied geophysical methods for detection of these mines.

59. Neumann (1977) presents an interesting case history of the
complete definition of a subsurface mine system by microgravimetry. An
initial survey with a grid spacing of 20 m, using a Model-D meter,
detected a negative anomaly of more than 100 µGal. This led to the
discovery and mapping of a mine including 11 chambers (at about 5-m
depth). In an attempt to evaluate the prospects of using microgravi-
metry to completely define the mine, including pillar and chamber loca-
tions, a more detailed survey was carried out with a 5-m station
spacing. Figure 25 presents the Bouguer anomaly map, where the original
survey points are identified by the large dots and the subsequent survey
points by small dots. The mapped mine is shown by the dotted outline
and cross hatching. It is apparent that small perturbations are present
on an otherwise clearly defined "local regional" field, which is
described by almost concentric circles. Making a regional-residual
separation results in the residual anomaly map in Figure 26, where the
chosen regional is indicated by the dashed contours. The residual anom-
aly field now defines negative and positive anomalies that correlate to
known locations of chambers and pillars, respectively. Note that the
contour interval in Figure 26 is 5 µGal. It should be possible to
obtain this quality result routinely from carefully conducted micro-
gravity surveys except at sites where there is a high lithological
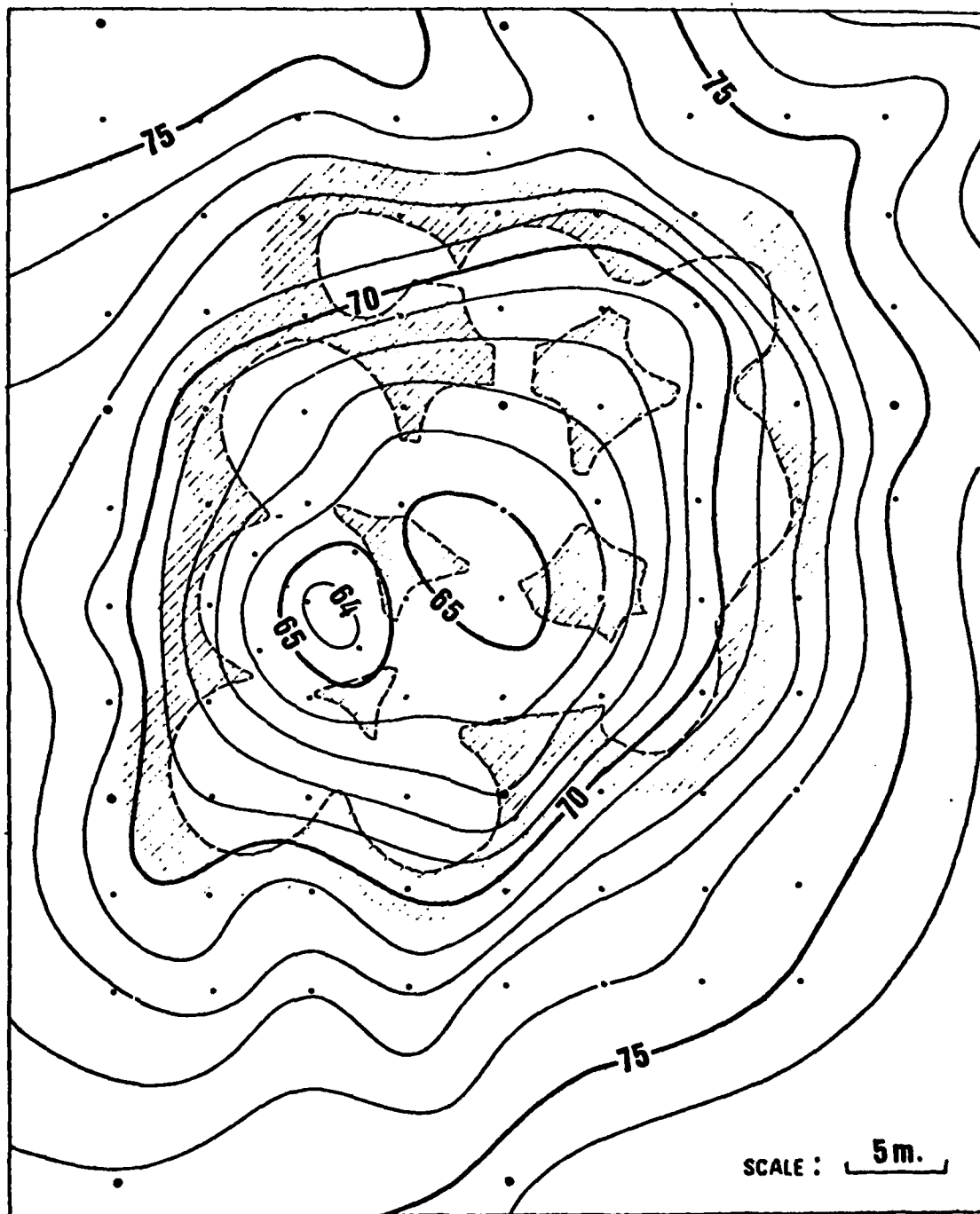noise level.

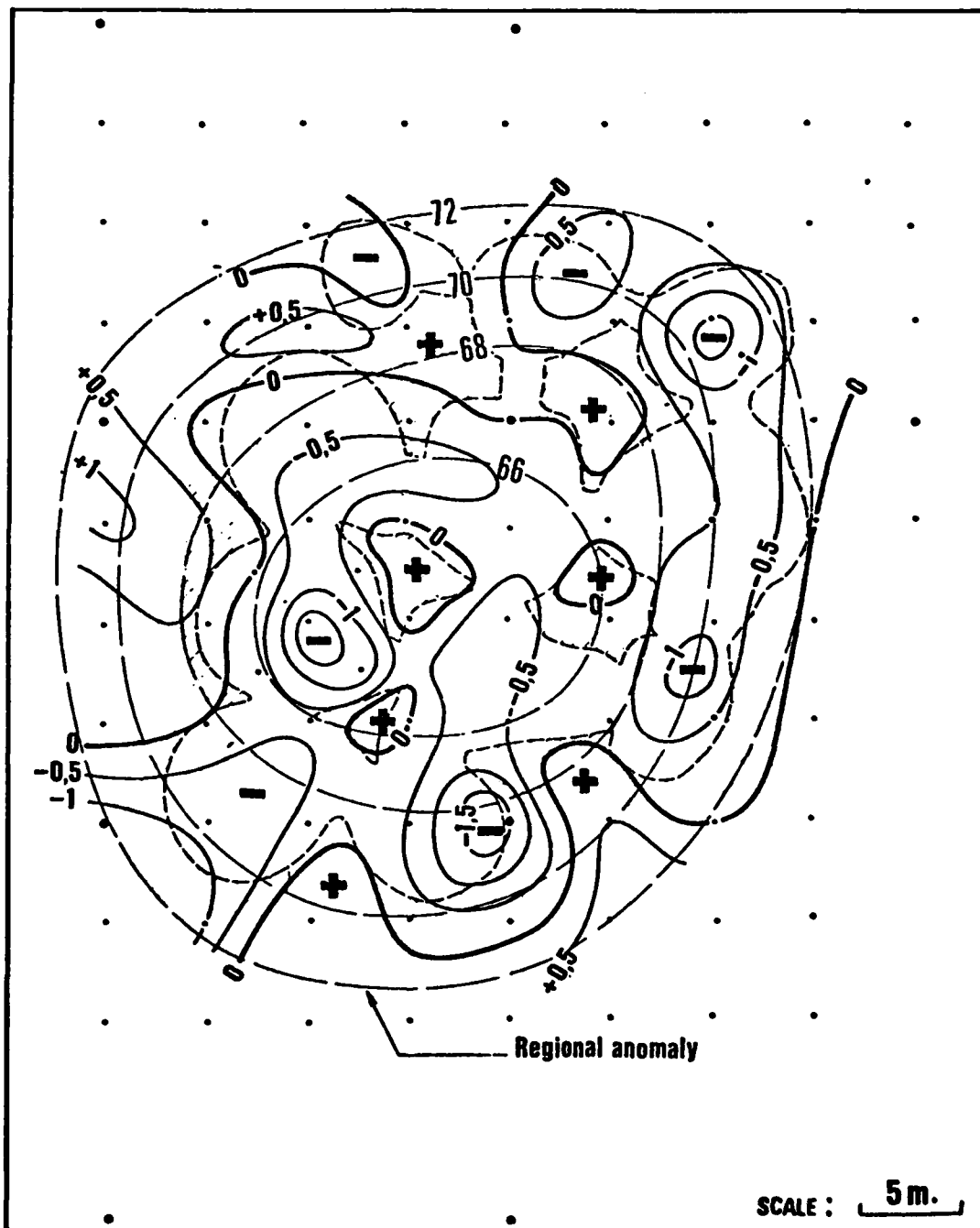Figure 25.   Bouguer gravity anomaly over underground mine (contour
interval--10 μGal)

67

Figure 26. Complete definition of subsurface mine by microgravity survey with regional and residual anomalies (residual contour interval--5 µGal)

60. Fajklewicz (1976) presents several interesting case histories on the use of a 2-m tower structure to conduct vertical gravity gradient surveys. Figure 27 shows the results of a tower vertical gradient survey across a brecciated fault zone. The observed tower vertical gradient profile agrees very closely with a theoretical tower vertical gradient profile calculated for a simplified model consisting of two truncated plates. The observed profile also agrees qualitatively with the theoretical (differential) vertical gradient profile for the model. The results of a tower vertical gradient survey conducted by Fajklewicz, as shown in Figure 28, successfully detected an unknown cavity created by subsurface mining.

Microgravity Survey at the Medford Cave Site, Florida

61. Medford Cave is located in Marion County, Florida, near Reddick. The cave system was mapped as a joint effect by the Southwest Research Institute and the Florida Highway Department in 1974. Figure 29 is the result of this mapping effort. Fountain et al. (1975) discuss the site and the results of various geophysical tests conducted there. The microgravity survey described here was conducted in the spring of 1979 and was the first of an extensive series of geophysical methods to be evaluated by the WES at the Medford Cave site. Since the microgravity survey will be discussed thoroughly in later reports under the projects cited in the Preface, showing correlations with other geophysical methods, only the most significant results will be presented here.

General site conditions

62. Medford Cave is located on private property, which is used primarily as pasture land.* The primary entrance to the cave is by a

---

* Permission to use the site was obtained by Mr. J. D. Gammage, State
  Materials and Research Engineer, Florida Department of Transportation,
  Gainesville, FL.

Figure 27. Gravity vertical gradient survey across a brecciated fault zone

70
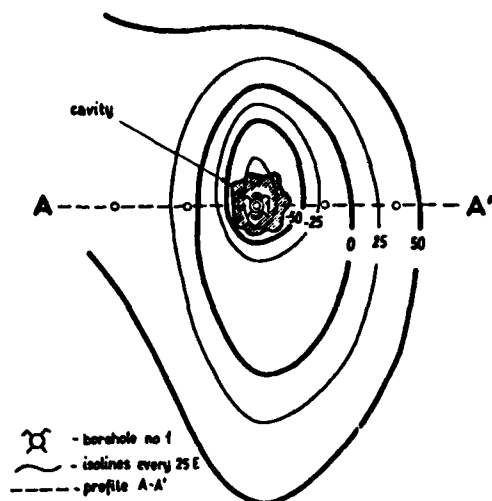
a. Surface distribution of the gravity
vertical gradient values over a detected
post-exploitation cavern
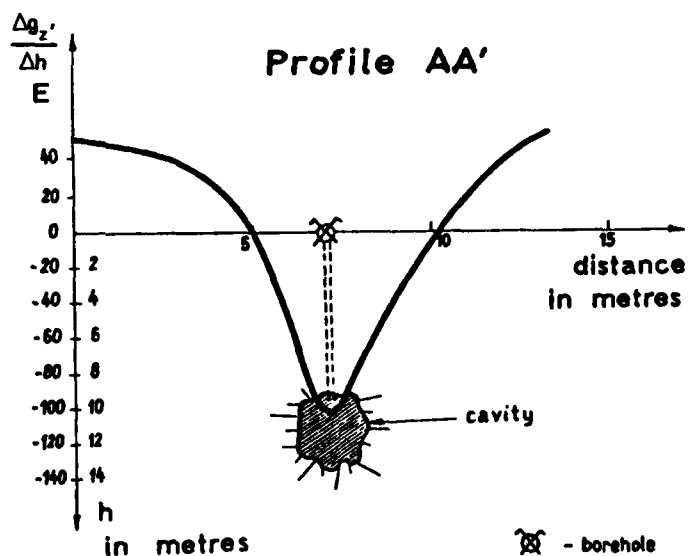
b. Distribution of the gravity vertical gradient
values in the profile AA', and drilled to cavern

(Courtesy of Fajkiewicz, 1976;
permission granted by Society
of Exploration Geophysicists)

Figure 28. Vertical gradient survey to detect subsurface mines

REFERENCE

SURFACE

SECTION A - A'

SURFACE

SECTION B - B' - B"

0 1   5 m

b. Cross sections

PRIMARY
ENTRANCE

ENTRANCE

SECTION C - C

ENTRANCE

ENTRANCE

0   10   25 FT
0   5   10 M
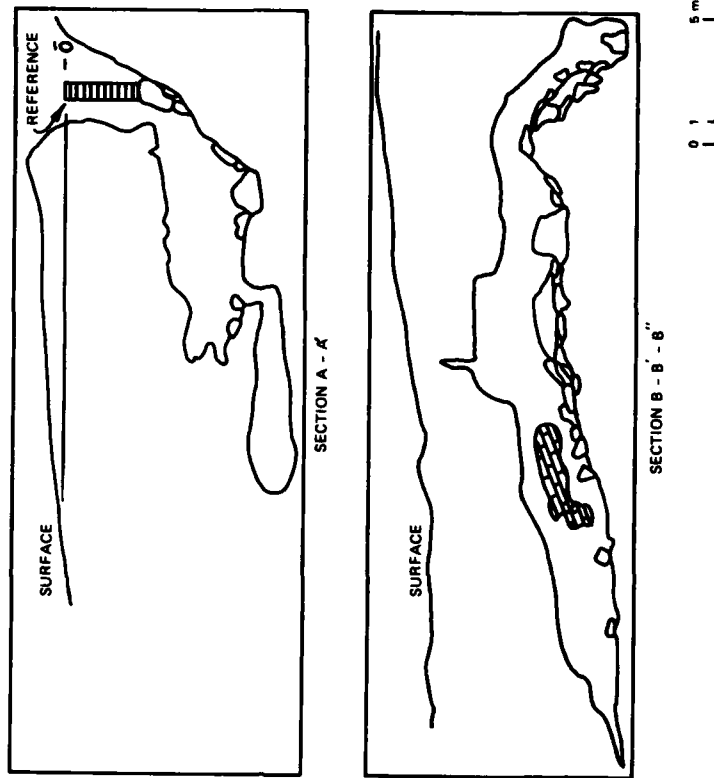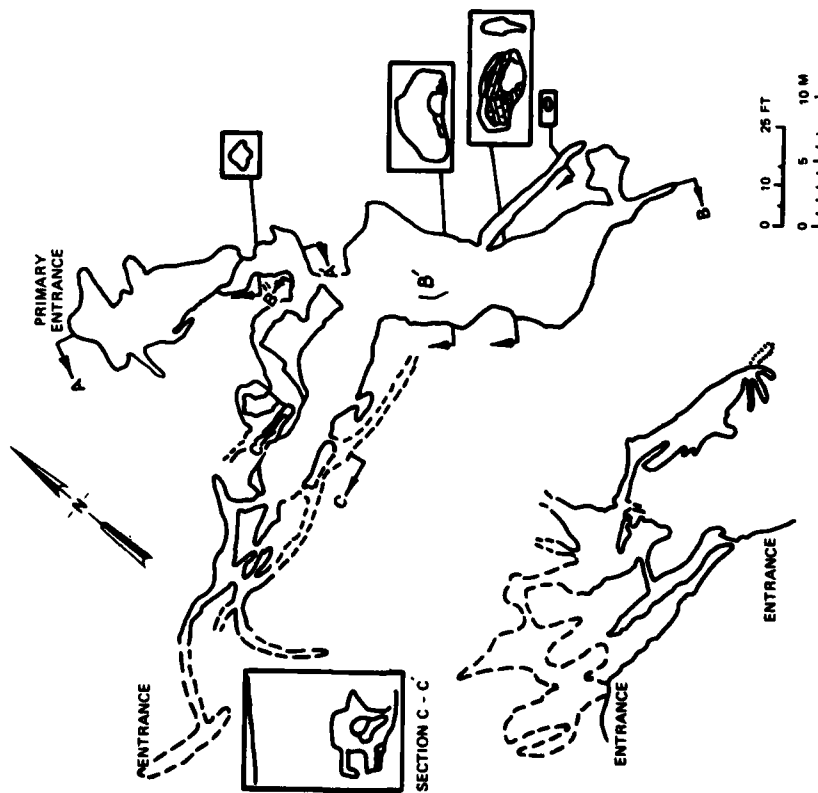
a. Plan view with selected cross sections

Figure 29. Medford Cave site map

vertical opening (about 3 m in diameter by 6 m deep) in a sink (Figure 29). There are three other sinks at the site, two of which have openings into portions of the cavity system large enough to permit a man to enter. Note in Figure 29 that connection between the southern portion of the cavity system (accessible through openings in the side of a large sink) and the northern portion has not been verified by direct exploration.

63. The cavity system has developed in soft, fossiliferous limestone (Crystal River Formation of the "Ocala Group" of limestone of Eocene age) near the crest of one of numerous small hills in the area. The terrain consists of gently rolling hills and valleys, and typical of karst areas, there is little to no surface drainage. In addition to sinkholes and subsurface cavities, the surface of the limestone (as verified by exploratory drilling) is solutioned to form limestone pinnacles with intervening pockets of clay. The surface soil cover is thin on crests of the hills, having a maximum thickness of about 1 to 1.5 m over the Medford Cave site.

Site topographic survey

64. A 10-ft (3-m) survey grid was established over a 260- by 260-ft (approximately 80- by 80-m) area, with the grid lines oriented north-south and east-west. At each grid point (every 10 ft or 3 m), a survey stake was driven flush with the ground surface. Relative elevations of the tops of the survey stakes were determined to ±0.01 ft (±0.3 cm). Figure 30a is a topographic map of the surveyed portion of the site, where the assumed elevation of point (0,0) is 150.00 ft. The highest elevation at the site is point (260,260), which is 26.57 ft (8.1 m) higher than point (0,0). Except for the three sinkholes in the surveyed area, the ground surface approximates an inclined plane dipping from northwest to southeast. Figure 30b is a simplified version of Figure 29a with grid axes superimposed. The topographic survey required the equivalent of 3 days for a 2-man crew.

Microgravity survey technique

65. Gravity measurements were made at 420 stations at the site, as shown in Figure 31, with LaCoste & Romberg Model D-4 gravity

73
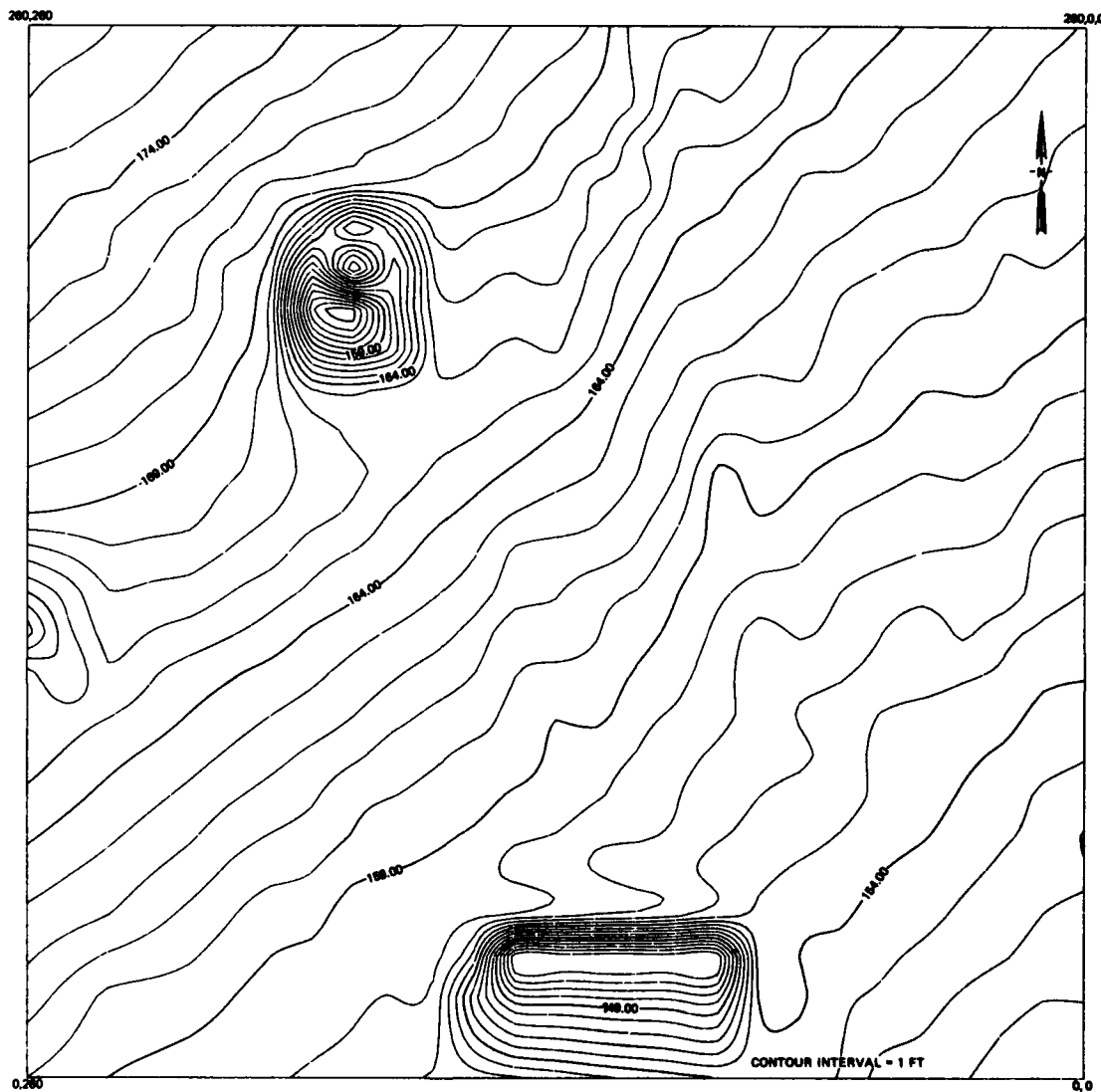
a. Topographic map of surveyed portion of site (assumed elevation of point (0,0) = 150.00 ft

Figure 30. Topographic survey of Medford Cave site (Sheet 1 of 2)

74

MEDFORD CAVE SITE
MARION COUNTY, FLORIDA
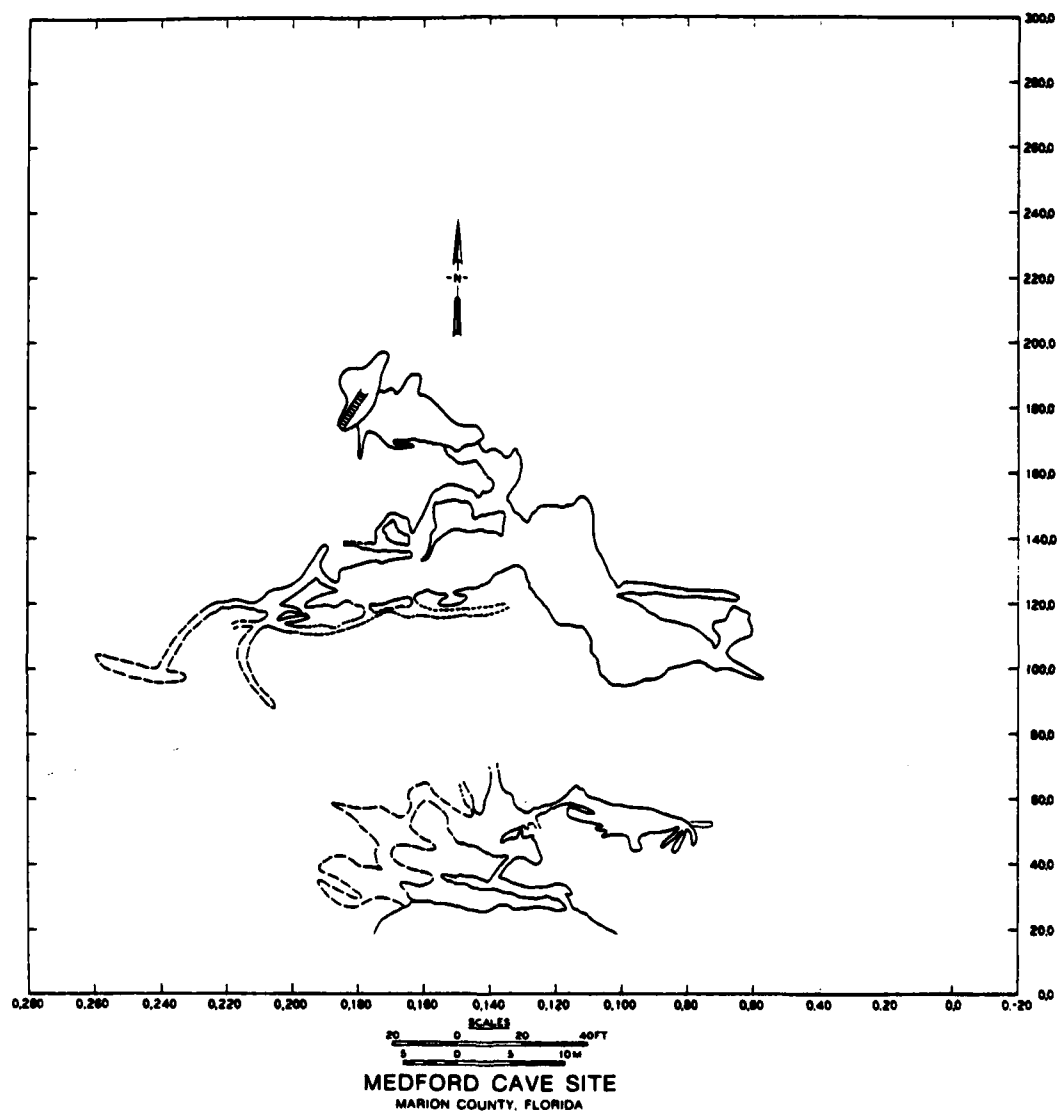
b. Site plan map with grid area

Figure 30. (Sheet 2 of 2)
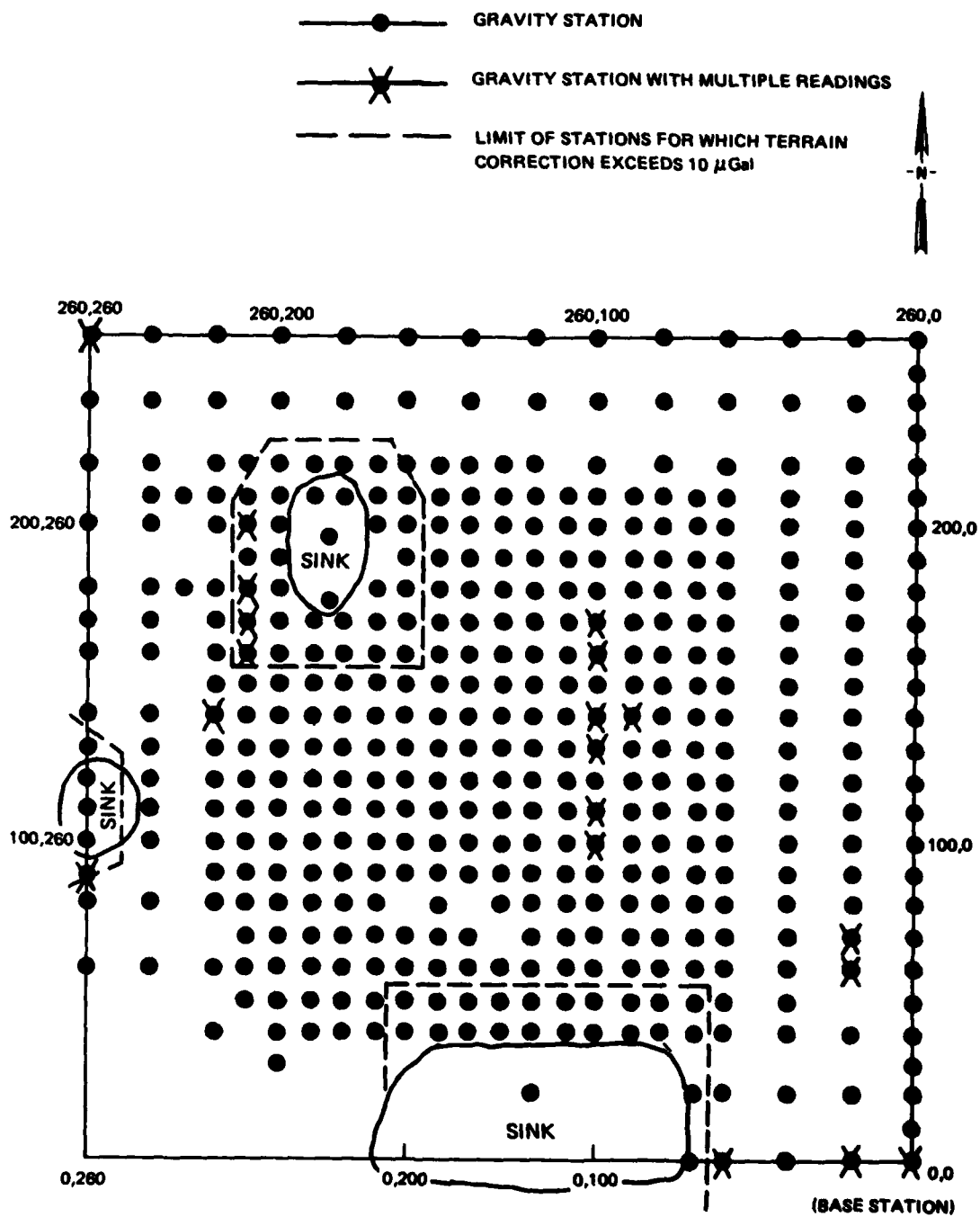
Figure 31. Station locations for microgravity survey of Medford Cave site

76

meter.* This survey was performed prior to the complete formulation of the recommended survey procedure presented in Part III. However, the survey procedure of Part III was adhered to quite closely except for two considerations: (a) the number of station reoccupations was only 5 percent of the total, and (b) several programs (see Part III) consisted of long, continuous profile lines. Because of a time constraint on the use of the gravity meter, it was decided to sacrifice repeat observations for a densification of coverage in the area over the known cavities at the site (Arzi, 1975). The perferability of short looping or "zigzag" programs to long, continuous programs was noted by Neumann** in a review of the data from the site following completion of the survey.

66. Grid point (0,0) was selected as the base station for the survey and was reoccupied once each hour (average rate). The flat baseplate is shown on the base station in Figure 4. The baseplate was leveled at each station, and its height above the survey stake recorded. Adjustments to level the gravity meter itself on the baseplate were minimal. At night, the gravity meter was operated in a tidal recording mode to produce a tidal record for comparison with the field "drift curve" and the theoretical tidal curve for the site. The survey required the equivalent of 7 days for one man.

Data corrections and processing

67. The required corrections to the field data and subsequent processing of the data were performed with the assistance of Neumann** and several of his colleagues. Steps used in correcting the gravity data are outlined in Part III. As a result of density measurements on soil and near-surface rock samples (weathered) from the site, a density of 1.9 g/cm^3 was used for the Bouguer and terrain corrections. The stations primarily affected by the terrain corrections were those close to the three sinks as indicated in Figure 31. All data corrections were

---

* The gravity meter was loaned to the WES by the U. S. Army Engineer District, Seattle.
** Personal communication with Robert Neumann, Compagnie Generale de Geophysique, Massy, France, 1979.
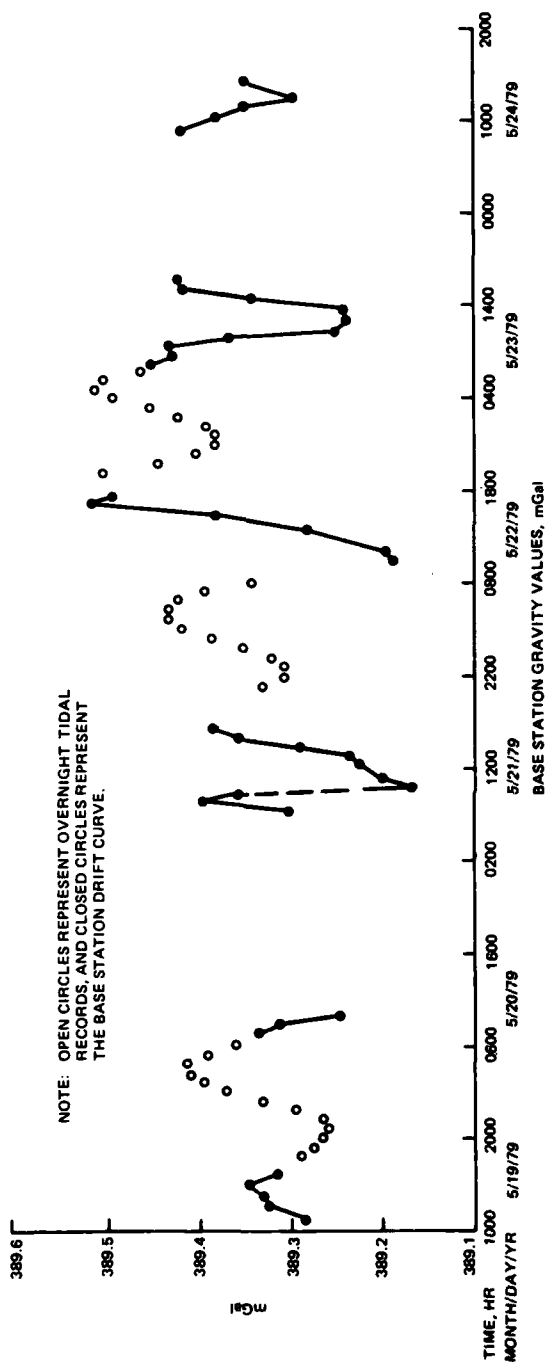
performed manually to allow maximum interaction with the data, and the detection of "high and/or low" programs. Entire programs that are anomalously "high" or "low" can be detected by careful examination of repeat readings at a station from different programs or from examination of neighboring station readings in areas with dense coverage. Explanation of the origin of these anomalous programs is not known, although a possible cause could be due to differences in time between readings at the first and last stations of a program and base station readings resulting in relative shifts in base station values.

68. The base station gravity values presented in Figure 32a represent the majority of the survey. The values have been free-air corrected for the height of the baseplate above the grid marker. Also shown (open circles) are the variations recorded overnight on three occasions. Since the overnight tidal records were recorded in a different location (i.e., local motel room), the segments have been shifted vertically to fit to the base station curve. The phase of the two sets of data agrees very well, but the amplitude variation of the field curve is more extreme. The time marked by an arrow corresponds to a base station reading following a strong jolt to the gravity meter. Because of the frequent base station reoccupations, the recovery period after the jolt is adequately defined. Significant errors can result for less frequent base station occupations in such cases. The theoretical tidal curve for the site shown in Figure 32b was computed using the equations of Longman (1959).

69. There is approximately a 4-hr phase difference between the theoretical and measured tidal curves; such phase delays are not uncommon.* Discounting the phase shift, there is good agreement between the amplitudes of the measured tidal curve (Figure 32a, open circles) and the theoretical tidal curve (Figure 32b). The long-term cumulative drift (nontidal) of the gravity meter appears to be about 2 µGal/hr, although there are nontidal meter drifts much larger than this that are

---

* For many locations, however, such as Vicksburg, Mississippi, for example, the agreement between theoretical and measured tidal curves, both in phase and amplitudes, is nearly exact.

NOTE: OPEN CIRCLES REPRESENT OVERNIGHT TIDAL RECORDS, AND CLOSED CIRCLES REPRESENT THE BASE STATION DRIFT CURVE.

a. BASE STATION DRIFT CURVE FOR PART OF SITE MICROGRAVITY SURVEY WITH OVERNIGHT TIDAL RECORDS
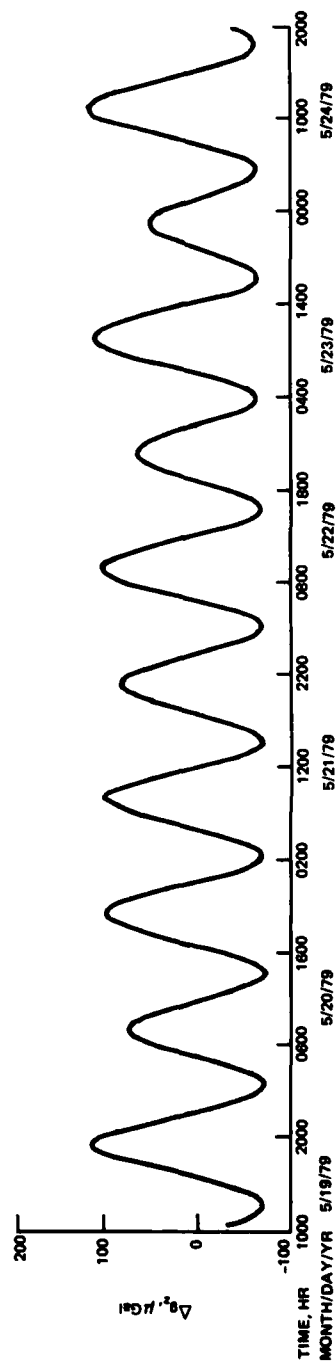
b. THEORETICAL EARTH TIDE FOR SITE

Figure 32. Field base station drift curve and theoretical and observed earth tidal records for Medford Cave site

79

not cumulative. In any event, frequent high-quality base station readings can correct for these time-dependent gravity variations.

Gravity anomaly maps

70. Figure 33 is the Bouguer gravity anomaly map for the site, where only the data from a 20-ft (6-m) grid of stations are included to produce the contour map. To this point, the gravity anomaly values are still completely relative. However, it is easily seen that the gravity anomaly values increase from an average of about 700 µGal on the western grid boundary to about 780 µGal on the eastern grid boundary. Assuming a linear regional gradient, the field increases from west to east at a rate of 0.3 µGal/ft or 3 µGal/10 ft (∿1 µGal/m). Subtracting this planar regional surface from the Bouguer anomaly surface of Figure 33 gives the residual anomaly map of Figure 34. Evidence of the validity of this regional-residual separation is given by the presence of the zero contour "winding everywhere" in the map.*

71. There are three major features of interest in Figure 34: (a) a large negative anomaly (-68 µGal in the center of the map) with directional trends northwest to southeast and to the west-southwest; (b) a localized negative anomaly (-41 µGal) centered at point (225,40) in the northeast part of the area surveyed; and (c) a large localized negative anomaly (-77 µGal) centered apparently at point (110,0). The first feature mentioned above is due to the large, northern portion of the known cavity system, has the same general directional trends, and satisfactorily outlines the known cavernous conditions at the site (even suggesting extension to a southern negative anomaly centered at point (160,50)). The other two features are due to unknown subsurface conditions; thus, confirmatory borings were planned to identify the causes of the anomalies.

72. The residual anomaly contour map using all gravity stations in Figure 35 is considerably more complex in appearance than Figure 34. Several other interesting negative anomalies appear, such as at locations (130,60), (165,90), and (180,100). An unexplained, localized, positive

---

* See second footnote on page 77.

Figure 33. Bouguer anomaly map for Medford Cave site microgravity survey (contour interval--0.02 mGal (20 μGal) and 20-ft station spacing data only)

81

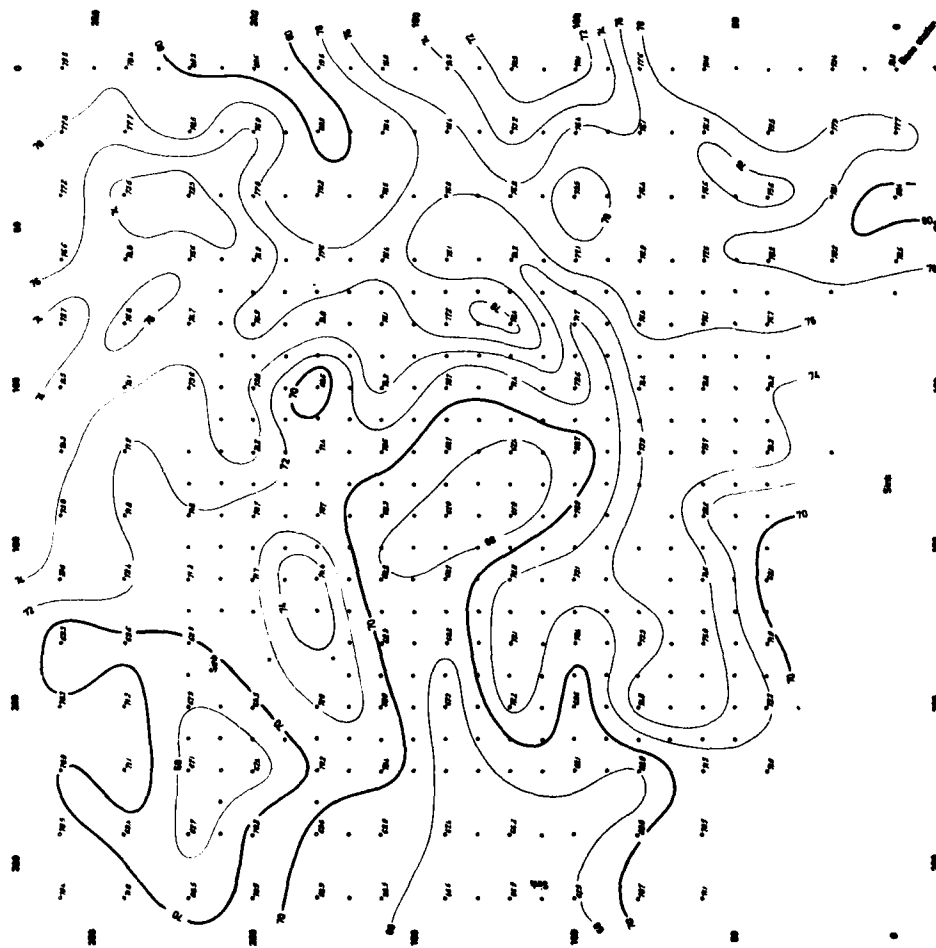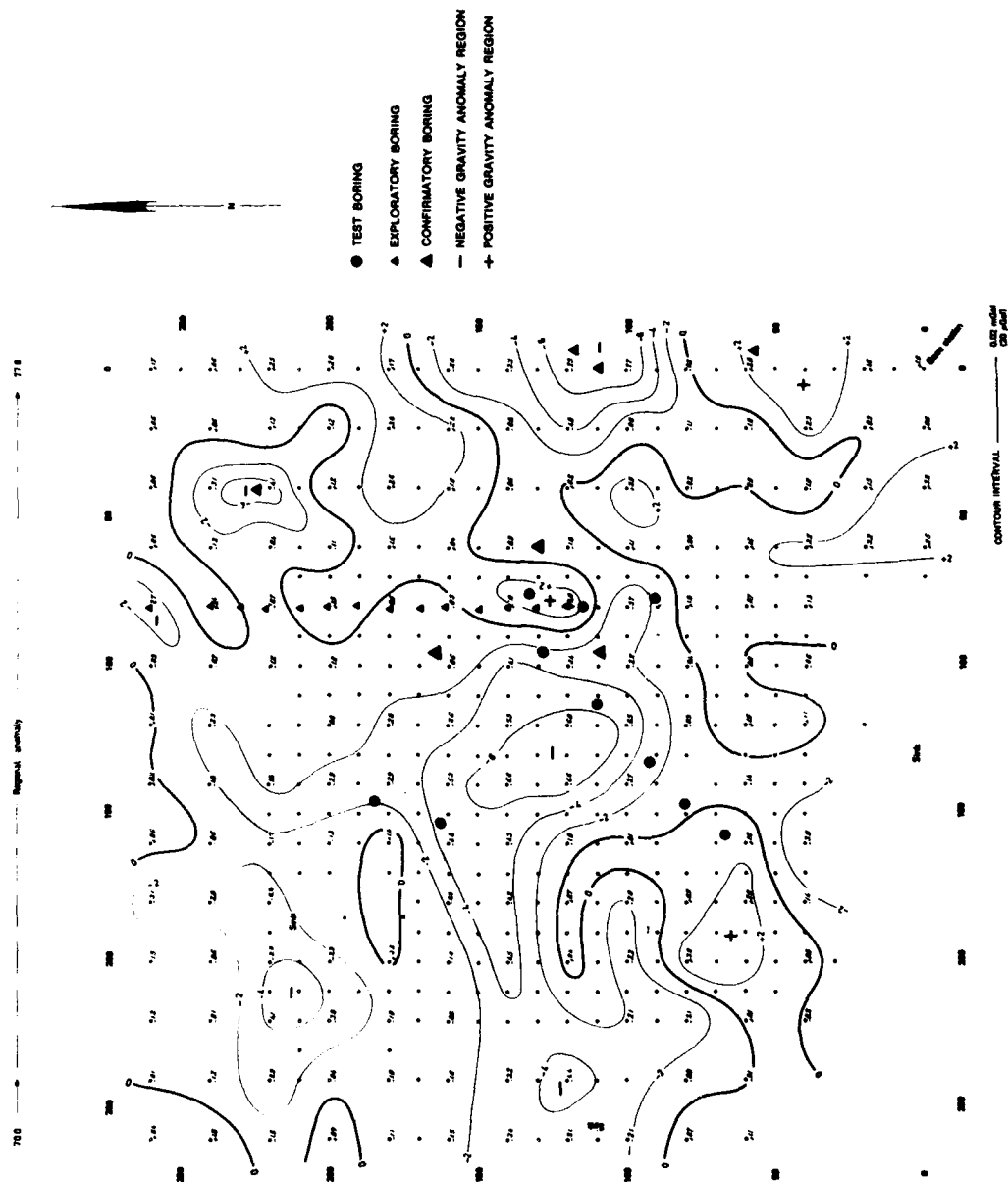Figure 34. Residual anomaly map for Medford Cave site microgravity survey (20-ft station spacing data only)
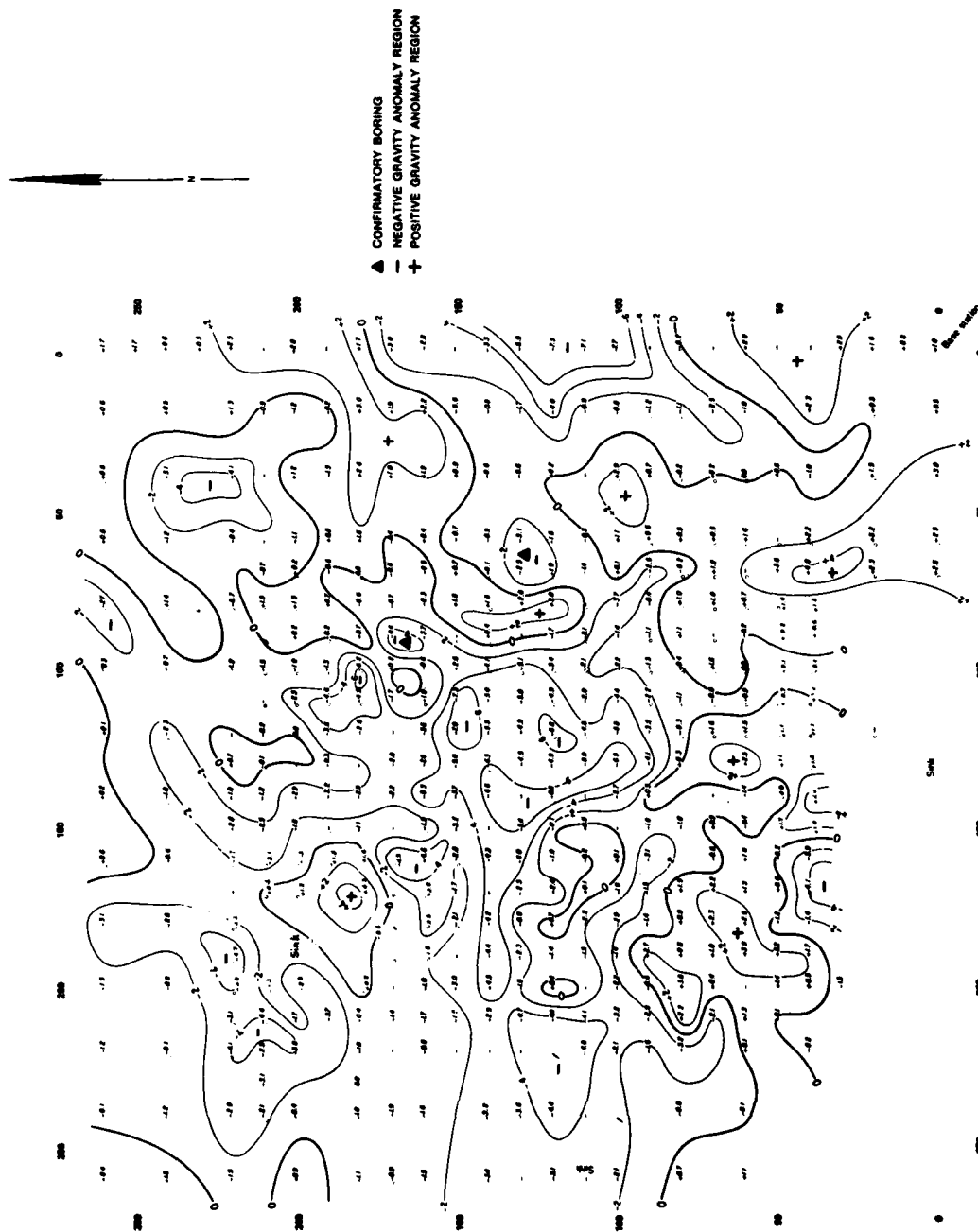
Figure 35. Residual anomaly map for Medford Cave site microgravity survey (contour interval--0.02 mGal (20 μGal) and all stations included)

▲ CONFIRMATORY BORING
－ NEGATIVE GRAVITY ANOMALY REGION
＋ POSITIVE GRAVITY ANOMALY REGION

anomaly occurs around point (185,170), which is near a known, rather large cavity, and now more prominently separates the central negative anomaly region from the negative anomaly feature (of unknown origin) just to the north and northwest of the primary cave entrance.

Site drilling program

73. Subsequent to the microgravity survey, a drilling program was undertaken. Locations of these borings are indicated in Figure 34, where boring symbols denote the objective of the boring: (a) test borings for use with subsurface geophysical test methods, (b) exploratory borings to determine a detailed geologic cross section along a north-south line, and (c) confirmatory borings to investigate geophysical anomalies. Most of the borings were cored and logged.

Correlation of microgravity and drilling results

74. Exploratory boreholes were placed on 10-ft (3-m) centers along the 80W north-south line from points (120,80) to (260,80), and test borings extended the profile line south to (90,80). A detailed geologic cross section was prepared from the core logs; Figure 36 presents a simplified version of this cross section. Above the geologic cross section is plotted the microgravity profile. There is excellent correlation between features of the microgravity profile and the geology. A -37-µGal anomaly occurs over the larger known cavity. The remainder of the microgravity profile gives an accurate "picture" of the top of rock topography--positive anomalies over the limestone pinnacles and negative anomalies over the clay pockets. A different choice for the regional field might have resulted in the negative anomaly over the large cavity being larger by say -10 µGal (-47-µGal magnitude), since the five values on the left of the gravity profile seem to be defining a relative zero value (though there are no core data in the area to substantiate this conjecture); this would also have made the anomalies over the clay pockets more negative.

75. Core logs in Figure 37 are from borings (225,40), (110,95), (110,0), and (117,-5). The boring at point (225,40) intercepts a shallow, partially clay-filled cavity at a depth of 9 to 14.5 ft (2.7 to 4.4 m), and the cavity is covered by 2.5 ft (0.75 m) of limestone and 6.5 ft

84
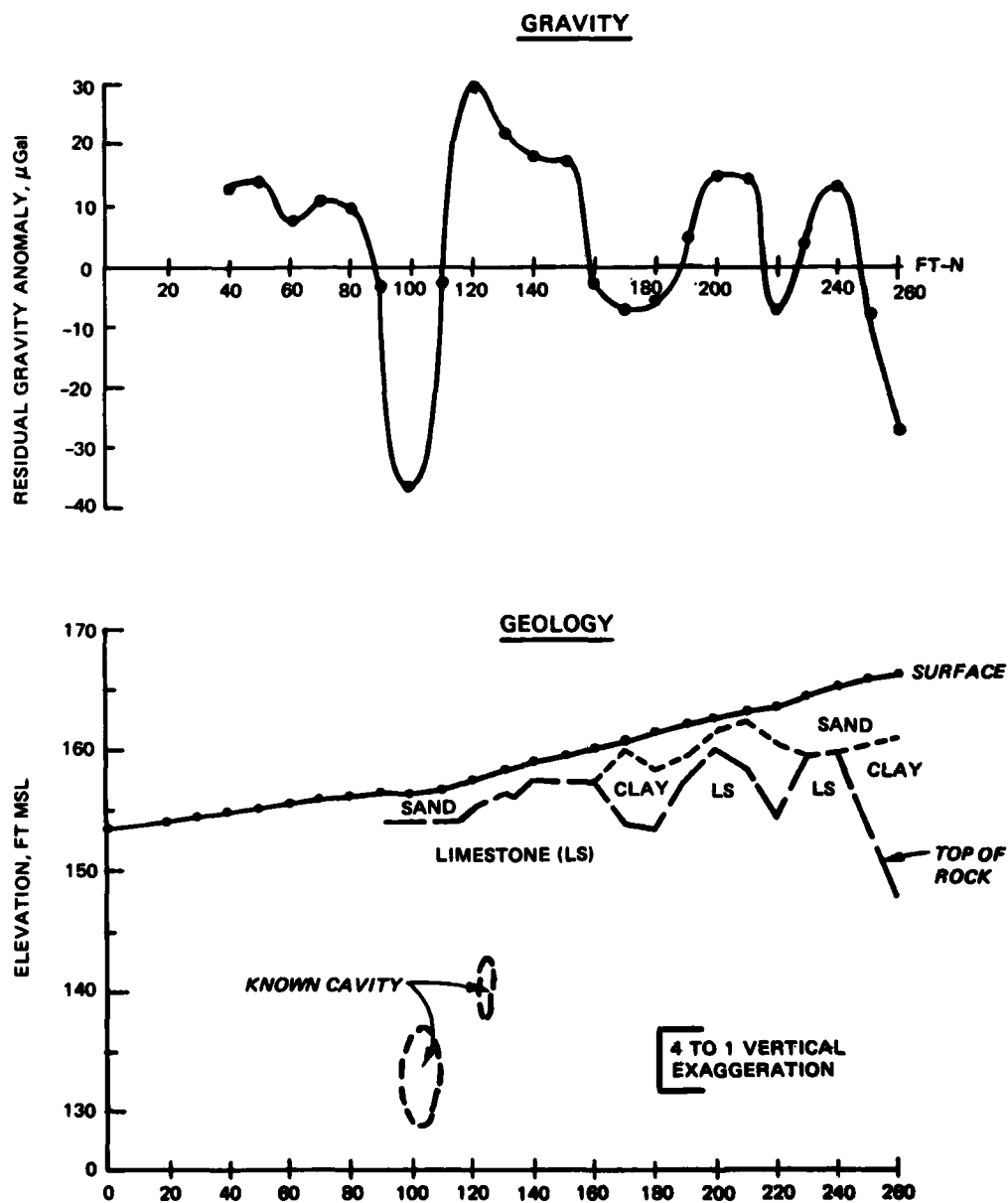
Figure 36. Geologic cross section and residual gravity profile along 80W north-south line

BORING (225, 40) — CORE RECOVERY

SAND, DK. BR. W/ORGANIC MATL.

SAND, LT. BR. W/SILT, CLAY, ROCK FRAG. — 40%

LIMESTONE, WHITE, SOFT POROUS, FOSSILIFEROUS

CAVITY

CLAY, BROWN, ? W/ROCK FRAG. — 83%

LIMESTONE, WHITE, SOFT, V. FOSSILIFEROUS, V. POROUS

V. SOFT (PASTE)

SOFT — 38%

CHERT, BR., HARD, W/LIMESTONE FILLED POROSITY — 28%

W/SMALL BROKEN PIECES OF CHERT

LIMESTONE, WHITE, SOFT, V. FOSSILIFEROUS, V. POROUS — 40%

BOH

BORING (110, 96) — CORE RECOVERY

SAND, CHAR. GRAY

SAND, TAN

LIMESTONE, WHITE

LIMESTONE, WHITE MED. HARD TO HARD, V. POROUS, V. FOSSILIFEROUS, SOME LARGE FOSSILS — 72%

LIMESTONE (AS ABOVE) — 78%

LIMESTONE, W/CHERT, SOFT TO HARD, MACROPOROSITY. SOFT — 68%

CAVITY

LIMESTONE, WHITE SOFT TO V. POROUS, V. FOSSILIFEROUS — 70%

LIMESTONE (AS ABOVE) — 83%

CAVITY

LIMESTONE, WHITE, V. SOFT — 38%

BOH

BORING (110, 0) — CORE RECOVERY

SAND, DK. BROWN V. CLAYEY

LIMESTONE, WHITE, SOFT TO MED. HARD, V. POROUS, V. FOSSILIFEROUS

CHERT, BR., HARD

CAVITY

CHERT, BR., HARD W/LARGE OPEN AND LS-FILLED POROSITY. SLIGHT TOOL DROPS — 43%

(AS ABOVE)

CAVITY

BOH

BORING (117, -5) — CORE RECOVERY

SAND, BROWN, V. CLAYEY

LIMESTONE, WHITE, SOFT — 100%

LIMESTONE, WHITE, SOFT TO MED. HARD, V. FOSSILIFEROUS — 100%

LIMESTONE (AS ABOVE)

CHERT

MASSIVE CORE LOSS. NO TOOL DROPS, BUT NO RECOVERY — 0

V. SOFT ZONE OR VOID

V. SOFT ZONE — 8%

SMALL AMOUNT OF CLAY, GRAY (MONTMORILLONITE)

VOID OR FILLED W/V. SOFT MATL. — 0

LIMESTONE, WHITE, SOFT, V. FOSSILIFEROUS — 70%

CHALKY

BOH

DEPTH, FT: 0, 5, 10, 15, 20, 25, 30, 35

DEPTH, M: 0, 1, 2, 3, 4, 5, 6, 7, 8, 9, 10

Figure 37. Core logs from borings placed to confirm presence of cavities or low density material beneath local negative gravity anomalies (BOH – bottom of hole)

(2.0 m) of sand. The interpretation of the negative gravity anomaly
is verified by the presence of the shallow cavity, although the greater
than typical soil thickness likely also contributes to the negative
anomaly. It is interesting to attempt a simple quantitative interpre-
tation for this anomaly. If it is assumed that the structure causing
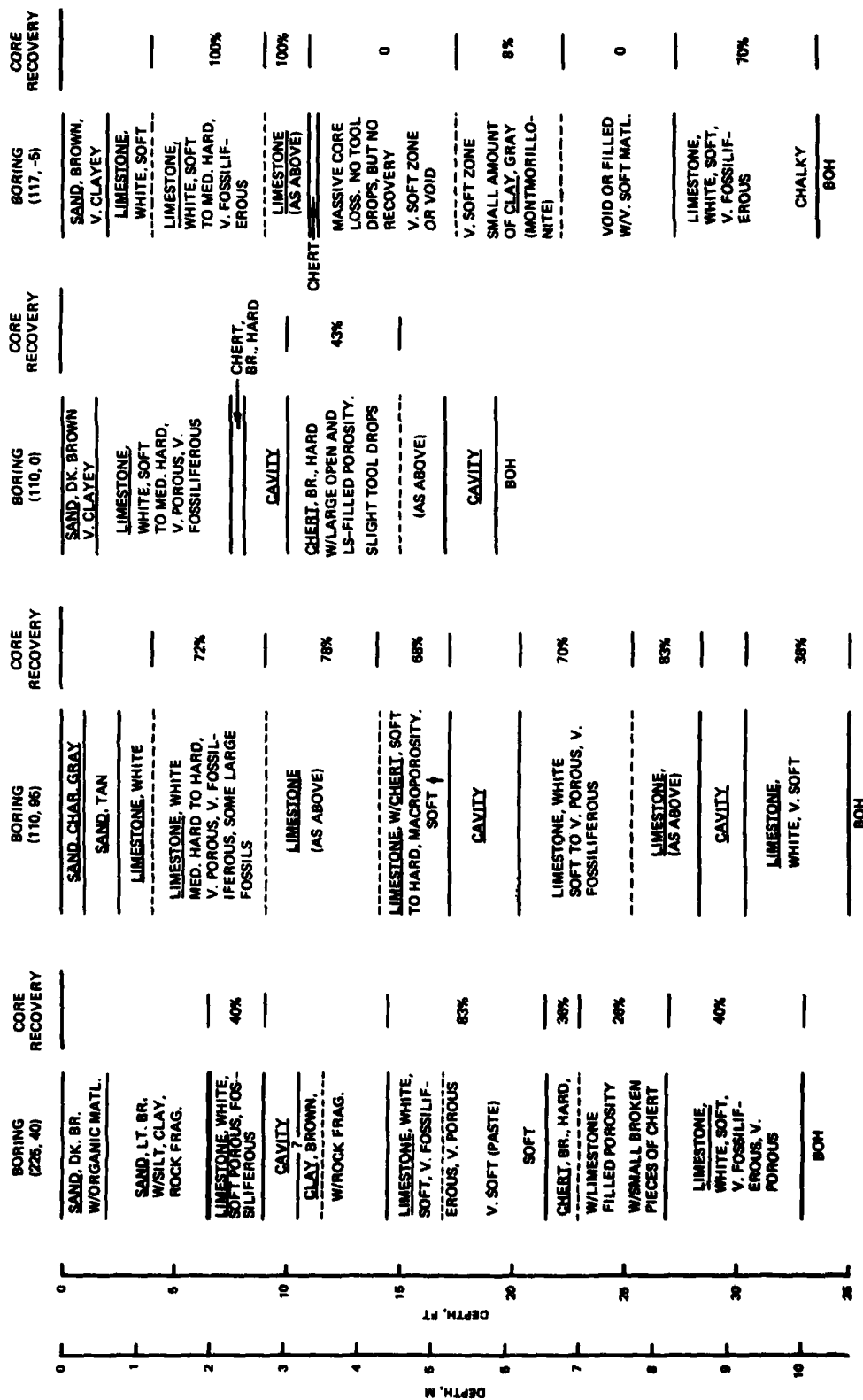the anomaly is spherical, then anomaly wavelengths of 9 to 15 ft (2.7
to 4.8 m) or depths to center of the spherical cavity of 11.7 to 19.5 ft
(3.6 to 5.9 m) are predicted. The lower estimate of depth to center
(11.7 ft) agrees fairly well with the boring log, although in general
the range of predicted depths is too large, due probably to an extended
area of thicker than typical soil cover.

76. Borings (110,0) and (117,-5) were in an area of negative
gravity anomaly but otherwise unknown subsurface conditions. Boring
(110,0) intercepted two open cavities and a zone of chert with very
large, open, and limestone-filled pores, with a total anomalous zone
thickness of 11 ft (3.4 m). This anomalous zone may have extended
deeper, but the diamond core bit broke off at a depth of 19.3 ft
(5.9 m). Boring (117,-5) only 9 ft (2.7 m) away from boring (110,0)
intercepted a total anomalous zone thickness of 16 ft (4.9 m).
Although there were no tool drops in this boring, only a small amount
of clay was recovered from the anomalous zone, suggesting the possible
presence of a very large clay-filled cavity. These data suggest that
the maximum negative gravity anomaly from this cavity would occur to
the east of the zero north-south survey line outside the microgravity
survey area.

77. Boring (110,95), in a negative gravity anomaly area, inter-
cepted a portion of the known cavity system at a depth 17.3 ft (5.3 m),
verifying approximately the original mapped depth. The boring apparently
penetrated a very large breakdown (limestone block) from 20.3- to 28.3-ft
(6.2- to 8.6-m) depth with a void beneath it. Limestone near the sur-
face in this boring is harder and denser than typical for the site.
Similar limestone (denser than typical, $\sim$0.2-g/cm^3 density contrast)
found near the surface in the vicinity of borings (120,80) to (140,80)
could explain the positive gravity anomaly in this vicinity in

Figure 36. Similarly, in the vicinity of the unexplained positive anomaly around (185,170), at about 3- to 5-ft (0.9- to 1.5-m) depth, a 5-ft- (1.5-m-) thick, hard, dense "molluscan" limestone ($\sim$2.3 to 2.4 g/cm^3) is encountered (probably the lower limestone member of the Hawthorne Formation of Miocene age). This could account for the positive anomaly, which apparently masks the anomaly caused by the cavity.

78. Borings (130,60) and (165,90) were placed in small negative anomaly areas (short spatial wavelength) with magnitudes of about -30 and -45 μGal, respectively. These negative anomalies appear as closed features on the anomaly map in Figure 35 (10-ft station spacing) but not in Figure 34 (20-ft station spacing). Boring (130,60) intercepted a clay-filled cavity extending from 8.7 to 18.3 ft (2.6 to 5.6 m) in depth. Boring (165,95) penetrated a clay pocket extending to a depth of 9 ft (2.7 m).

Summary

79. The microgravity survey at the Medford Cave site correlates very well with site geology. Even very subtle features on the residual anomaly maps can be indicative of real geology of interest in site investigations. With only one exception (near 185,170), all previously known cavernous conditions at the site were adequately mapped by the microgravity survey. All negative anomalies in areas with previously unexplored subsurface conditions, which were drilled in the confirmatory boring program, were found to be due to air- or clay-filled cavities or clay pockets in the top of the limestone surface. Cavities reliably detected by the microgravity survey ranged in depth from 9 to 25 ft (2.7 to 7.6 m) below the surface and were as small as 3 ft ($\sim$1 m) in vertical dimension.

80. It is possible for deeper objectives, such as cavities below the top of rock, to be masked by near-surface density variations. However, in geotechnical site investigations even the shallow density variations, such as clay pockets and limestone pinnacles, are exploration objectives. These shallow variations are a source of lithological "noise," but even in the presence of this significant noise source, the microgravity survey adequately mapped the known cavity system at the

88

site and led to the discovery of other unknown cavities. Since it is sometimes possible for the anomalies caused by deeper-seated sources (such as cavities below top of rock) to be masked by the anomalies due to shallower sources (i.e., by lithological noise), an ideal condition for conducting a microgravity survey might be at a site where the over-burden has been stripped away. However, at this stage, the option to abandon the site if foundation problems are encountered may no longer be available, the terrain corrections can become more difficult because of excavations, and construction noise (vibrations) can cause problems. As reported by Arzi (1975), these last two possibilities are not severe limitations.

81. The total labor in the field represented by the topographic survey and the microgravity survey was 13 "man-days." The best that could be expected from a two-man rotary rig drill crew (no geologist of inspector) in an equivalent field time would be about eight 50-ft-deep NX diamond core drill holes. For a similar "nonresearch-oriented" microgravity survey, data reduction and processing to produce anomaly maps are estimated to require about an additional 10 to 15 man-days. Thus, microgravimetry is found to be a very time- and cost-effective method for site exploration.

PART VI: A FIELD STUDY OF GRAVITY GRADIENT TECHNIQUES

Selection of Test Case

82. There has been much speculation on the feasibility and
utility of gravity gradient determinations (Evjen, 1936; Hammer and
Anzoleaga, 1975; Thyssen-Bornemisza et al. 1972). However, no defini-
tive study has been reported. This study is a preliminary attempt at a
definitive evaluation of gravity gradient techniques. Three criteria
guided the selection of the test case: (a) the anomalous structure
should be precisely defined; (b) the anomaly both in g_z and the gradi-
ents should be large (in a "microgravimetric sense") and should have
a relatively short wavelength; and (c) the structure should approximate
two-dimensional conditions. These criteria seemed most easily satisfied
by a shallow man-made structure. The structure chosen was the concrete-
lined drainage channel shown in Figure 38. Since the structure is at
the surface, the gravity anomaly is large and has a short wavelength.
Also, since the channel extends to either side of the bridge for at
least 100 m with no significant change in cross section, the structure
is approximately two-dimensional. The bridge itself is the only known
major non-two-dimensional (i.e., three-dimensional) aspect of the site.
Pertinent dimensions are given in the diagram in Figure 39, which will
also be the basis for two-dimensional model calculations.*

Survey Procedure

83. The survey over the drainage channel consisted of 16 sta-
tions over a 55-m line perpendicular to the channel along one side of
the bridge. The approximate center of the channel is at the 33-m

---

* Two-dimensional model calculations were accomplished using a computer
   program TALGRAD, which utilizes the algorithm of Talwani et al. (1959)
   to compute g_z profiles caused by an arbitrary number of polygonal
   cross-sectional structures. The program also allows for the computa-
   tion of $\Delta g_z/\Delta z$ and $\Delta g_z/\Delta x$ along the profile for arbitrarily speci-
   fied Δz and Δx.

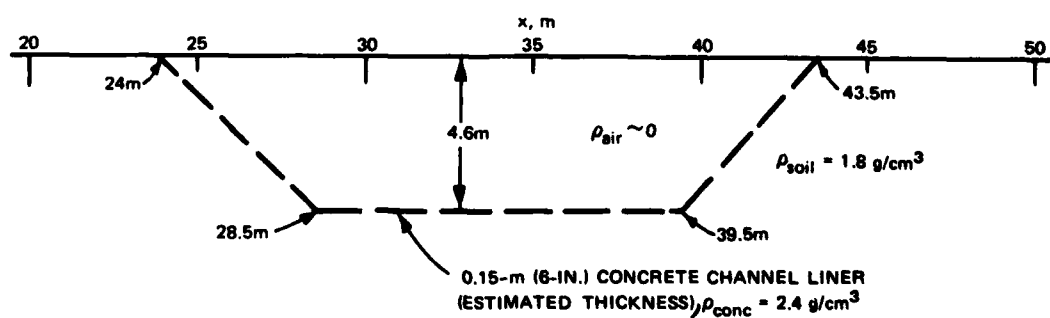Figure 38. Concrete-lined drainage channel chosen for gravity gradient field study

Figure 39. Geometry of drainage channel

position, which is also the location of the center bridge support (two columns and cross beam). At each station, g_z measurements were made at the ground surface elevation and at a nominal elevation of 1.3 m vertically above the ground station. No elevation or Bouguer corrections were necessary for the data (no elevation change). The data were corrected for latitude change in the station location in the usual manner. Linear drift corrections were applied to the data utilizing base station reoccupations, and the drift curves were compared with theoretical earth tide curves calculated for the site to verify consistent gravimeter performance.

Results

84. Results of the two-dimensional model calculations and the measured gravity data (at the ground surface elevation) are compared in Figure 40. The model profile results agree in anomaly amplitude and width with the measured data, with a major deviation being the approximately 70-µGal positive anomaly (relative to the model profile) between 30 and 36 m. However, this is precisely where the three-dimensional aspects of the structure, i.e., the bridge columns and cross beam, should make a positive contribution to the measured gravity profile. The positive contribution due to the column directly beneath the profile line should be about 30 µGal, with the remainder of the 70-µGal anomaly accounted for by the other column, the cross beam, and the remainder of the bridge. Negative anomalies (relative to the model profile) of unknown origin occur at the 15-, 20-, 49-, and 55-m locations. It is possible only to speculate regarding the origin of these negative anomalies (since drilling is not a possible option in this case). One possibility is the existence of regions of low-density fill material adjacent to the channel, perhaps associated with utility culverts.

85. Finite difference approximations ɔ the horizontal and vertical gradients of g_z along the profile were computed for the two-dimensional model and from the measured field data. Figures 41 and 42 present the horizontal and vertical gradient profiles, respectively, for
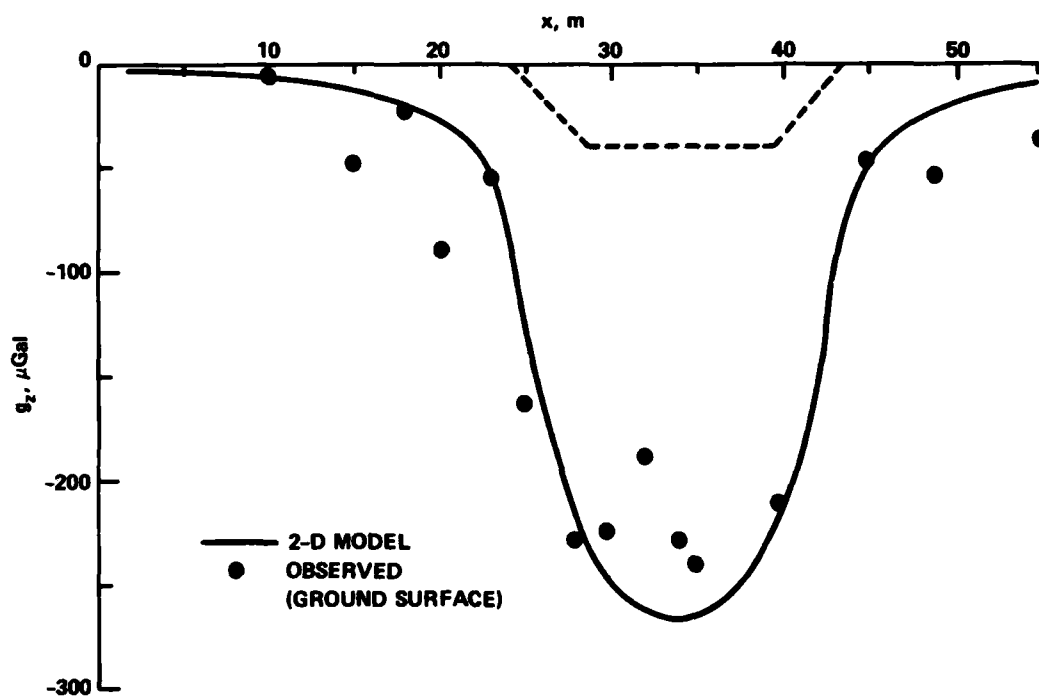
Figure 40. Gravity profiles across drainage channel--observed
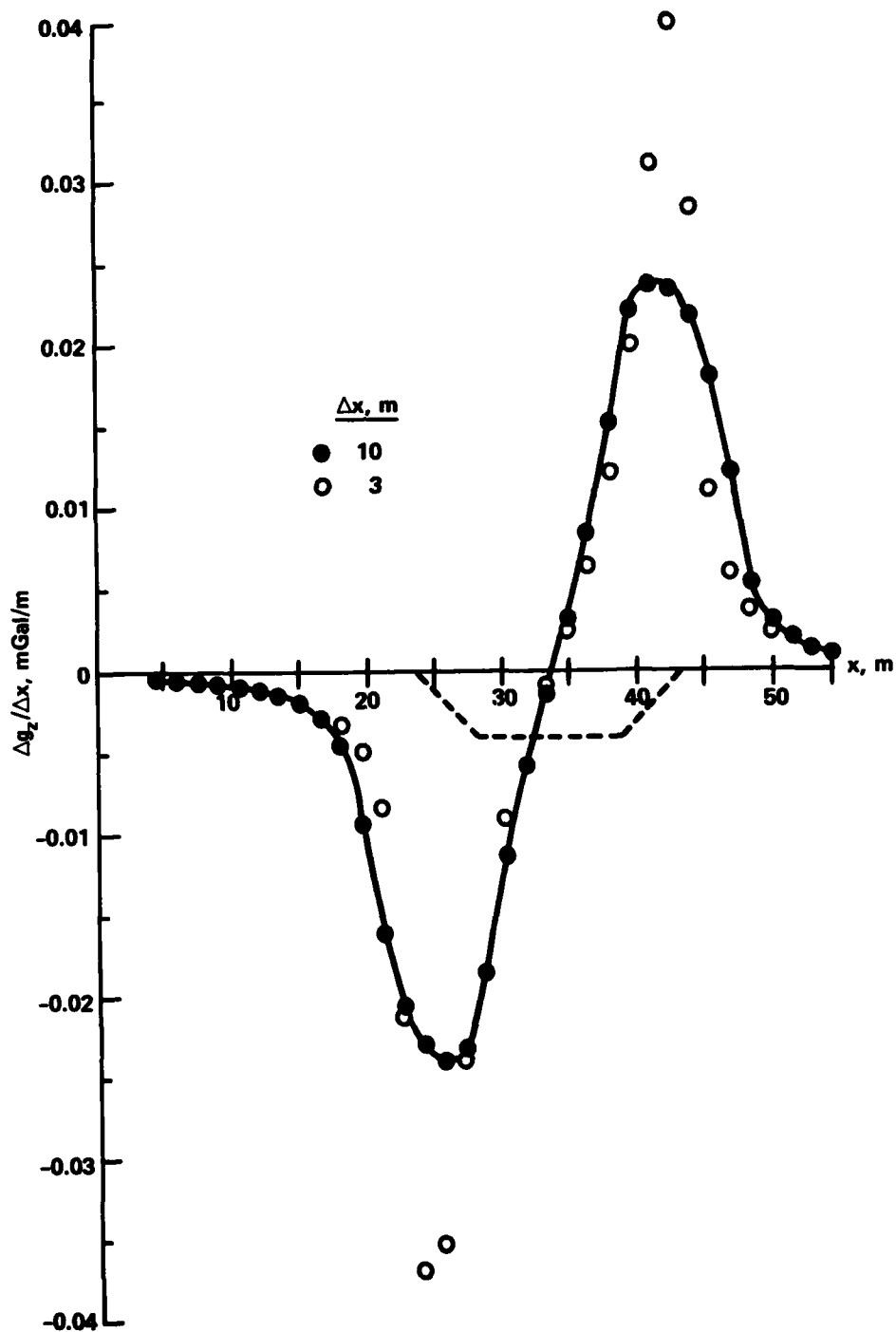and calculated from two-dimensional (2-D) model

93

Figure 41.   Analytical horizontal gradient profile
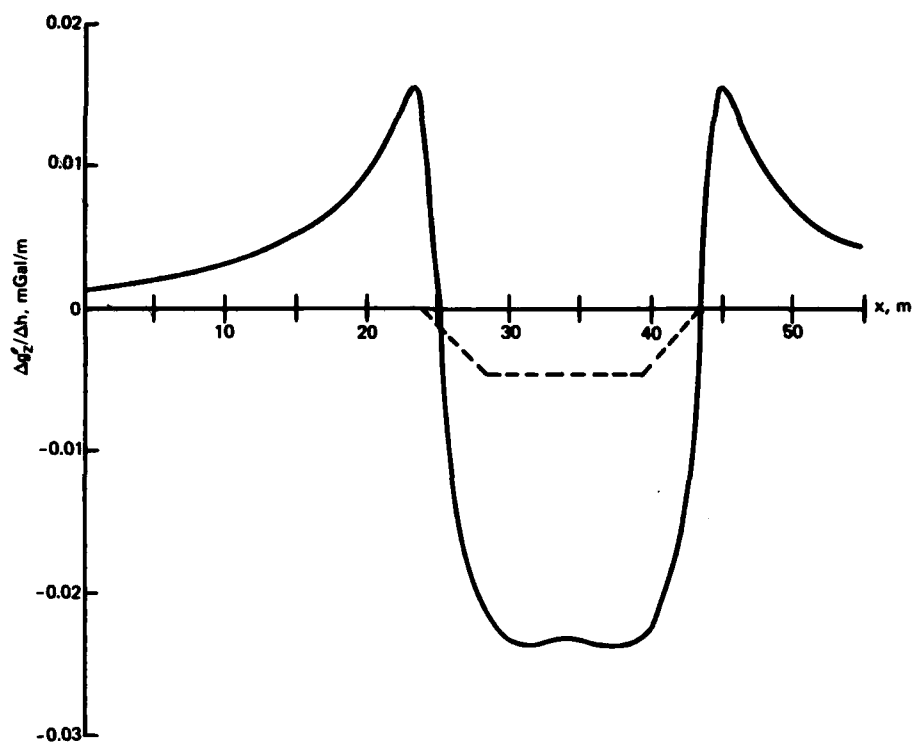for two-dimensional model

94

Figure 42. Analytical vertical gradient profile for the two-dimensional model with $\Delta h = 1.3$ m (gradient calculations made every 1.5 m along profile line, then plotted and connected with smooth curve)

the two-dimensional model. For the horizontal gradient (Figure 41), profile values were computed for $\Delta x = 3$ m and $\Delta x = 10$ m* . The finite difference approximation $\Delta g_z/\Delta x$ to $\partial g_z/\partial x$ should become better as Δx decreases; clearly, the horizontal gradient profile for $\Delta x = 3$ m is sharper and has greater amplitude than the profile for $\Delta x = 10$ m , as expected. The vertical gradient profile (Figure 42) was computed for $\Delta h = 1.3$ m , corresponding to the nominal value used for the field

* Calculated horizontal gradient values are plotted at the midpoint of the Δx-interval in Figure 41 as well as in Figure 43. For the $\Delta x = 10$ m case in Figure 41, calculated values are plotted every 1.5 m along profile line and connected with a smooth curve; while for the $\Delta x = 3$ m calculations, only selected values are shown (open circles) for comparison.

measurements. Note that the four corners of the trapezoid are fairly well defined in Figure 42 by the vertical gradient profile.

86. Horizontal and vertical gradient profiles in Figures 43 and 44 were determined from the field data. The horizontal gradient values are shown for various values of Δx (corresponding to various possible combinations of stations); however, the dashed line connects points for $\Delta x = 10$ m . The comparison between the analytic model (Figure 41) and the horizontal gradient profile (Figure 43) is quite good for the curves for $\Delta x = 10$ m , both in general shape and in amomaly amplitude and width. Also, the general trend of increasing anomaly amplitude and sharpness with decreasing Δx is seen in the measured data in Figure 43. The measured vertical gradient data presented in Figure 44 (note the different gradient axis scale compared with Figure 42) are erratic, and only with a certain amount of smoothing do the results resemble the results in Figure 42 for the two-dimensional model. There are several possible reasons for the erratic nature of the vertical gradient data:

  a. The value $\Delta z \sim 1.3$ m is too small for the vertical separation between measuring stations due to the probable error in the measurements, i.e., a larger Δz would result in a larger $\Delta g_z'$ and hence decrease the significance of the probable error.

  b. The vertical gradient determination is more strongly affected by the three-dimensional aspects of the structure than the horizontal gradient determination.

  c. The vertical gradient is known to be strongly influenced by very shallow density fluctuations, so a preferable procedure might be to make the lower g_z measurement some small distance, about 0.2 m, above the ground surface.

The two large positive values of measured vertical gradient between 30 and 35 m are due to the bridge pillars and beams; the negative vertical gradient excursion at 15 m is associated with the negative gravity anomaly noted earlier at that location. In a positive sense, however, the measured vertical gradient results in Figure 44 demonstrate the enhancement of an anomaly caused by a shallow source (the bridge support) relative to a local regional field (the field due to the channel itself).
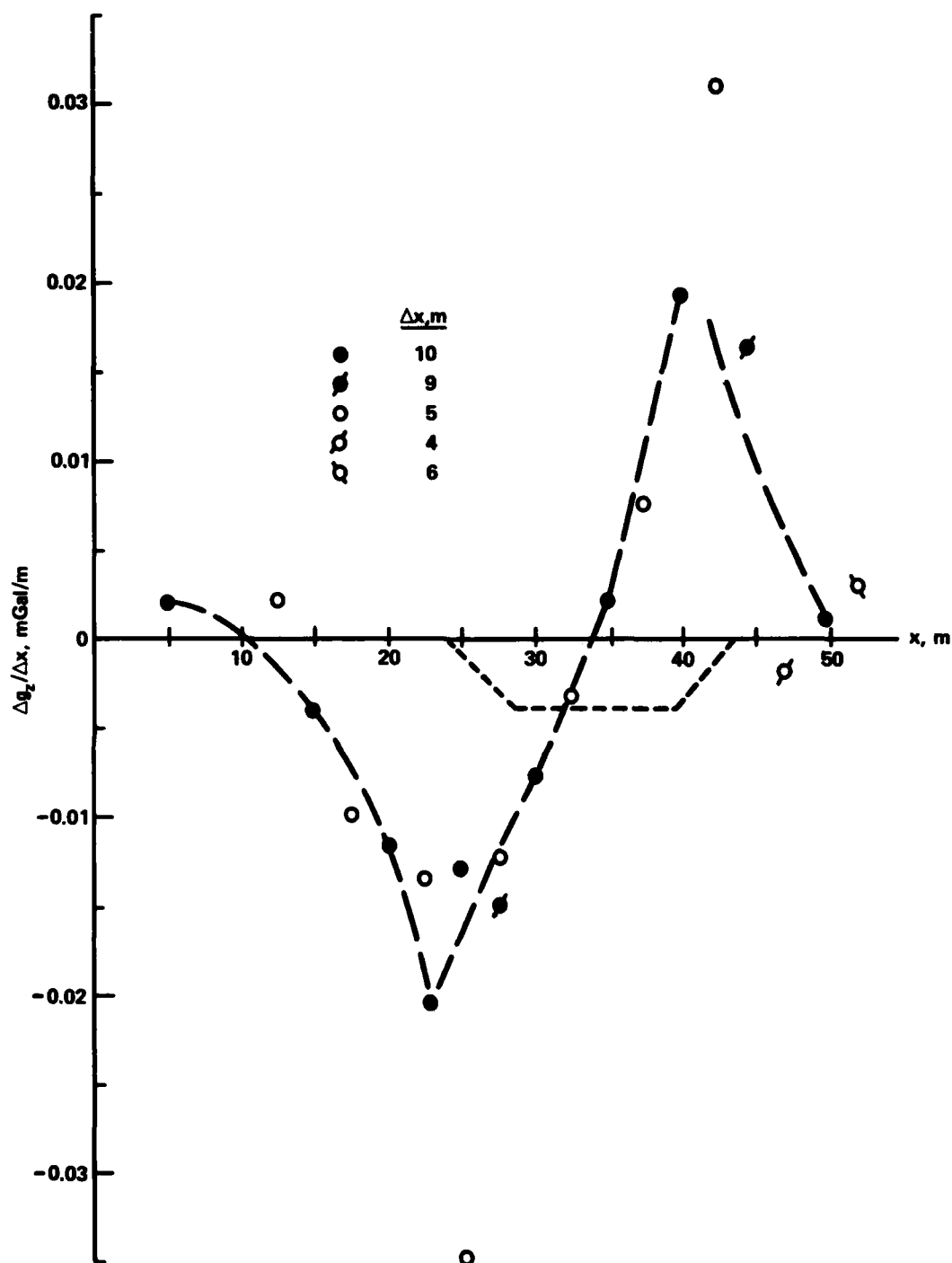
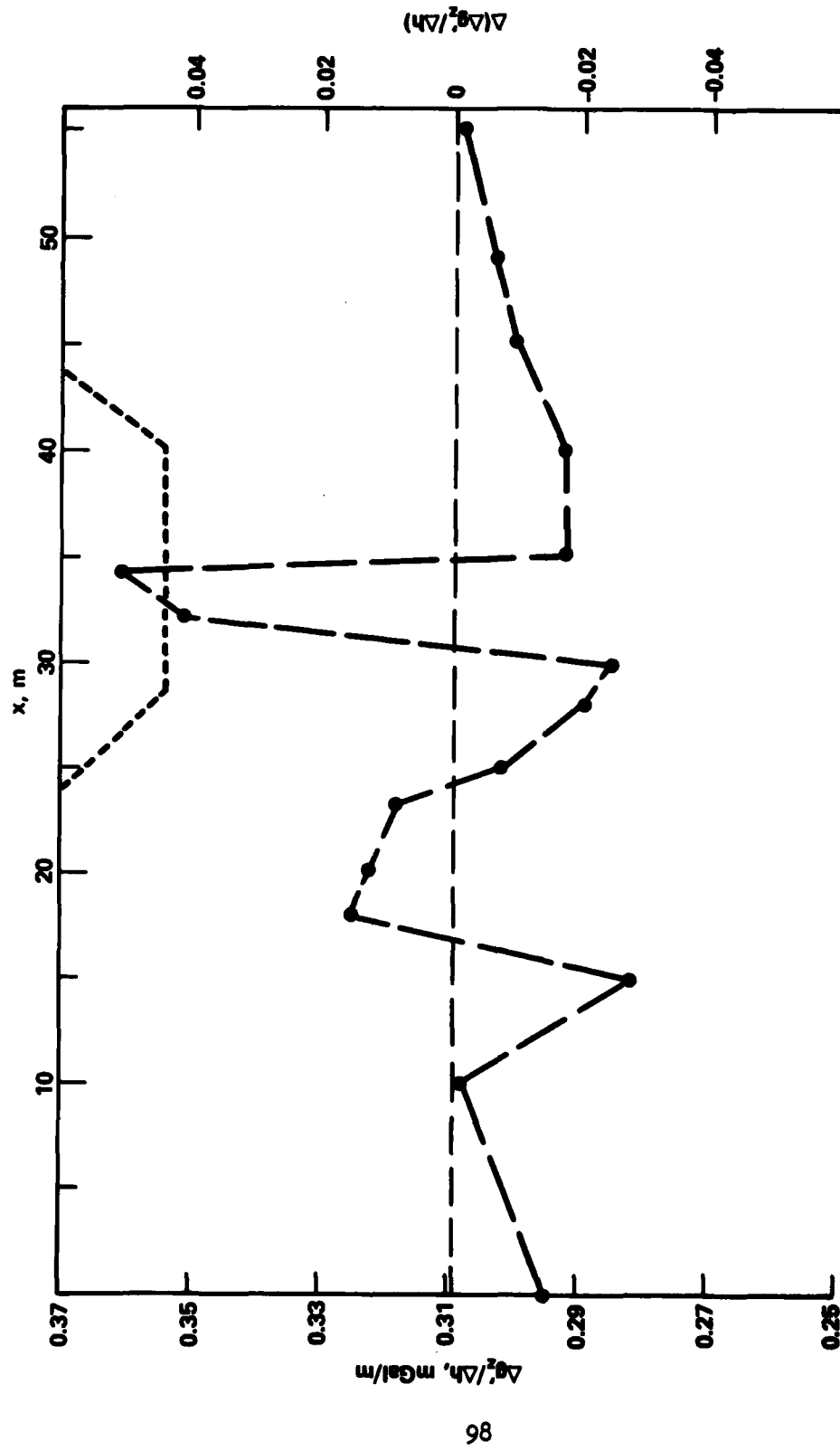Figure 43. Measured horizontal gradient profile across drainage channel

97

Figure 44. Measured vertical gradient profile across drainage channel with
Δh ~ 1.3 m

Calculation of Vertical Gradient Profile
from the Horizontal Gradient Profile

87. Utilizing the horizontal gradient profile from the two-dimensional model calculations (Figure 41), the vertical gradient profile shown in Figure 45 was computed using the Hilbert transform relation and computer program mentioned earlier. Except for the sign reversal (caused by assuming the z-axis vertically downward for the two-dimensional model results), the vertical gradient profiles shown in Figures 42 and 45 agree very well qualitatively. The lower amplitudes and frequency content of the profile computed by the Hilbert transform are not unexpected; however, the comparison would improve if the profile itself were longer and/or a smaller Δx were used for the horizontal gradient profile.

88. Similarly, a vertical gradient profile shown in Figure 46 was computed from the horizontal gradient profile of the measured data (Figure 43) over the structure using the Hilbert transform. To facilitate comparison among the various vertical gradient determinations (measured and computed), the vertical gradient curves from Figures 42, 44, 45, and 46 are plotted in Figure 47 to the same scales and using the same sign convention for all four curves. There is good qualitative agreement between all the curves except for the anomalies on the observed vertical gradient curve noted earlier, which are due to shallow anomalous features. The curve, which is the Hilbert transform of the observed horizontal gradient profile, is seen to exhibit lower spatial frequency behavior than the other curves. It is expected that this condition would improve if the observed horizontal gradient profile were more densely sampled. To investigate this possibility, all possible combinations of g_z data were utilized to give a horizontal gradient data value every 2.5 m along the profile (instead of every 5 m with $\Delta x = 10$ m as was used for Figure 46), and then the Hilbert transform was taken of this more densely sampled profile. The results shown in Figure 48 confirm that transforming the more densely sampled profile yields a vertical gradient profile that more closely resembles the

99

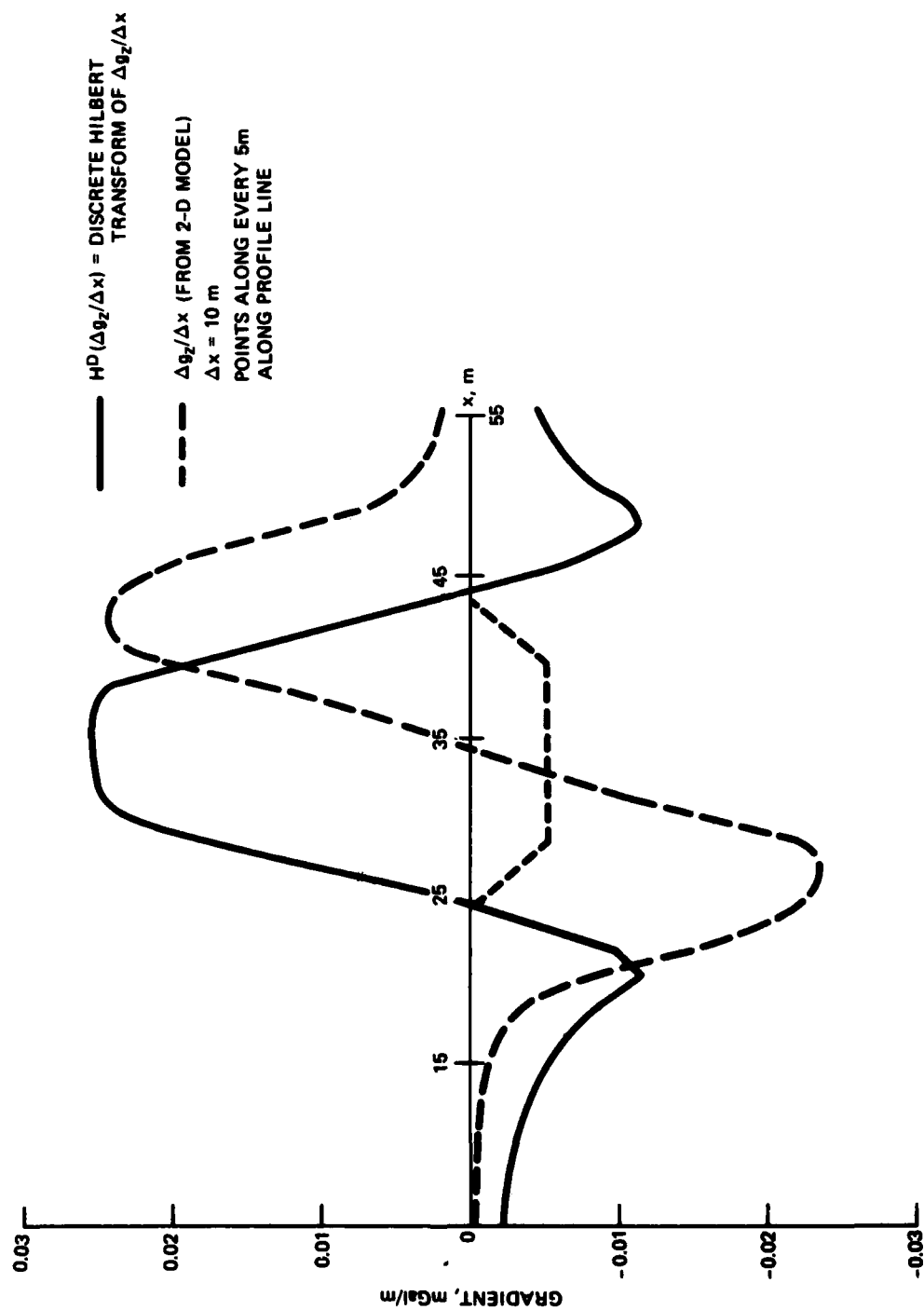Figure 45. Calculation of vertical gradient profile from the theoretical horizontal gradient profile for the two-dimensional (2-D) model by a discrete Hilbert transform

100
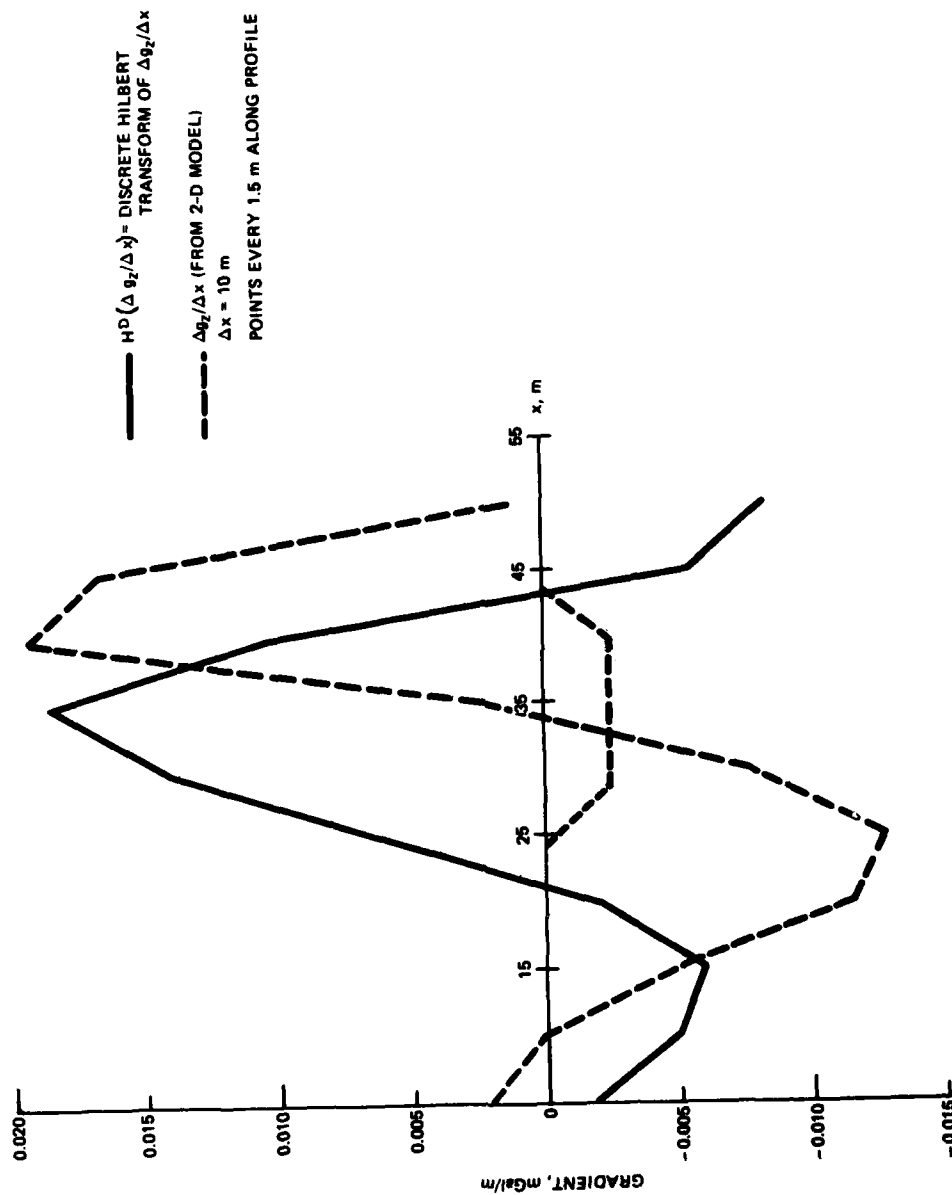
Figure 46. Vertical gradient profile calculated from measured horizontal gradient profile by a discrete Hilbert transform

101

Figure 47. Comparison of measured and computed vertical gradient profiles across the drainage channel
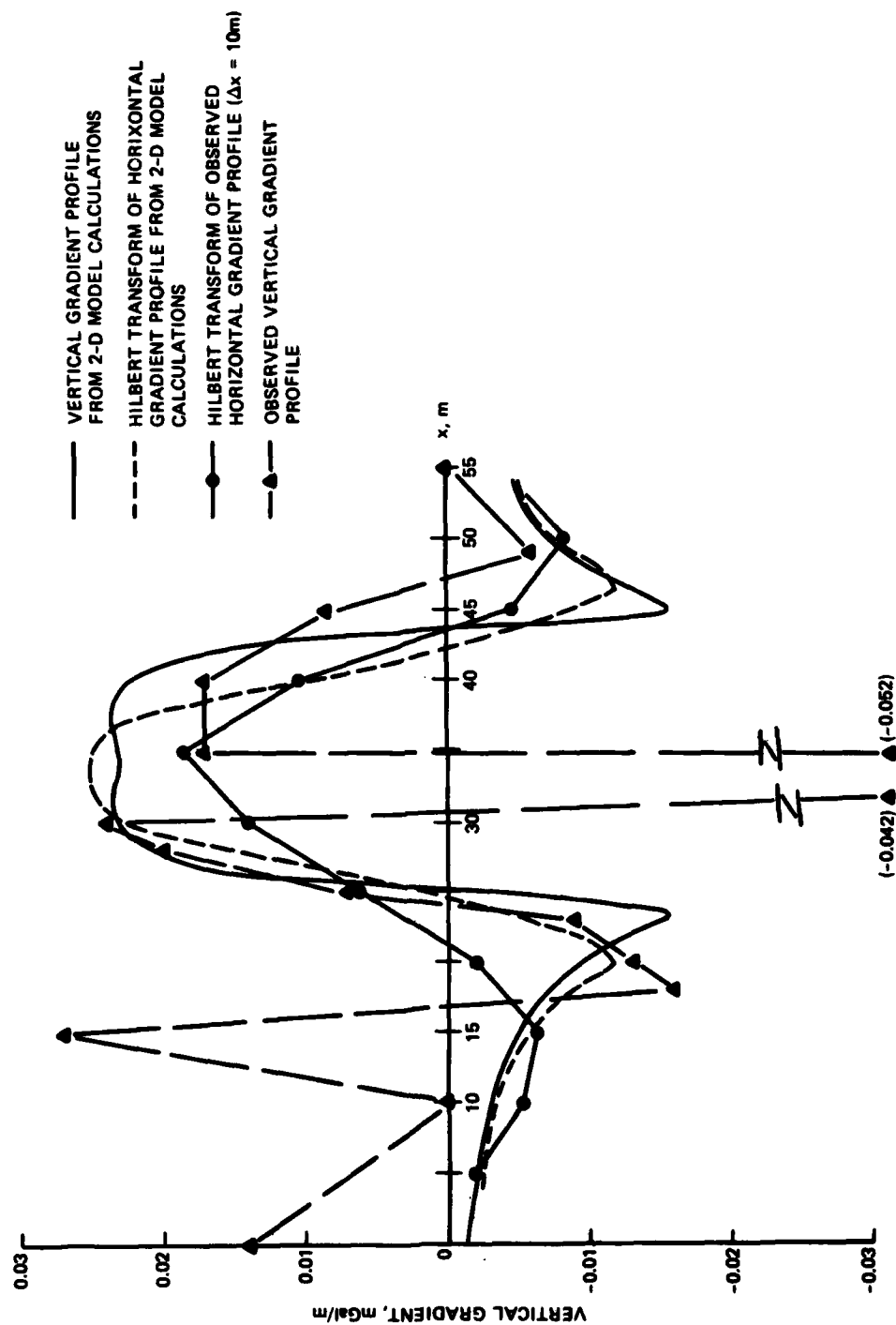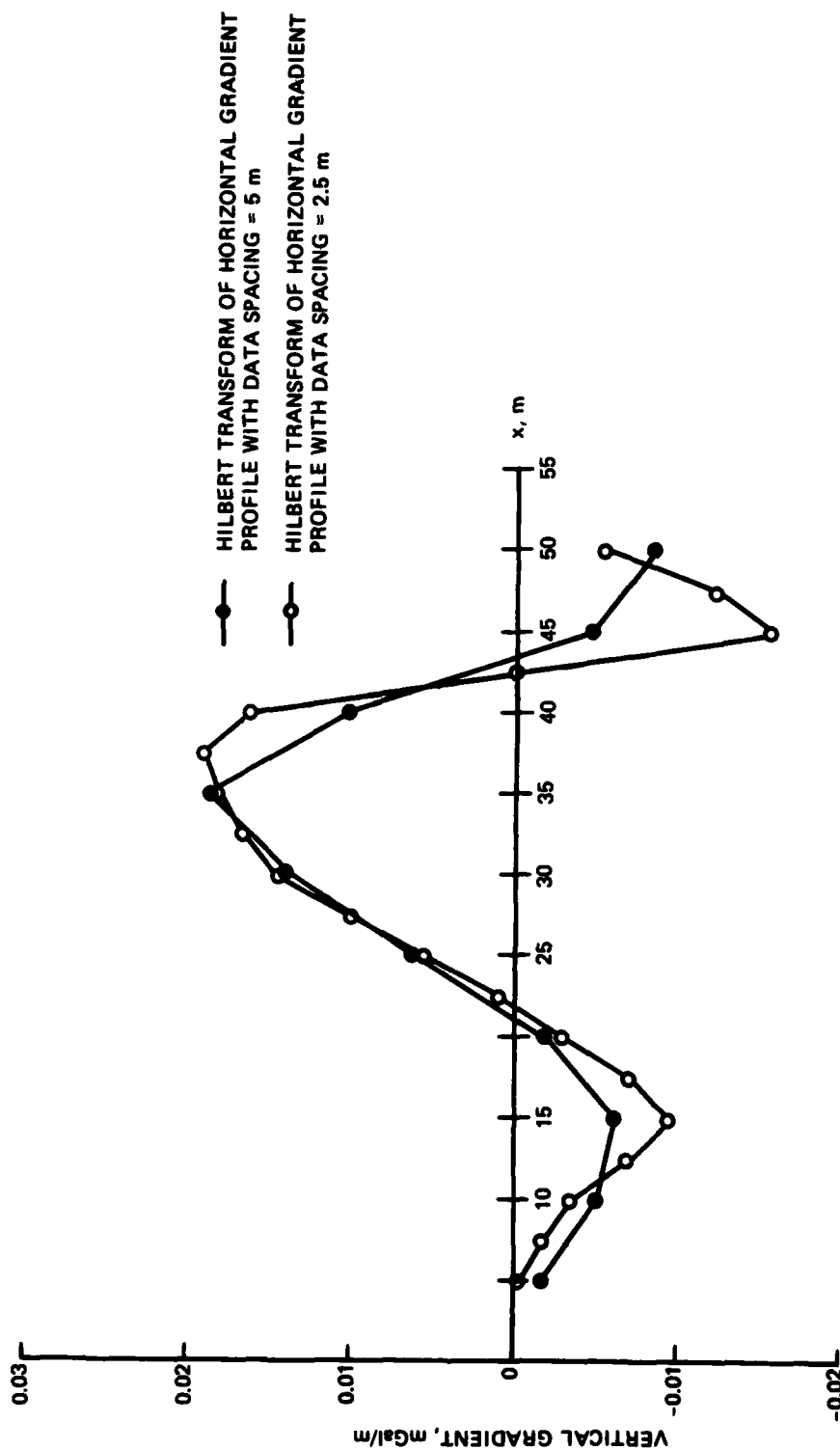
Figure 48. Comparison of vertical gradient profiles calculated from observed horizontal gradient profiles by a discrete Hilbert transform (two curves correspond to different data spacings along the horizontal gradient profiles)

analytical profile from the two-dimensional model calculations. Thus, the procedure for determining the horizontal gradient profile from field measurements and then calculating the vertical gradient profile via the Hilbert transform is very promising.

Utilization of Gravity Gradients

89. The motivations for determining gravity gradients have been discussed previously. A complete discussion of the possibilities for utilization of gradient data for subsurface structure delineation is beyond the scope of this report. Thus, the concepts under consideration will only be covered briefly.

90. A very promising technique for displaying the gradient data is a gradient space plot, i.e., $g_{z,z}$ versus $g_{z,x}$. In such a space, each point will correspond to a given profile position or value of x . As an example, the gradient profile data for the two-dimensional model (Figures 41 and 42) result in the gradient space plot in Figure 49. Corresponding points along the profile and the plot are indicated, and the manner in which the geometry of the structure might be deduced is indicated.

91. Another promising technique involves the concept of the analytic signal (Bracewell, 1965) along the profile, defined by $A(x) = g_{z,x}(x) - ig_{z,z}(x)$. Note that the gradient space plot is just a complex plane plot of the components of $A(x)$. The amplitude of $A(x)$ is defined in the usual manner, $a(x) = |A(x)| = (g^2_{z,x} + g^2_{z,z})^{1/2}$. Above a two-dimensional structure with corners, $a(x)$ will be the superposition of symmetrical, bell-shaped curves, one for each of the corners. The properties of the bell-shaped curves determine the profile position and depth of the structural corner causing the signal. Thus, the decomposition of the $a(x)$ signal into bell-shaped curves represents in principal the solution of the structural problem.
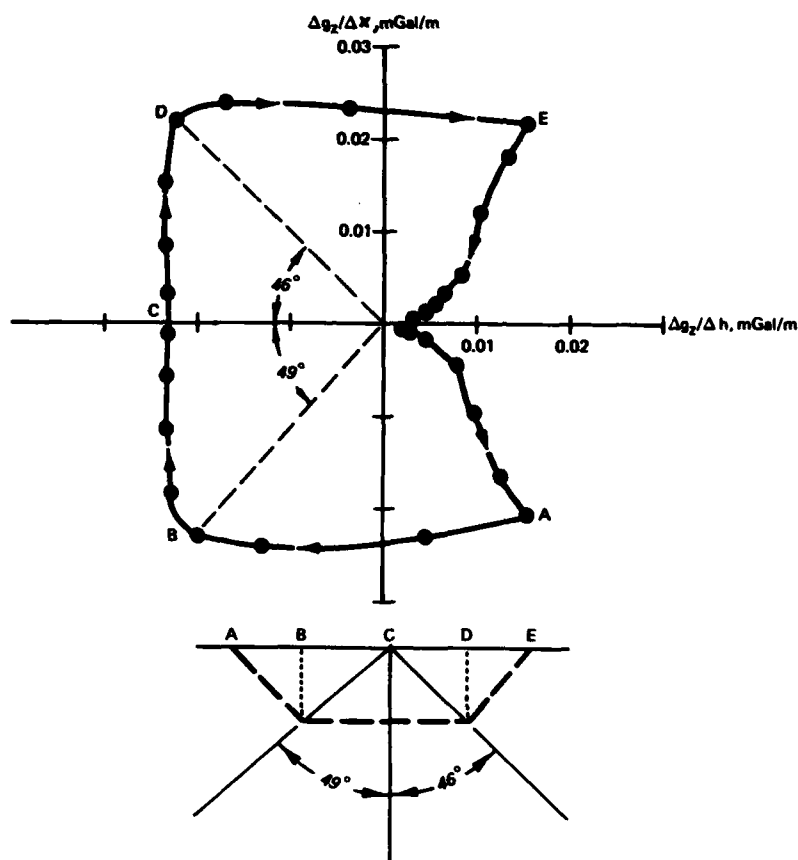
Figure 49. Gravity-gradient space plot for
two-dimensional model

Summary

92. The horizontal gravity gradient profile has been adequately
determined from a microgravimetric survey and compared with the results
of a two-dimensional model study. The theoretical model results were in
agreement with the measured profile. Measurement of the vertical gradient profile with a relatively short tower structure ($\Delta z = 1.3$ m) was
erratic at some profile locations due presumably to both known and unknown shallow anomalous conditions, but otherwise was in qualitative
agreement with the theoretical model results. Utilization of the Hilbert transform allows the vertical gradient profile to be calculated from

the horizontal gradient profile (which eliminates the need for use of a tripod). For cases in which the assumption of a two-dimensional, polygonal cross-sectional geometry is approximately valid, use of the gradient profiles permits a unique structural interpretation. Future work in this research effort should concentrate on: (a) continued attempts to determine vertical gradient profiles across known structures using larger values of Δz than in the past; (b) further study of the application of the discrete Hilbert transform to calculate vertical gradient profiles from measured horizontal gradient profiles; and (c) in-depth studies of interpretative methods using the gradient data.

PART VII: ASSESSMENT OF MICROGRAVIMETRIC SURVEYS FOR DETECTION
OF ELEVATION CHANGES CAUSED BY RESERVOIR IMPOUNDMENT

Introduction

93. One of the primary observable effects of the impoundment of
large reservoirs is the deflection of the earth's surface, presumably
due to the imposed load. For small reservoirs, elevation changes may be
immeasurably small, while for large reservoirs, elevation changes are
easily observed. Also associated with reservoir filling (as well as
with subsequent seasonal changes in reservoir level) are changes in
groundwater levels and the forcing of pore fluid deep into basement
rocks. The objective of this phase of the study is to assess the
potential of microgravimetric surveys for the detection of elevation
changes caused by reservoir impoundment. The possibility of studying
subsurface mass movements (pore fluid diffusion, groundwater table
fluctuations, etc.) by coupling microgravity surveys with precise sur-
face leveling surveys is also considered.

Microgravimeters and Detectable Elevation Changes

94. The normal free-air gravity gradient is approximately
0.3086 mGal/m (0.09405 mGal/ft).* An elevation change of 1 cm (0.0328
ft) at a given gravity survey point, with no associated mass loss or
gain in the subsurface, would produce a change in the vertical component
of the gravitational attraction of about 0.003 mGal or 3 µGal. Studies
have shown that with careful <u>repeat</u> gravity measurements of stations in
a survey net with a LaCoste & Romberg Model-D gravimeter,** it is possible
to obtain solutions to the survey net with a precision and accuracy in
the estimate of relative gravity values of 1 to 2 µGal (Lambert and
Beaumont, 1977; McConnell et al., 1974; and Neumann, 1972) with a high

---

*   1 Gal = 1 cm/sec^2.
** The LaCoste & Romberg Model-D Gravimeter has a reading sensitivity
    of about 1 µGal.

confidence level. Thus, using a true "microgal" instrument, such as the
Model-D, with extreme care, it should be possible to detect elevation
changes or differences of 1 cm (~0.03 ft) by repeat surveys of the same
gravity survey net at different times. The precision and accuracy
achieved in "routine" microgravity site surveys with the Model-D meter
to determine relative gravity variations is 3 to 6 μGal (Arzi, 1975;
Butler, 1979; Lambert and Beaumont, 1977; and McConnell et al., 1974).
Thus, even in this context, elevation changes or differences of 2 cm
should be detectable by repeat surveys.

Crustal Deflection Observations and Calculations

95. Downward crustal deflections have been observed following
the impounding of many reservoirs. Elevation changes of 20 cm (0.66 ft)
have been measured at Lake Mead, Arizona, agreeing very closely with
elastic deflection calculations (Westergaard and Adkins, 1934). At
Lake Kariba, Rhodesia, the third largest man-made lake in the world,
deflections along a carefully repeated level traverse were as great as
13 cm (0.43 ft) next to the reservoir and agreed almost exactly with
elastic deflection calculations (Gough and Gough, 1970a, b). The calcu-
lation for Lake Kariba predicted a maximum deflection directly beneath
the reservoir of about 25 cm (0.82 ft). Similar calculations have been
made for four other smaller reservoirs (Beck, 1976; Green, 1973; Gupta,
1976; and Lee, 1972). The calculated maximum vertical deflections and
total surface loads represented by the six reservoirs are summarized
below.

108

Reservoir	Total Surface Load kg	Calculated Maximum Vertical Deflections cm
Kariba (Rhodesia)	1.5×10^{14}	25.0
Mead (USA)	4×10^{13}	20.0
Gordon (Tasmania)	1.5×10^{13}	7.0
Hsinfengkiang (China)	1.2×10^{13}	10.0
Oroville (USA)	4.4×10^{12}	5.5
Hendrick Verwoerd (South Africa)	3.2×10^{12}	3.2

Note: 1 kg = 1.1×10^{-3} tons; 1 cm = 0.0328 ft.

96. Using the data tabulated above, Figure 50 presents a rough picture of the relation of total surface load and maximum calculated elastic deflection and/or observed deflection. The dashed line indicates the trend of the data. The data for the six reservoirs suggest a consistent relation between total surface load and deflection. The reservoirs have a different areal extent and varying water depths distributions; of course, for the field observations all of the complexities of different geologies are present. Despite these differences, these data seem to imply that the total load is the key parameter in determining deflection. For the Oroville Reservoir, results of measurements of elevation change near the reservoir are smaller than corresponding values from the calculation (Figure 50). However, the elevation change data for Oroville are complicated by the question of how much of the total observed elevation change is due to reservoir loading and how much is due to the 1975 Oroville earthquake (Beck, 1976; Savage et al., 1977).

Associated Gravity Changes

Elevation change alone

97. Considering the free-air gravity changes due to the elevation changes and neglecting any other effect at this point, the maximum to be expected from reservoir impoundment would be about 75 µGal for an
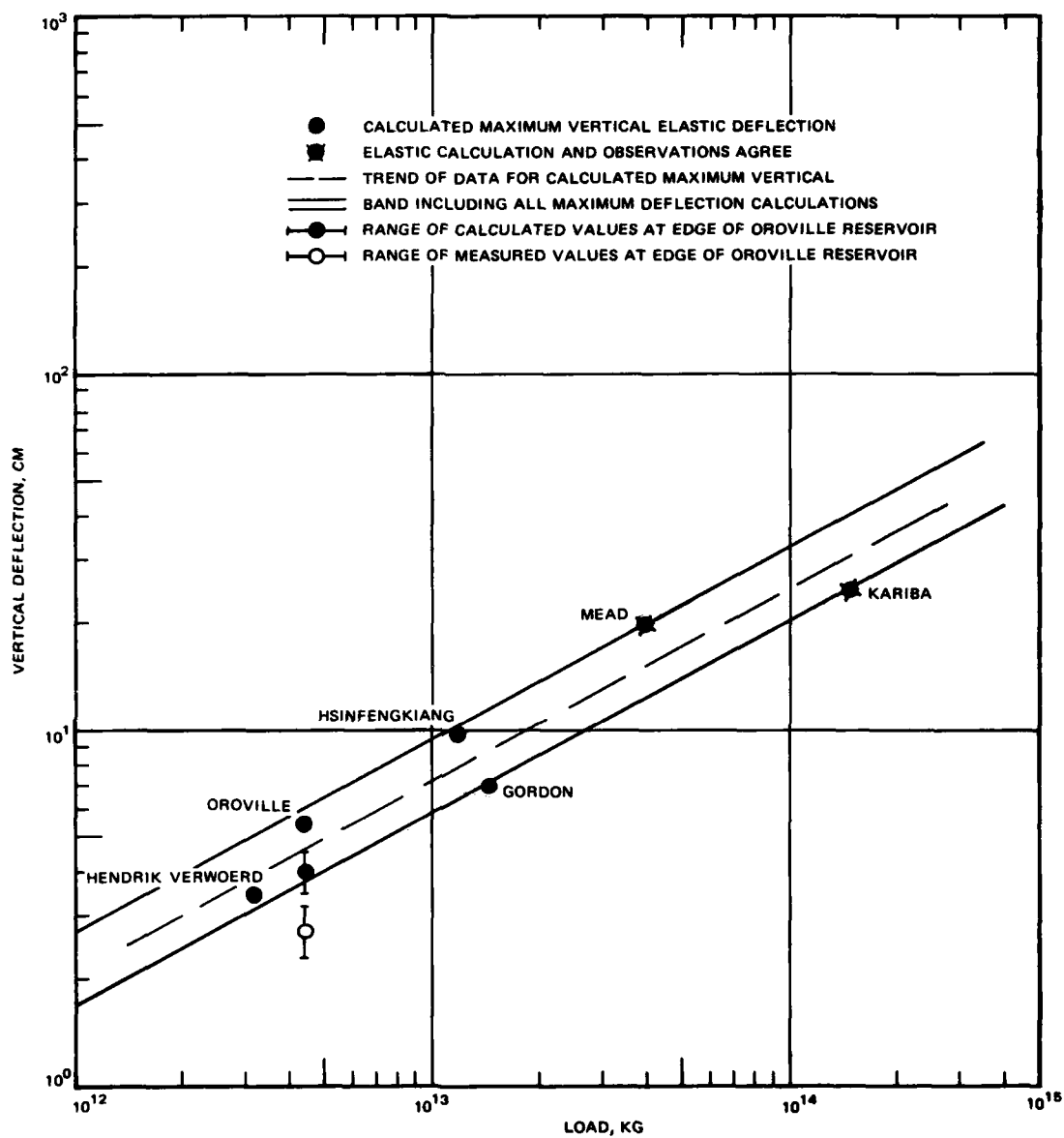
Figure 50. Vertical deflections, calculated and observed, as a function of total surface load for six reservoirs

"elastic-type" crustal deflection. However, cases in which a large earthquake occurs in the vicinity of a reservoir may exhibit locally greater elevation and gravity change (Guha et al., 1974). A deflection of 75 μGal is an upper limit from a practical point of view since the corresponding deflection would probably be directly under the reservoir. For Lake Kariba, 20 cm (0.66 ft) represents about the maximum deflection accessible to measurement, or about a 60-μGal gravity change. A 60-μGal gravity change is well within the detectability limits of the Model-D gravity meter and could possibly be detected with standard gravity instruments, such as the Worden or LaCoste & Romberg Model-G, with careful survey procedures. On the lower end of the spectrum, it seems that with the utmost care in surveying the gravity traverses, a gravity change as small as 3 μGal may be ultimately detectable with a reasonable degree of confidence with an instrument having microgal precision and accuracy such as the Model-D. A 3-μGal gravity change implies a 1-cm (0.03-ft) elevation change (assuming no other interfering effects). From Figure 50, this seems to imply that microgravimetry will be of possible usefulness in detecting vertical deflections of the crust only for reservoirs representing loads of the order of 10^{12} kg (1.1 x 10^9 tons or a value of 0.81 million acre-ft) or greater.

Interfering time effects

98. The assessment thus far has made the rather idealistic assumptions that there are no interfering effects, i.e., that gravity differences are solely due to elevation changes. Introduction of the time factor is the primary source of interfering effects. The following is a partial list of time-related phenomena affecting the assessment:

<u>a.</u> Even though observed deflections agree with elastic deflection calculations, the response time for deflections probably cannot be "instantaneous" considering the geologic scale.

<u>b.</u> Filling of the reservoir will not only raise the water table around the reservoir but force water deep into basement rock, and the time lapse for water to diffuse following reservoir filling may be hundreds of days.

<u>c.</u> Reservoir level fluctuations will cause groundwater level fluctuations with time lags similar to that discussed in item <u>b.</u>

    <u>d</u>.   Rainfall percolation into the subsurface can have a
significant effect on gravity readings by causing
seasonal fluctuations in groundwater levels.

    <u>e</u>.   Earth-tide effects must be included in the gravity data
analysis.

    <u>f</u>.   Long-term drift in gravity meter.

    <u>g</u>.   Background noise level.

99. The groundwater level changes (items <u>b-d</u>) cause mass changes
that cannot be separated from elevation changes in the overall gravity
effect without <u>independent</u> information on <u>either</u> the groundwater level
variations or the elevation changes. Item <u>a</u>, of course, implies that a
long-term monitoring program will be involved, i.e., reading a survey
net two or three times a year over a several-year period before and
after reservoir filling. The data can be corrected for earth-tide
variation by the use of theoretical earth-tide programs or a base sta-
tion gravity tidal recording meter.

100. The subsurface mass changes represented by groundwater level
fluctuations and caused by rainfall and reservoir level fluctuation
are considered to be a major problem. One solution is to coordinate
precise leveling surveys with the gravimetry. While this would not
have the effect of determining elevation changes directly with gravi-
metry, it would allow the separation of elevation effects from mass
change effects in the gravity data. This separation would be of con-
siderable importance in assessing the overall effects of reservoir
impoundment (such as the possible role played by water movement and
pore pressure increases in triggering earthquakes). It would be neces-
sary in this regard to begin the gravity survey several years before
impoundment in order to have knowledge of the effects on gravity readings
caused by normal, seasonal groundwater fluctuations. Another feasible
solution to the problems of subsurface mass change effects on the gravity
data is to locate the gravity stations on outcrops of "impermeable"
bedrock if possible; this would at least minimize the effects. A third
possibility is to correlate the gravity surveys with independent infor-
mation on groundwater level fluctuations provided by piezometers or other
instruments. Knowledge of the groundwater level at the time of each

survey would allow the separation of gravity changes caused by elevation changes from those caused by groundwater level changes. In general, previous work has indicated 10- to 30-μGal changes in some areas resulting from seasonal water table fluctuations (Lambert and Beaumont, 1977). Changes in the 30- to 40-μGal range have been observed by the author in repeat surveys over a test area before and after heavy rains (presumably caused by very shallow groundwater concentrations).

Survey procedure

101. The survey procedure itself is of crucial importance. The same meter should be used over the complete traverse, and each traverse should be completed in the minimum time possible. One procedure for randomizing reading and long-term drift errors (items $\underline{f}$ and $\underline{g}$ in paragraph 98) is to use more than one instrument for the survey; however, it is essential that each instrument be used over the complete traverse and the data be reduced separately prior to combination. The survey grid points should be substantial concrete monuments extending below the depth of seasonal volume change (frost heave, thermal expansion, etc.) or at least about 0.5 m (1.64 ft) below ground surface. Gravity meter elevation relative to the monument should be repeated to within 0.3 cm (0.01 ft) or closer to keep errors from this source to ±1 μGal or less. Also, reading should be synchronized to the tidal variation, so that repeat readings at stations are taken at similar points on the tidal curve as earlier readings. This synchronization of repeat readings will accomplish two important things: (a) the readings will be at about the same position on the meter measuring screw to avoid errors from screw irregularities; and (b) soil and rock beneath the stations will be in similar states with respect to tidal loading. Typical background noise levels (from cultural and natural sources) for microgravimetric surveys are in the 5- to 10-μGal range, although during large earthquakes, the noise level can easily exceed the total tidal variation. Thus, for a several-hour period following large earthquakes, obtaining gravity readings in a survey net will be impossible. With the capacitive readout capability on the Model-D meter, it is easy to monitor the background noise level. If required, the station reading can be

113

obtained as the mean of several readings over a 10-min period; a preferable procedure is to continuously record the gravimeter output on a chart recorder for at least 10 min.

Comments and conclusions

102. In spite of the stringent survey demands and time-dependent interfering effects, it seems that repeated microgravity surveys show promise of being a valuable tool for studying elevation changes and/or mass change effects associated with reservoir impounding. A reservoir representing a total post impoundment load of the order of 10^{12} kg (1.1×10^9 tons or 0.81 million acre-ft) or greater is a candidate for microgravimetric studies for determing elevation changes.

103. Of great importance, both from the standpoint of understanding crustal deflection and earthquake-inducing mechanisms and from the standpoint of assessing the usefulness of microgravimetry for studying reservoir-induced elevation changes, is the need for a study (theoretical and observational) of the response times of crustal deflection to load application and the time lag between reservoir filling and the arrival of pore pressure changes as a function of depth and distance from the reservoir. Considering the nature of the geologic system involved, it is difficult to imagine that the vertical deformations occur "instantaneously" as the reservoir load is applied, even though the final deformations agree very closely with purely elastic deformation calculations.

104. It is interesting to note, as a conclusion to this assessment, that the length of the traverse line is not a limiting factor in assessing the accuracy of a microgravity survey. However, for even the most precise and accurate level survey, the accuracy degrades at least as fast as $\alpha_n L^{1/2}$ where L is the survey line length in km and α_n depends on the order of the survey with a range of 0.5 to 6 mm (Lambert and Beaumont, 1977; Savage et al., 1977). A possible example of this level survey degradation is given in Savage et al. (1977).

PART VIII: MICROGRAVIMETER AS TIDAL RECORDING
INSTRUMENT AND SEISMOMETER

105. Use of the microgravimeter to record the solid earth tide
has been discussed previously. For the Model-D meter equipped with
electronic output, the meter is set on the baseplate and the output is
monitored with a chart recorder, resulting in a time record of the
variation of gravimeter output. The tidal gravity variation at a point
on the surface depends primarily on two factors: (a) variation in gravi-
tational attraction due to varying positions of the sun and moon (and to
a smaller extent the planets) with respect to the point; and (b) ampli-
fication of the magnitude predicted by (a) due to yielding of the solid
earth in response to the varying attractive force, i.e., elevation of
the point actually varies with time.

106. Using the equations of Longman (1959), it is possible to
calculate the theoretical tidal effect at any point on the earth's
surface. The equations include a compliance or gravimetric amplifica-
tion factor to account for yielding. Comparison of observed and meas-
ured earth tide records can in principle yield a determination of this
factor for any location; typical values range from 1.138 to 1.240
(Garland, 1977). Observations of the earth tide can give information not
only on gross earth structure but also on anomalous tidal yielding in
areas of major faults or other significant tectonic features.

107. The theoretical and observed earth tide for Vicksburg,
Mississippi, are compared in Figure 51 for a three-day period (16-18 May
1980). The phases of the two curves in Figure 51 agree quite well.
Amplitudes of the minima and secondary maxima of the two curves agree
closely; however, the primary maxima of the measured tidal curve are
nominally 50 µGal larger than the corresponding maxima on the theoret-
ical curve. There are two possible explanations for the amplitude
differences: (a) a small portion of the amplitude difference could be
due to using a compliance factor that is too small for the site (1.160
was used); and (b) the electronic output of the gravimeter is nonlinear
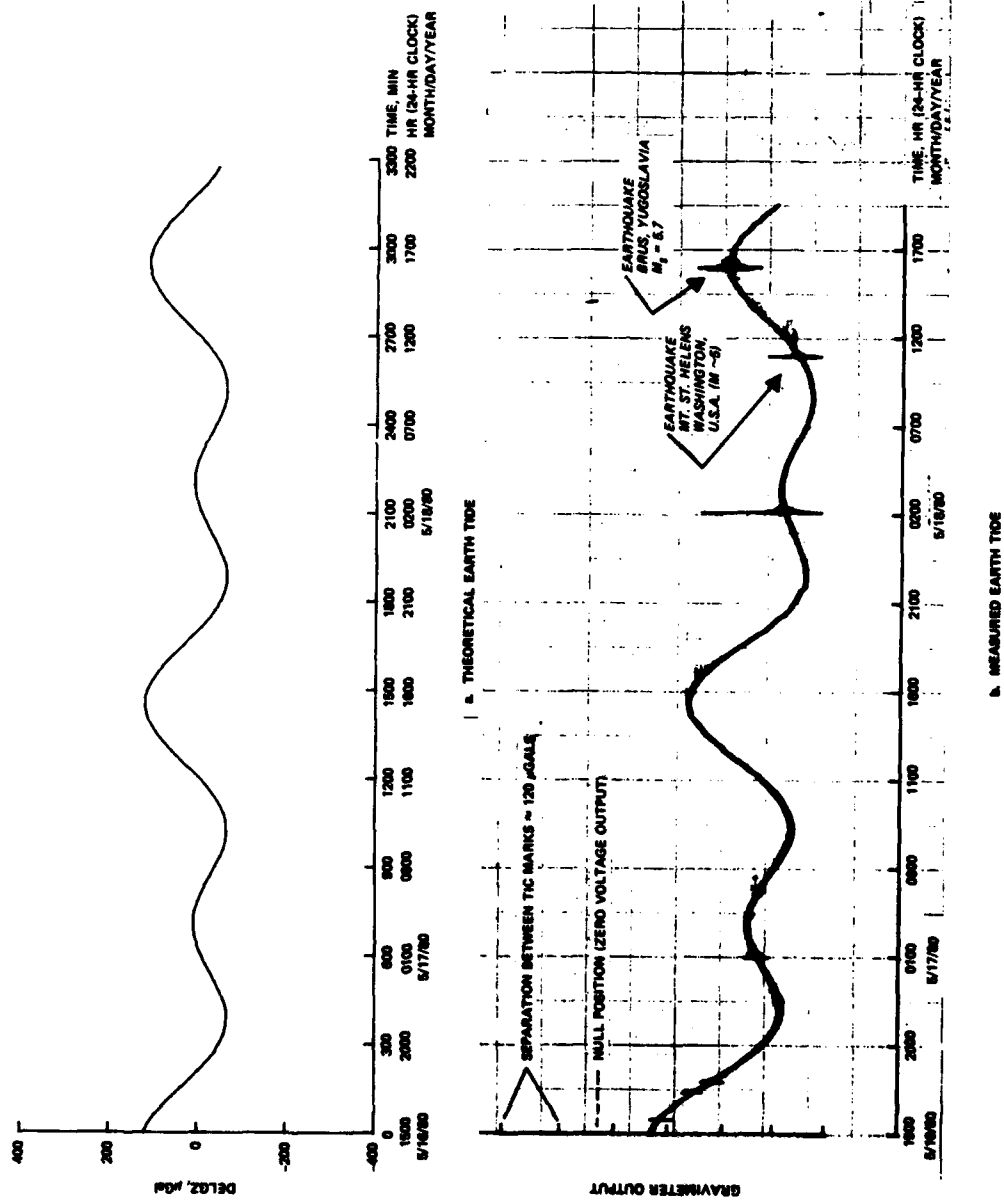relative to the null position (McConnell et al., 1974). Since the

115

Figure 51. Comparison of theoretical earth tide and earth tide measured with Model-D gravimeter at Vicksburg, Mississippi, for three-day period

116

position of the tidal variation relative to the meter null position will vary because of the superimposed approximately 2 µGal/hr drift, the gravimeter tidal curve would require frequent nonlinearity calibrations if used for quantitative tidal variation studies. The vertical scale of the measured curve was generated about the actual output position at 1930 hr on 18 May. At this time, drift has carried the tidal variation curve to within about 120 µGal of saturation of the electronic output on one side of the null position.

108. The three events superimposed on the tidal record on 18 May in Figure 51 are earthquakes and illustrate another interesting application of the microgravimeter as a long-period vertical seismometer. Figure 52 presents four other earthquakes recorded with the gravimeter at Vicksburg, Mississippi (note that the scale factors are different from those in Figure 51). The Kuril Islands earthquake record in Figure 52 is clipped (meter output saturated) on the bottom. Gravimeter records of earthquakes can be used to study the fundamental modes of free oscillation of the earth (Linton et al., 1979). Also, monitoring gravimeter tidal variation overnight during field surveys for the occurrence of large earthquakes will alert field parties as to the source of larger than normal background noise.
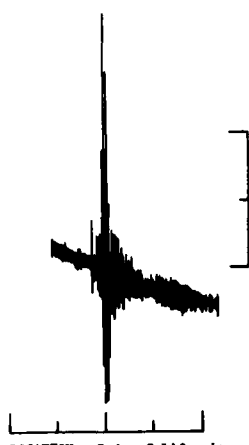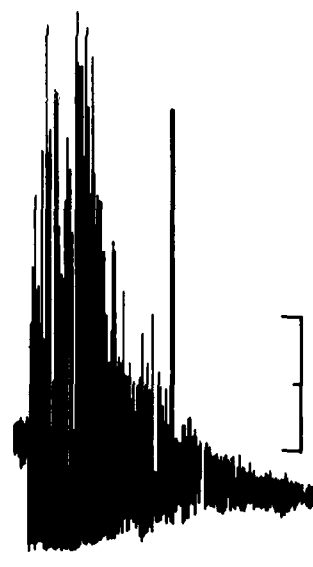
LOCATION: Baja, California

ϕ_0 - 26.3N
λ_0 - 112W

Time: 07:43:46.5 GMT
        26 November 1978
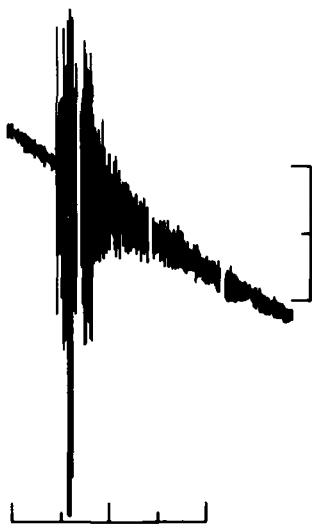
Magnitude: 5.1 M_s

LOCATION: Southern Kuril Islands
            (750 mi NE of Tokyo)

ϕ_0 - 44.7N
λ_0 - 145.7E

Time: 14:01:51.7 GMT
        6 December 1978
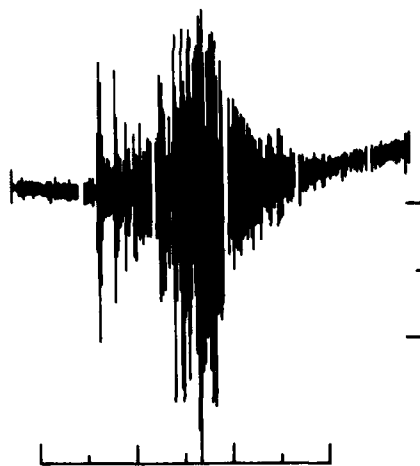
Magnitude: 7.0 M_s

LOCATION: Off Mexico

ϕ_0 - 9.02N
λ_0 - 104.18W

Time: 23:57:47.9 GMT
        25 December 1978

Magnitude: 6.5 M_s

LOCATION: Taiwan

ϕ_0 - 23.65N
λ_0 - 122.42E

Time: 11:23:14.9 GMT
        23 December 1978

Magnitude: 6.7 M_s

Comments: Two reported killed

1 HR (HORIZONTAL)

100 μGal (VERTICAL)

Figure 52.   Earthquake records made at Vicksburg, Mississippi, with
LaCoste & Romberg Model-D microgravimeter in tidal recording mode

118

PART IX: SUMMARY AND CONCLUSIONS

109. This study attempts to assess the applicability of micro-
gravimetric techniques to a wide range of geotechnical problems. Aspects
of potential theory relevant to the discussion are reviewed. Field pro-
cedures and data correction requirements for high-resolution gravity
surveys are discussed in detail. With care in carrying out the field
survey and data correction, it is possible to keep probable errors to
5 µGal or less. Choosing a conservative detectability threshold of 10
µGal, the detectability by microgravity surveys of simple structures,
which can approximate real structures of interest in geotechnical site
investigations, is assessed. It is noted that due to the nonuniqueness
of the inverse gravity problem, although it may not be possible to state
positively what is present in the subsurface at a site on the basis of
a microgravity survey alone, it is possible to place bounds on what is
not present in the subsurface (i.e., to state the maximum size and depth
of anomalies that may be present).

110. Four case histories of the use of microgravity surveys for
detection of subsurface cavities are presented. While cavities are only
one of a number of geotechnical problems to which microgravimetry can be
advantageously applied, the detection and delineation of subsurface
cavities is one of the most challenging geotechnical problems. In the
Medford Cave site investigation, the microgravity study revealed subtle
features of complex near-surface geology (Figure 36). Yet even in the
presence of the lithological noise introduced by complex near-surface
geological variations, the Medford Cave microgravity survey successfully
detected deeper known and previously unknown cavernous conditions at the
site.

111. The results of a preliminary attempt to conduct a definitive
field evaluation of gravity gradient techniques are presented. A man-made
structure simulating a block-faulted geometry was selected. The micro-
gravity survey across the structure again demonstrates the ability to
define and delineate small shallow structures of interest (Figure 40).
Comparison of the observed gravity profile and horizontal and vertical

119

gravity gradient profiles to two-dimensional model profile calculations is quite good. Use of the discrete Hilbert transform relation to calculate a vertical gradient profile from the measured horizontal gradient profile is successfully demonstrated. Gravity gradient techniques for delineation of shallow geologic structures are very promising.

112. Application of repeat microgravity surveys for determination of elevation and elevation change is assessed with particular emphasis on elevation changes caused by reservoir impoundment. It is concluded that elevation changes as small as 1 cm should ultimately be detectable with a reasonable degree of confidence. Also, reservoirs representing a total postimpoundment surface load of the order of 10^{12} kg or greater are candidates for microgravity survey nets for elevation change monitoring. Similar applications of repeat microgravity surveys are for monitoring elevation changes associated with subsidence caused by fluid withdrawal and with tectonic subsidence or uplift.

113. Other uses for microgravimetric techniques are briefly discussed in the review of the state of the art and the case histories. An application of great potential value is the use of gravity data to estimate mass requirements for remedial grouting programs and for verification of effectiveness of grouting programs. Grouting program applications of microgravimetry should be applied and evaluated at Corps of Engineers construction projects when suitable test cases are encountered. Regional studies of seasonal groundwater-level fluctuations and estimates of aquifer porosity are another area that should be thoroughly studied. Another important application, which has not been discussed, is the use of borehole microgravimeters to determine in situ bulk densities. Considerable effort has been devoted to developing borehole microgravimeters. Some of the principles and applications of borehole gravimetry are covered in the papers by Healy (1970), Hearst and McKague (1976), and Snyder (1976).

114. Microgravimetry has many varied applications to geotechnical problems. It should be carefully considered for general use in geophysical site investigations as well as the specialized applications

summarized in this study. It is important that the geotechnical community be aware of the potential as well as the limitations of the techniques.

REFERENCES

Arzi, A. A. 1975. "Microgravimetry for Engineering Applications," Geophysical Prospecting, Vol 23, No. 3, pp 408-425.

Beck, J. L. 1976. "Weight-Induced Stresses and the Recent Seismicity at Lake Oroville, California," Bulletin of the Seismological Society of America, Vol 66, pp 1121-1131.

Boubaker, K. 1973. "Rapid Method of Quantitative Interpretation in Microgravity Measurement," Third Cycle Doctorate Diploma, University of Paris, VI.

Bracewell, R. 1965. The Fourier Transform and Its Application, McGraw-Hill Company, New York.

Butler, D. K. 1979. "Assessment of Microgravimetric Techniques for Site Investigations," 49th International Meeting of the Society of Exploration Geophysicists, New Orleans, La.

Cabrera, D. H. 1973. "Methods of Relief Correction in Micro-Gravity Corrections," Optional Thesis, Ecole des Mines de Paris.

Carmichael, R. W., and Henry, G. 1977. "Gravity Exploration for Groundwater and Bedrock Topography in Glaciated Areas," Geophysics, Vol 42, pp 850-859.

Chico, R. J. 1964. "Detection of Caves by Gravimetry," International Journal of Speleology, Vol 1, pp 101-108.

Colley, G. C. 1963. "The Detection of Caves by Gravity Measurements," Geophysical Prospecting, Vol 11, pp 1-9.

Coons, R. L., Woolard, G. P., and Hershey, G. 1967. "Structural Significance and Analysis of Mid-Continent Gravity High," Journal of the American Association of Petroleum Geologists, Vol 51, pp 2381-2409.

Domenico, S. N. 1967. "Detail Gravity Across San Andreas Fault Zone," Geophysics, Vol 32, pp 297-301.

Eaton, G. P., Martin, N. W., and Murphy, M. A. 1964. "Application of Gravity Measurements to Some Problems in Engineering Geology," Engineering Geology (AEG), Vol 1, pp 6-21.

Evjen, H. M. 1936. "The Place of the Vertical Gradient in Gravitational Interpretations," Geophysics, Vol 1, pp 127-136.

Fajklewicz, Z. J. 1976. "Gravity Vertical Gradient Measurements for the Detection of Small Geologic and Anthropomorphic Forms," Geophysics, Vol 41, pp 1016-1030.

Fountain, L. W., Herzig, F. X., and Owen, T. E.. 1975. "Detection of Subsurface Cavities by Surface Remote Sensing Techniques," Report No. FHWA-RD-75-80, Federal Highway Administration, Washington, D. C.

Garland, G. D. 1977. The Earth's Shape and Gravity, Permagon Press, New York.

Geldart, L. P., Gill, D. E., and Sharma, B. 1966. "Gravity Anomalies of Two-Dimensional Faults," Geophysics, Vol 31, pp 372-397.

Gough, D. I., and Gough, W. I. 1970a. "Stress and Deflection in the Lithosphere Near Lake Kariba, 1," Geophysics Journal Report of the Astron Society, Vol 21.

_____. 1970b. "Load-Induced Earthquakes at Lake Kariba," Geophysics Journal Report of the Astron Society, Vol 21.

Grant, F. S., and West, G. F. 1965. Interpretation Theory in Applied Geophysics, McGraw-Hill Book Company, New York.

Green, R. W. E. 1973. "Seismic Activity Observed at the Hendrik Verwoerd Dam," International Colloquim on Seismic Effects of Reservoir Impounding, The Royal Society, London.

Guha, S. K. et al. 1974. "Case Histories of Some Artificial Crustal Disturbance," Engineering Geology, Vol 8, pp 59-77.

Gupta, H. K. 1976. Dams and Earthquakes, Elsevier Scientific Publishing Company, New York.

Hall, D. H., and Hajnal, Z. 1962. "The Gravimeter in Studies of Buried Valleys," Geophysics, Vol 27, pp 939-951.

Hammer, S. 1953. "Usefulness of High-Quality Gravity Surveys," The Oil and Gas Journal.

Hammer, S., and Anzoleaga, R. 1975. "Exploring for Stratigraphic Traps with Gravity Gradients," Geophysics, Vol 40, pp 256-268.

Hammer, S., Nettleton, L. L., and Hastings, W. K. 1945. "Prospecting for Chromite in Cuba," Geophysics, Vol 10, pp 34-49.

Healy, D. L. 1970. "Calculated In Situ Bulk Densities from Subsurface Cavity Observations and Density Logs, Nevada Test Site and Hot Creek Valley, Nye County, Nevada," U. S. Geological Survey Professional Paper 700-B, pp 1352-1362.

Hearst, J. R., and McKague, H. L. 1976. "Structure Elucidation with Borehole Gravimetry," Geophysics, Vol 41, pp 491-505.

Janle, P., Makris, J., and Menzel, H. 1971. "Experimental Investigations of the Vertical Gradient of Gravity," Bollettino di Geofisica Teoria ed Applicata, Vol 13, pp 254-263.

Jung, K. 1961. Schwerkraftverfahren in der Angewandten Geophysik, Geest und Portig, Leipzig.

LaFehr, T. R. 1979. "Gravity and Magnetic Methods," Geophysical Methods in Geotechnical Engineering, American Society of Civil Engineers Convention, Atlanta, Ga.

Lambert, A., and Beaumont, C. 1977. "Nano Variations in Gravity due to Seasonal Groundwater Movements--Implications for the Gravitational Detection of Tectonic Movements," Journal of Gerphysical Research, Vol 82, pp 297-306.

Lee, T. 1972. "A Method for Computing the Deformation of the Crust Caused by the Filling of Large Lakes," Bulletin of the Seismological Society of America, Vol 62, pp 1597-1610.

Linton, J. A., Smylie, D. E., and Jansen, O. G. 1979. "Gravity Meter Observation of Free Modes Excited by the August 19, 1977, Indonesia Earthquake," Bulletin of the Seismological Society of America, Vol 69, pp 1445-1454.

Longman, I. M. 1959. "Formulas for Computing the Tidal Acceleration due to the Moon and Sun," Journal of Geophysical Research, Vol 64, pp 2351-2355.

McConnell, R., Hearty, D., and Winter, P. 1974. "An Evaluation of the LaCoste & Romberg Model-D Microgravimeter," Seventh Meeting of the International Gravity Commission, Paris.

Nettleton, L. L. 1971. "Elementary Gravity and Magnetics for Geologists and Seismologists," Monograph Number 1, Society of Exploration Geophysicists, Tulsa, Okla.

Neumann, R. 1967. "High Accuracy Gravimetry Application of the Detection of Cavities," Geophysical Prospecting, Vol 15.

_____. 1972. "High Precision Gravimetry--Recent Developments," Report to Paris Commission of European Association of Engineering Geologists, Compagnie General de Geophysique, Massy, France.

_____. 1973a. "Microgravimetry--Experimentation of Vertical Gradient," Compagnie Generale de Geophysique, Massy, France.

_____. 1973b. "Gravity Measurement Prospecting Applied to the Detection of Underground Cavities," Compagnie Generale de Geophysique, Massy, France.

_____. 1973c. "Gravimetrical Prospecting--Course in Geophysics," Geophysical Treatise, ed. M. Coulomb, Vol 1, Chap. 22, Masson.

_____. 1974. "Seeking Cavities by Gravity Measurement Prospecting," Compagnie Generale de Geophysique, Massy, France.

_____. 1977. "Microgravity Method Applied to the Detection of Cavities," Symposium on Detection of Subsurface Cavities, U. S. Army Waterways Experiment Station, CE, Vicksburg, Miss.

Oldenburg, D. W. 1974. "The Inversion and Interpretation of Gravity Anomalies," Geophysics, Vol 39, pp 526-536.

Parasnis, D. S. 1966. Mining Geophysics, Elsevier Publishing Company, New York.

Pick, M., Picha, J., and Vyskocil, V. 1973. Theory of the Earth's Gravity Field, Elsevier Scientific Publishing Company, New York.

Savage, J. C., et al. 1977. "Geodetic Measurements of Deformation Associated with the Oroville, California, Earthquake," Journal of Geophysical Research, Vol 82, pp 1667-1671.

Sneddon, I. H. 1972. The Use of Integral Transforms, McGraw-Hill Company, New York.

Snyder, D. D. 1976. "The Borehole Bouguer Gravity Anomaly - Application to Interpreting Borehole Gravity Surveys," Society of Professional Well Log Analysts, Seventeenth Annual Logging Symposium.

Speed, R. C. 1970. "Gravity Anomalies from Cavities in Salt Beds I - The Surface Field," Third Symposium on Salt, Northern Ohio Geological Society, Vol 2, pp 367-385.

Talwani, M., Wonzel, S. L., and Landisman, M. 1959. "Rapid Gravity Computations for Two-Dimensional Bodies with Application to the Mendocino Submarine Fracture Zones," Journal of Geophysical Research, Vol 64, pp 49-59.

Telford, W. M. et al. 1976. Applied Geophysics, Cambridge University Press, New York.

Thyssen-Bornemisza, S. 1965. "A Short Note on Double-Track Profiling with the Gravity Meter," Geophysics, Vol 30, pp 1135-1137.

Thyssen-Bornemisza, S., Groten, E., and Bazhaw, W. 1972. "Correction of Accurate Gravity Surveys by Carefully Observed Vertical Gradients of Gravity," Geophysical Prospecting, Vol 20, pp 17-27.

Thyssen-Bornemisza, S., and Stackler, W. F. 1956. "Observation of the Vertical Gradient of Gravity in the Field," Geophysics, Vol 21, pp 771-779.

Torge, W. 1971. "Determination of the Calibration of the LaCoste & Romberg Gravimeters and Time Variations in the Calibrations," Bollettino di Geofisica Teorica ed Applicata, Vol 13, pp 298-306.

Westergaard, H. M., and Adkins, A. W. 1934. "Deformation of the Earth's Surface Due to Weight of Boulder Reservoir, Technical Memorandum No. 422, U. S. Bureau of Reclamation, Denver, Colo.

Wolters, R. (editor). 1973. Proceedings, Symposium on Sink-Holes and Subsidence Engineering--Geological Problems Related to Soluble Rocks, International Association of Engineering Geology, Hanover, Germany.